28

ORNL
MASTER COPY

ORNL-3047
UC-34 - Physics

ELECTRONUCLEAR RESEARCH DIVISION

ANNUAL PROGRESS REPORT

FOR PERIOD ENDING MARCH 1, 1960

OAK RIDGE NATIONAL LABORATORY
operated by
UNION CARBIDE CORPORATION
for the
U.S. ATOMIC ENERGY COMMISSION

Printed in USA. Price $2.00. Available from the

Office of Technical Services
Department of Commerce
Washington 25, D.C.

LEGAL NOTICE

This report was prepared as an account of Government sponsored work. Neither the United States, nor the Commission, nor any person acting on behalf of the Commission:

A. Makes any warranty or representation, expressed or implied, with respect to the accuracy, completeness, or usefulness of the information contained in this report, or that the use of any information, apparatus, method, or process disclosed in this report may not infringe privately owned rights; or

B. Assumes any liabilities with respect to the use of, or for damages resulting from the use of any information, apparatus, method, or process disclosed in this report.

As used in the above, "person acting on behalf of the Commission" includes any employee or contractor of the Commission, or employee of such contractor, to the extent that such employee or contractor of the Commission, or employee of such contractor prepares, disseminates, or provides access to, any information pursuant to his employment or contract with the Commission, or his employment with such contractor.

ORNL-3047
Physics
TID-4500 (16th ed.)

Contract No. W-7405-eng-26

ELECTRONUCLEAR RESEARCH DIVISION

ANNUAL PROGRESS REPORT

For Period Ending March 1, 1960

Robert S. Livingston, Director

DATE ISSUED
FEB 7 1961

OAK RIDGE NATIONAL LABORATORY
Oak Ridge, Tennessee
operated by
UNION CARBIDE CORPORATION
for the
U.S. ATOMIC ENERGY COMMISSION

SUMMARY

Heavy ions (27-Mev N^{+++}) produced in the ORNL 63-Inch Cyclotron are used in investigations of heavy-ion elastic scattering, the evaporation of light particles, nucleon-transfer reactions, and nucleon-exchange reactions. Surface-barrier counters are being developed for use as heavy-ion detectors.

For work with 22-Mev protons from the ORNL 86-Inch Cyclotron, a new selective counting system permits simultaneous recording of proton, deuteron, triton, and alpha-particle spectra; data are recorded on IBM cards for analysis in a high-speed computer. Present studies concern (p,d), (p,t), and (p,α) reactions, anomalous scattering, and elastic scattering from isobars. Studies of elements in the rare-earth group continue with a detailed study of the nuclear levels in Yb^{169}.

Design problems for the construction of spiraled sector coils for Cyclotron Analogue II were solved. The major components of this azimuthally-varying-field approx 500-kev electron cyclotron were designed and are now being fabricated.

Construction of the Oak Ridge Isochronous Cyclotron is well advanced. A new cyclotron building is being built, the main magnet was fabricated and is being tested, and other components are being designed and fabricated. Precise field measurements in a quarter-scale magnet are being used to determine the design of the complex pole-tip windings required for isochronous operation for a wide range of particles and energies.

CONTENTS

SUMMARY iii

1. HEAVY-PARTICLE PHYSICS 1
   Elastic Scattering 1
   Light Particles from Nitrogen-Induced Reactions 5
   Surface-Barrier Counters 8
   Angular Distribution of N^{13} from N^{14} on N^{14} 12
   The Exchange Transfer Reaction $Al^{27}(N^{14},Mg^{27})O^{14}$ 14
   Optical Model Calculations 16

2. PHYSICS RESEARCH WITH 22-Mev PROTONS 20
   (p,d) and (p,t) Reactions 21
   Anomalous Scattering 25
   (p,α) Reactions 26
   Elastic Scattering from Isobars 27
   Nuclear Levels in Yb^{169} 27
   Applied Physics 31

3. CYCLOTRON OPERATION 36
   Time Dependence of the Beam in the 86-Inch Cyclotron 36
   The 86-Inch Cyclotron Dee Voltage Regulation 39
   Operation of the 86-Inch Cyclotron 40
   Operation of the 63-Inch Cyclotron 42

4. ACCELERATOR DEVELOPMENT 44
   Cyclotron Analogue II 44

5. THE OAK RIDGE ISOCHRONOUS CYCLOTRON 54
   Design Studies 55
   Cyclotron Components 66
   Instrumentation and Controls 76
   The ORIC Building 79

PUBLICATIONS 83

ANNOUNCEMENTS 86

1. HEAVY-PARTICLE PHYSICS

The heavy-ion physics program continues to exploit the 28-Mev nitrogen ions produced in the ORNL 63-Inch Cyclotron. In the following sections are described investigations of heavy-ion elastic scattering and the interpretation of these results, experiments on the evaporation of light particles from the $N^{14} + F^{19}$ reaction, angular-distribution measurements of transfer reactions, measurement of the total cross section for an exchange-transfer reaction, and the development of surface-barrier counters for use as heavy-ion detectors.

Elastic Scattering

The coincidence technique for the identification and measurement of absolute differential cross sections for the elastic scattering of nitrogen ions from light elements was described in a previous report.[1] By virtue of this method, elastic-scattering events can be differentiated from other processes, such as inelastic scattering or transfer reactions. Cross sections as small as several tenths of an mb/sr (millibarns/steradian) can be measured in this way. Since the time of the last report the scintillation counters have been replaced by barrier counters, and while this has made much of the work easier, it does not differ in principle from the system employing scintillation detectors. Basically, two counters in coincidence are arranged so that one counts the scattered particle and the other the recoiling one. From pulse-height information in each counter and from the angular position of each, an elastic-scattering event may be identified.

This method was used to investigate the elastic scattering of nitrogen on beryllium (in the previous report the data extend only to 90° c.m.), nitrogen on carbon at three energies, and nitrogen on aluminum. The results are shown graphically in Figs. 1.1–1.3.

An attempt was made to analyze the data in terms of the sharp cut-off model which proved so successful in the previous analysis of N^{14}-N^{14} scattering. The attempt was unsuccessful in N-Be scattering, and in N-C scattering at all three energies. This should not be surprising since

---

[1] Electronuclear Ann. Prog. Rep. Oct. 1, 1958, ORNL-2740.

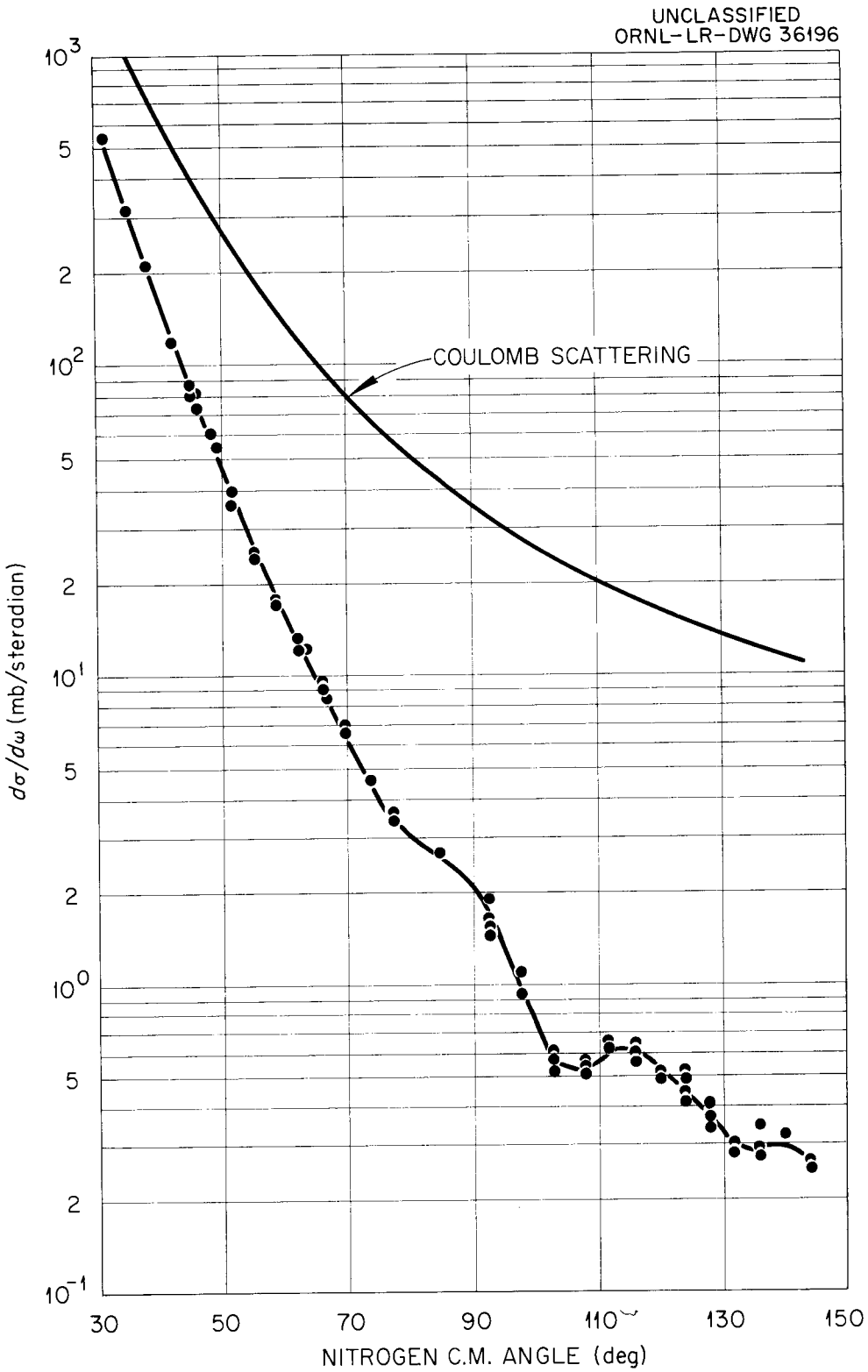

Fig. 1.1. The Differential Cross Section of N^{14}-Be^9 Elastic Scattering as a Function of the Nitrogen Center-of-Mass Angle. All experimental points are shown except at 85°, where many points were taken and only an average is shown. The upper curve is the cross section for Coulomb scattering.

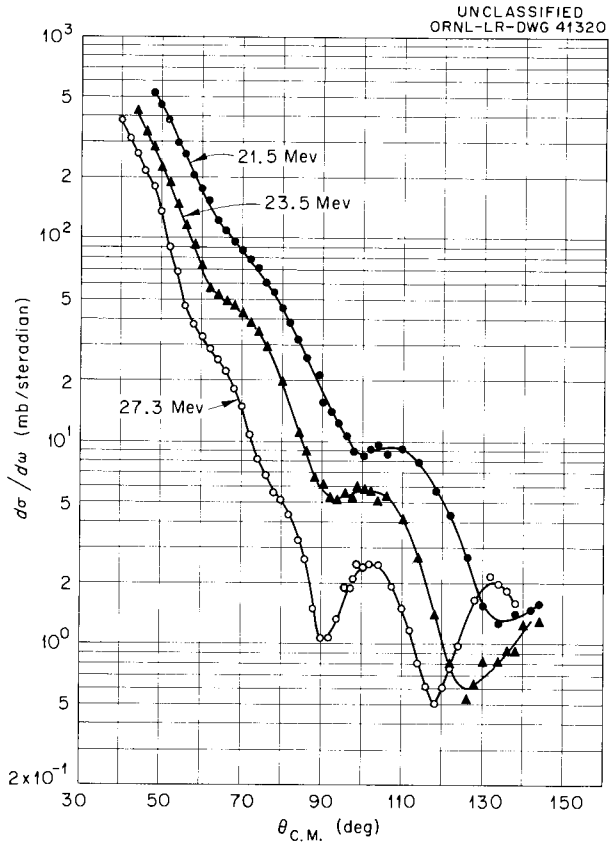

Fig. 1.2. The Differential Cross Section of N^{14}-C^{12} Elastic Scattering at 27.3, 23.5, and 21.5 Mev as a Function of the Nitrogen Center-of-Mass Angle. Mean energies in the target are shown.

it was found in the analysis of alpha-particle scattering that the sharp cutoff model applies if $\sigma/\sigma_c > 1/\eta$ ($\eta = Z_1 Z_2 e^2/hv$); in these experiments η is of the order of three, and $\sigma/\sigma_c < 1/\eta$ over nearly the whole angular region.

In the case of N-Al scattering $\eta = 10.3$; this leads one to expect a much more classical situation. Indeed, the sharp cutoff model does reproduce the data to the point where σ/σ_c approaches $1/\eta$ (see Fig. 1.4). From this fit one may obtain an interaction distance R, which turns out to be $R = 1.68(A_1^{1/3} + A_2^{1/3})$ f. A semiclassical scattering theory recently developed by Ford and Wheeler was also used to interpret the data. This theory pictures the nucleus as having a diffuse, nonabsorbing surface and a totally absorbing core. It has two free parameters: θ_r, the rainbow angle related to a nuclear interaction distance R; and $\underline{q}$, a parameter

related to the surface thickness ΔR. The best fit, also shown in Fig. 1.4, was obtained for a rainbow angle of 94°; this corresponds to $R = 1.59(A_1^{1/3} + A_2^{1/3})$ and a value of $\underline{q}$ such that $\Delta R = 0.83$ f.

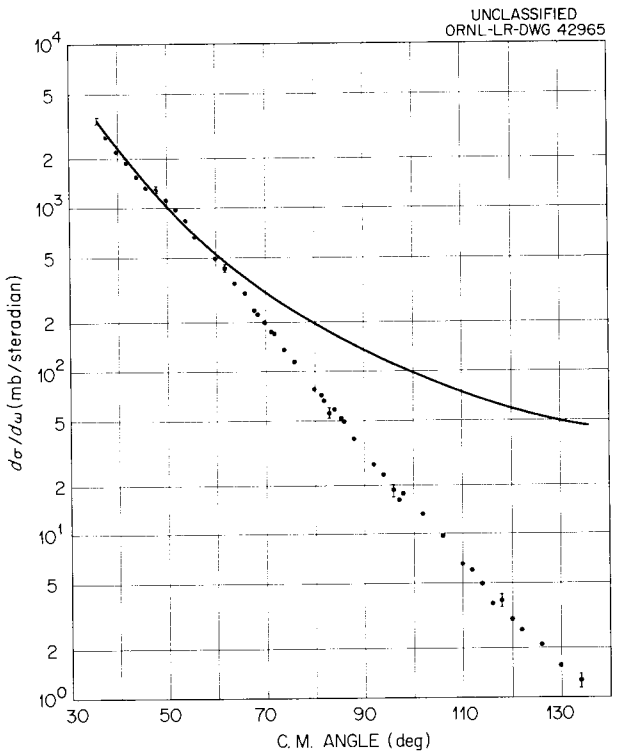

Fig. 1.3. The Differential Cross Section of N^{14}-Al^{27} Elastic Scattering as a Function of the Nitrogen Center-of-Mass Angle. The dots are the experimental results, and the smooth curve is the cross section for Coulomb scattering.

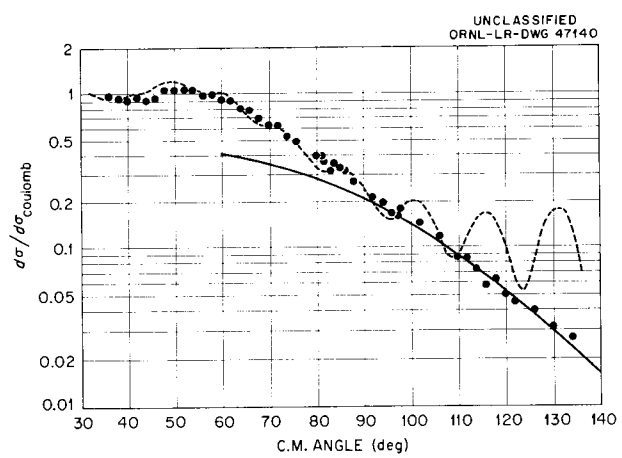

Fig. 1.4. The Ratio of the Elastic to the Coulomb Cross Section for N-Al Scattering at 27.3 Mev. The dashed line is the sharp cutoff calculation and the solid line the rainbow scattering calculation.

Light Particles from Nitrogen-Induced Reactions

Previous reports[2-5] have described work done at the Laboratory on the energy and angular distributions of protons, deuterons, and alpha particles from reactions induced by approx 27.5-Mev N^{14} ions. The work on light-particle spectra from N^{14}-induced reactions has been continued with the study of alpha particles from the nitrogen bombardment of an F^{19} target. This target nucleus was chosen because the high, 20.9-Mev, Q value of the $F^{19}(N^{14},\alpha)Si^{29}$ ground-state transition permits a large range of alpha-particle energy to be observed with little chance of significant contribution due to target impurities. Thus far, alpha-particle energy spectra have been obtained at laboratory angles of 20, 35, 50, 65, and 80°.

Equipment and Procedure

To perform this experiment with the existing 24-in.-diam scattering chamber at the 63-Inch Cyclotron, a counter telescope was designed whose total length is only 7-1/4 in. The short length is due largely to the use of the small six-stage Du Mont 6365 photomultiplier tube. In order to determine a lower limit for the intrinsic pulse-height resolution of these phototubes, a preliminary experiment was performed in which 23-Mev protons from the 86-Inch Cyclotron were scattered from a thin gold foil onto an NaI(Tl) crystal optically coupled to the Du Mont 6365. For each of the two phototubes tested in this manner, the observed peaks had a full width at half maximum of less than 3.5%. In the particle-selective experiment itself a CsI(Tl) crystal was used because of its relatively linear alpha-particle response;[6] the resolution for 18-Mev alpha particles varied from 7 to 10% full width at half maximum, depending on target thickness.

---

[2] C. D. Goodman and J. L. Need, Phys. Rev. 110, 676 (1958).

[3] A. Zucker, Nuclear Phys. 6, 420 (1958).

[4] M. L. Halbert and A. Zucker, Phys. Rev. 114, 132 (1959).

[5] A. Zucker, R. S. Livingston, and F. T. Howard, Proceedings of the Conference on Reactions Between Complex Nuclei, Gatlinburg, Tenn., May 5–7, 1958, ORNL-2606 (Sept. 17, 1958).

[6] C. B. Fulmer, private communication.

The particle-selective scheme, described by Goodman and Need,[2] involves the simultaneous display of the two counter outputs as x and y coordinates on an oscilloscope face. A block diagram of the electronics used for the present experiment is shown in Fig. 1.5. For pulse amplification the A-8 preamplifier and amplifier[7] were chosen because the high gain and low noise level compensate the comparatively low gain of the Du Mont 6365. Other advantages of the A-8 amplifier for this application included (1) good impedance matching with the 1000-ohm RG 65/U delay line used and (2) compatibility with the crossover-pickoff gate pulse generator,[8] which facilitates accurate particle selection.

The particle-selective adjustments had to be complete before it was possible to measure the energy-calibrating alpha-particle groups. This

[7]G. G. Kelley, IRE National Convention Record, part 9, p 63 (1957).

[8]E. Fairstein, Instrumentation and Controls Ann. Prog. Rep. July 1, 1957, ORNL-2480, pp 1-5.

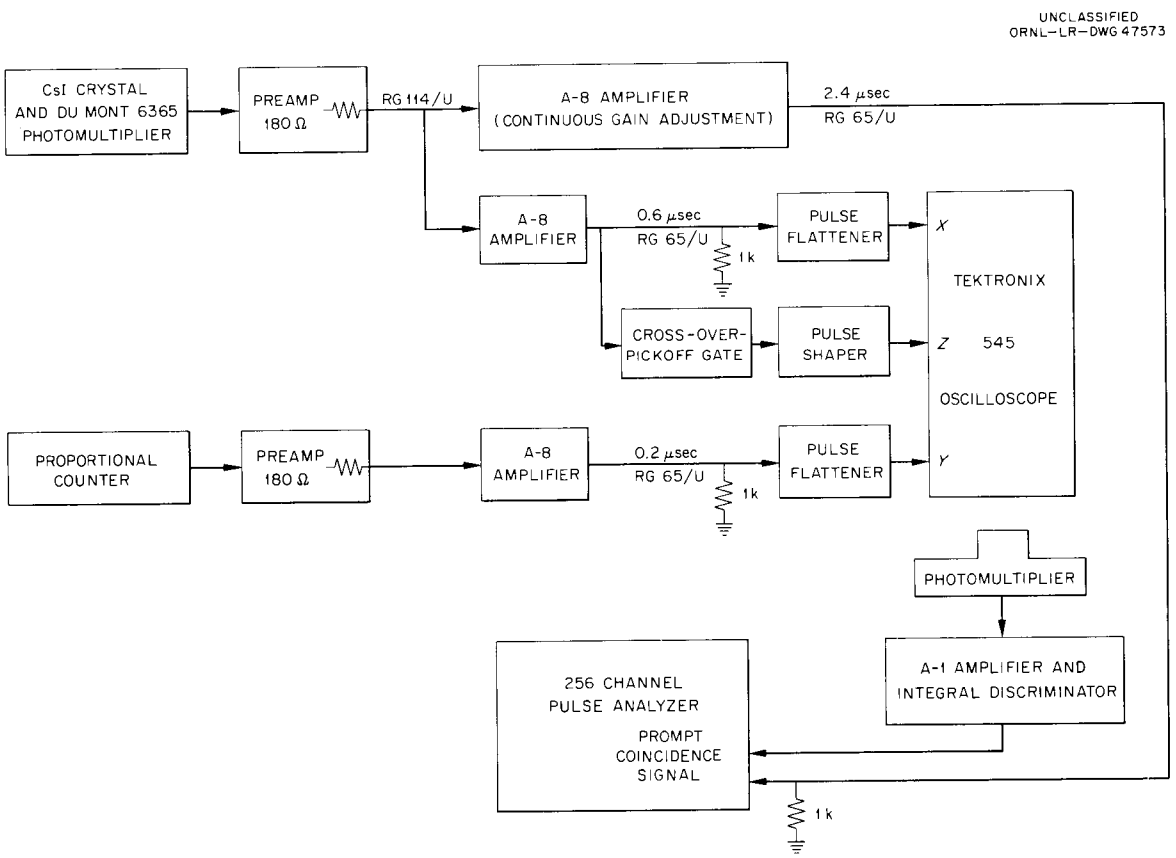

Fig. 1.5. Block Diagram of Circuits Used in the Particle-Selective System.

made it convenient to amplify the scintillation counter signal in two parallel amplifiers.

The energy-calibrating alpha-particle groups used were the ground- and first-excited-state transitions of the $N^{14}(d,\alpha)C^{12}$ reaction. A solid deuterated polyethylene target was placed in the N^{14} beam; a hot solution of the polyethylene in kerosene was used to form an approx 0.1-mg/cm^2 coating on one side of a 1-mg/cm^2 nickel foil. Such targets withstood a beam of about 2×10^{10} nitrogen ions/sec for about 8 hr before charring.

For the F^{19} target an approx 0.1-mg/cm^2 layer of NiF_2, prepared by high-temperature fluorination of nickel plates, followed by etching away of the metallic nickel, was used. Since these targets were not uniform and were supported by 1-mg/cm^2 nickel foil backings, only approximate angular distributions of the reaction particles have been feasible so far.

Results

Experimental results include alpha-particle spectra from reactions induced in the F^{19} targets by the nitrogen ion beam at angles from about 25 to 95° c.m. In each case the energy spectra are fitted to the predictions of a simple exponential energy-level density, exp (E^*/T), where the assumed reaction is $F^{19}(N^{14},\alpha)Si^{29}$, E^* is the excitation energy in the residual nucleus, and the nuclear temperature T is a constant at a given angle. The fit in each case extends over a range of at least 14 Mev in E^* and is better than a fit using $E^{*1/2}$ in the exponential of the level-density expression.[9] This feature of the observed alpha-particle spectra is illustrated by a typical spectrum at about 80° c.m. in Fig. 1.6.

The resulting values of the nuclear temperature decreased from about 3.0 to about 2.3 Mev as the center-of-mass angle was increased. These fits can be compared with those for alpha-particle spectra from the N^{14} bombardment of oxygen,[4] where the nuclear temperature decreases from about 2.4 to about 2.2 Mev in the angular range 0 to 75° c.m.

---

[9] T. Ericson, Nuclear Phys. 11, 481 (1959).

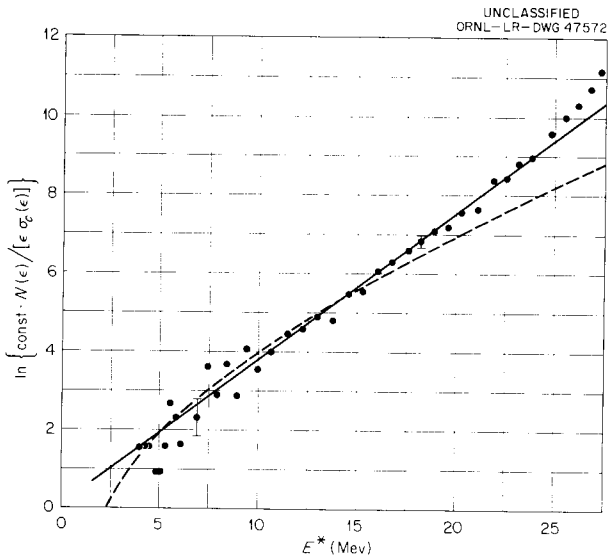

Fig. 1.6. Alpha-Particle Energy Spectrum at 65° Lab (about 80° c.m.) from N^{14} Bombardment of an F^{19} Target. The ordinate is such that a fit to the prediction of a simple exponential energy level density appears as a straight line (full curve). The dashed curve shows a fit to the prediction using $E^{*1/2}$ in the exponential of the energy level density expression.

Preliminary results on the angular distribution of alpha particles from N^{14} bombardment of F^{19} show a marked anisotropy, the differential cross section decreasing about a factor of 10 for E* = 8 Mev from 25 to 93° c.m. This factor decreases as E* is increased; for E* = 24 Mev the factor is about 4. Qualitatively these results are similar to those for alpha particles from nitrogen bombardment of oxygen.[4] In neither case can anything be said at this time regarding symmetry of the differential cross sections about 90° c.m.

An experiment is now in progress to measure the proton spectra from N^{14} bombardment of the F^{19} targets.

Surface-Barrier Counters

There has long been a need for a heavy-ion detector with good resolution and linear pulse-height response. The development of a germanium surface-barrier counter by Mayer and Gossick[10] and the subsequent

[10] J. Mayer and B. Gossick, Rev. Sci. Instr. 27, 407 (1956).

improvements and measurements on it by Walter et al.[11] pointed the way toward filling this need.

The advantages of these counters over the CsI(Tl) scintillation counters formerly used for heavy-ion detection are many. The new counters are capable of extremely good resolution, better than can be achieved with the best gridded ionization chambers.[12] Their pulse-height response is proportional to energy. They are compact, inexpensive, and relatively insensitive to magnetic fields. Their rise time is very fast. No windows are needed. Their sensitive volume may be varied simply by changing an external bias. They are insensitive to gamma rays, neutrons, and fast charged particles. They have shown excellent pulse-height stability. They may be biased reliably and cheaply with batteries.

The depth of the sensitive region is calculated as follows. At the surface of a semiconductor there normally exists a large number of trapping sites for electrons. With n-type material, these surface states remove mobile electrons from the interior until equilibrium is established, leaving behind fixed positive charges (ionized donors). The potential drop across this asymmetric double layer is known as the barrier height. It is frequently assumed that all the mobile electrons are removed down to a certain depth D and that none beyond D are disturbed (Schottky exhaustion-layer theory). Then, by solving Poisson's equation with appropriate boundary conditions, D is easily calculated in terms of the dielectric constant K, the net donor concentration N, and the barrier height V_0. If a negative external bias V is applied to the surface, D is given by

$$D = \sqrt{\frac{K(V_0 + V)}{2\pi eN}} ,$$

where e is the electronic charge. In this work a silicon counter has been operated routinely with $D \approx 30\ \mu$ (7.2 mg/cm^2). With higher purity (smaller N) or higher bias (larger V), counters with much greater barrier depth can undoubtedly be made.

---

[11] F. J. Walter et al., Study of Germanium Surface Barrier Counters, ORNL CF-58-11-29 (Nov. 28, 1958).

[12] J. L. Blankenship and C. J. Borkowski, Proc. Seventh Scintillation Symposium, Washington, D.C., February 1960 (to be published).

Since the capacity C_b of a barrier of area A is given by $C_b = KA/4\pi D$, operation with as large a D as practical is advantageous because it increases the signal pulse height and thus improves the signal-to-noise ratio.

The response of two counters to N^{14} ions and Po^{210} alphas was measured. One was made of 40 ohm-cm germanium by M. V. Goldman of this Division; it operates at 77°K. The other is a room-temperature silicon counter (50 ohm-cm) donated to us for testing by J. L. Blankenship of the Instrumentation and Controls Division. The area of each is 5 × 5 mm.

Figure 1.7 shows how the counters are connected. The preamplifier was designed especially for surface-barrier counters by E. E. Fairstein of the Instrumentation and Controls Division. It has a gain of 1000 and low noise (approx 5 μv rms equivalent noise at input). The amplifier is an A-1D modified for increased inverse feedback.

The pulser is useful not only for checking the circuit but also for measuring certain barrier characteristics. For example, C_b was measured as a function of bias and found to vary linearly with $(V_0 + V)^{-1/2}$, as expected from the exhaustion-layer theory. The energy loss per electron-hole pair was determined by using the pulser to inject a known charge and then comparing the output pulse height with that from Po^{210} alphas. The results were 3.3 ± 0.3 ev for silicon and 2.8 ± 0.3 ev for germanium.

The response of the silicon counter to N^{14} ions was measured in two ways. First, nickel absorbers of known thickness were inserted in the

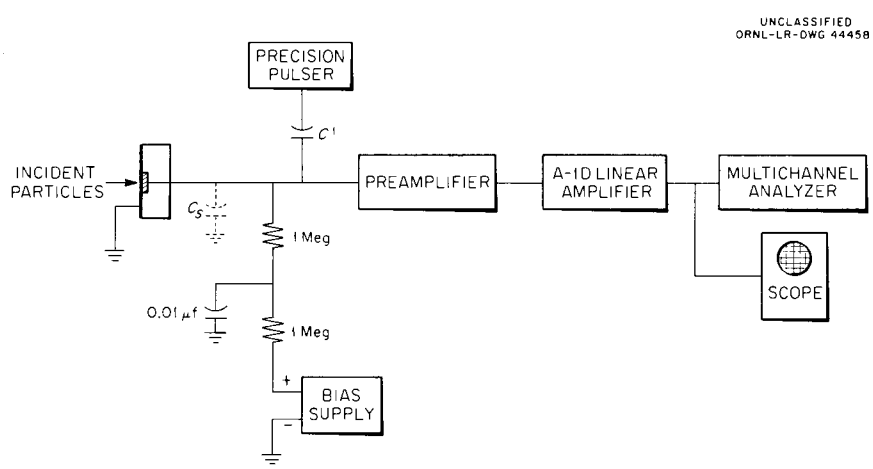

Fig. 1.7. Circuit for Surface-Barrier Counter. C^1 is approx 1 pf.

external beam of the cyclotron, and the pulse height of N^{14} scattered through 90° by a thin gold target was recorded. The results are given as the open circles in Fig. 1.8. The same type of measurement was also made for a germanium counter at liquid-nitrogen temperature; again a linear response was obtained. The accuracy of this method was limited mainly by uncertainty in the range-energy curve[13] for N^{14} in nickel.

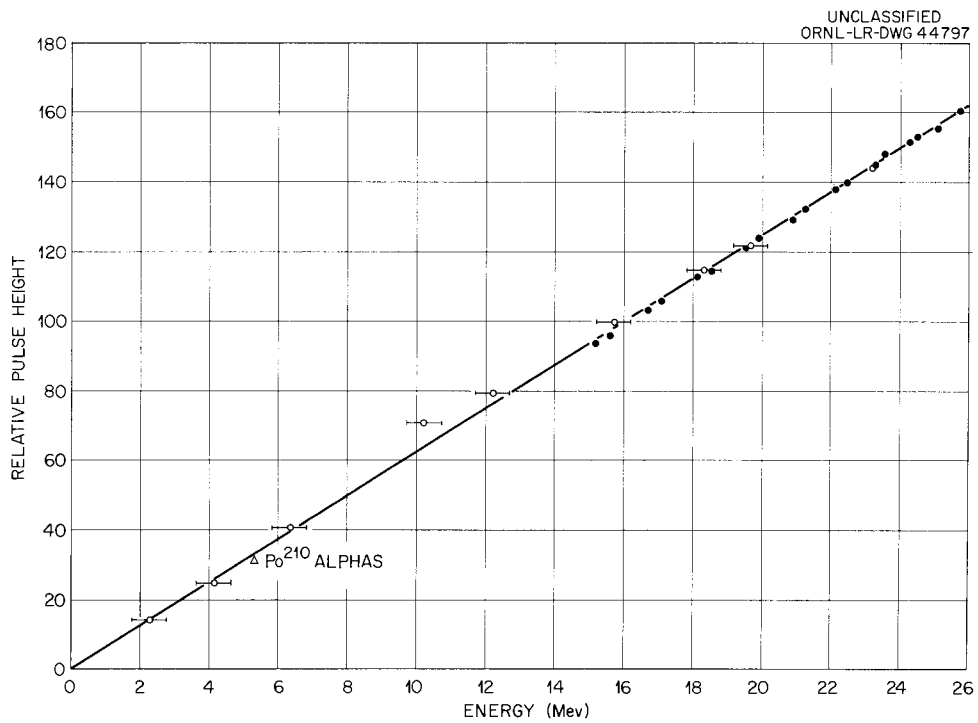

Fig. 1.8. Response of Silicon Surface-Barrier Counter to N^{14} Ions.

The silicon-counter response to N^{14} was also determined by scattering N^{14} at various angles from a thin aluminum absorber. In this way the response from 15 to 25 Mev was measured quite accurately for the silicon counter. These data are shown as solid dots in Fig. 1.8. The ratio of pulse-height response to N^{14} energy for these points has an rms deviation of only 0.5%, which is comparable with the experimental error expected.

It was found that the pulse height as a function of bias for both N^{14} ions and Po^{210} alpha particles, after correction for the variation

[13] H. L. Reynolds, D. W. Scott, and A. Zucker, Phys. Rev. 95, 671 (1956).

in C_b, reached saturation well before the bias value predicted by equating D to the particle range. This suggested that the sensitive depth was greater than D. To study this point further, pulse-height spectra for various bias voltages were obtained for a continuous energy distribution of alpha particles from nuclear reactions produced by N^{14} bombardment of carbon. These spectra show a sharp cutoff above a certain pulse height, corresponding to alphas with a range equal to the sensitive depth. It was found that the sensitive depth is about 15 μ greater than the barrier depth D. This excess sensitive depth is probably due to diffusion into the barrier region of holes produced below it.

Angular Distribution of N^{13} from N^{14} on N^{14}

The angular distribution of N^{13} produced in the $N^{14}(N^{14},N^{13})N^{15}$ reaction has been studied. Earlier investigations[14] have shown that the above reaction proceeds by a transfer mechanism; the N^{13} is produced by a particle (a neutron in this case) being exchanged between the projectile and the target nucleus. The N^{13} is not the result of compound-nucleus formation with the subsequent emission of an appropriate number of light particles. Angular distributions are of interest because they distinguish between reaction mechanisms. Compound-nucleus products tend to be isotropically distributed, while products of transfer reactions should be emitted preferentially at an angle corresponding to the distance between the interacting nuclei at which the particle exchange occurs.

The target used is Cymel resin 248-8, a nitrogen-bearing resin with the following approximate composition: nitrogen 24%, carbon 52%, oxygen 16%, and hydrogen 8%, by weight. Attempts made to produce a thin self-supporting Cymel foil that could withstand the beam were unsuccessful. The experiments described here were done with targets of Cymel foils on 0.12-mg/cm^2 aluminum backing.

The angular distribution is obtained by stopping the radioactive N^{13} with a set of suitably placed catcher foils; annular rings of aluminum are attached to a circular metal disk placed at a known distance

---

[14] H. L. Reynolds and A. Zucker, Phys. Rev. 101, 166 (1956).

from the target. This distance together with the two radii of a particular aluminum ring yield the tangents of the two angles subtended by the ring.

To obtain a meaningful distribution those N^{13} nuclei formed when the residual N^{15} nuclei are left in excited states must be eliminated. At all angles N^{13} energies can be determined from the reaction kinematics for N^{15} nuclei left in either the ground or excited states. Aluminum absorber foils are then placed in front of the catcher foils to halt the undesired and less energetic N^{13} nuclei.

After a 20-min bombardment the foils are detached from the metal disk and the catchers separated from the absorbers. The catchers are then folded and counted directly in Geiger counters. The amount of N^{13} present is found by resolving the decay curves. The activity contributions due to the aluminum backing in each catcher are determined by bombarding the backing with no Cymel but with the same catcher and absorber arrangement.

The angular distribution obtained with 26.5-Mev N^{14} ions is shown in Fig. 1.9. The quantity plotted vs c.m. angle is proportional to

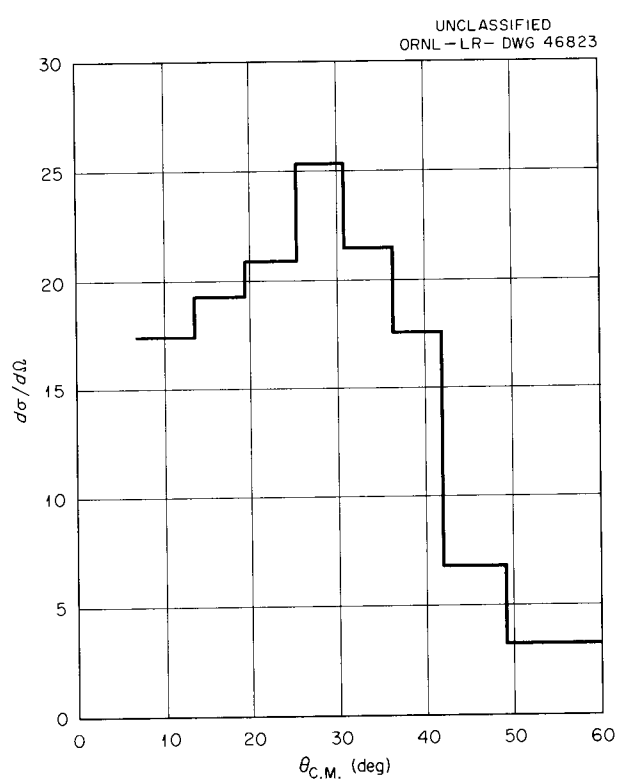

Fig. 1.9. Angular Distribution of N^{13} from the Reaction $N^{14}(N^{14},N^{13})N^{15}$.

$d\sigma/d\Omega$. The figure represents an average of many runs. These are corrected for varying beam intensities. The runs are normalized to one another by arbitrarily making the peak activities (25.5 to 31°) equal for all bombardments. This eliminates differences due to varying target thicknesses.

The results agree with the hypothesis that the reaction proceeds by the transfer of a neutron between the interacting nuclei. Since small angles represent distant collisions, the transfer probability should decrease as the angle becomes small. The distribution does indeed fall off at small angles. Large angles correspond to close collisions. The distribution drops as the angle increases, as expected, because of competition from the compound-nucleus formation probable for close collisions. The peak of the distribution can be related to the distance of closest approach for the two interacting N^{14} nuclei by using a simple classical formula for scattering by an inverse-square repulsive force field:

$$D = [Z_1 Z_2 e^2/2E][1 + \csc(\theta/2)] \quad ;$$

D in turn may be related to r_0 by the expression

$$D = r_0(A_1^{1/3} + A_2^{1/3}) \quad .$$

For $\theta = 28°$,

$$r_0 = (2.75 \pm 0.20) \times 10^{-13} \text{ cm} \quad .$$

This r_0 is large when compared with the value of 1.5×10^{-13} cm found by other methods. Perhaps a more realistic method to obtain the distance of closest approach is to plot $d\sigma/dD$ vs c.m. angle, where $d\sigma/dD$ is proportional to $(d\sigma/d\Omega)\sin^3(\theta/2)$. The distribution then changes and the peak shifts to $\theta = 39°$. For the above formula this θ gives

$$r_0 = (2.12 \pm 0.10) \times 10^{-13} \text{ cm} \quad .$$

The r_0 thus calculated is still rather large. The data indicate, therefore, that transfers occur when the two nuclei are widely separated.

The Exchange Transfer Reaction $Al^{27}(N^{14},Mg^{27})O^{14}$

The thick-target yield was measured for the $Al^{27}(N^{14},Mg^{27})O^{14}$ reaction, which may be described as a simultaneous transfer of a neutron

from one nucleus and a proton from the other. Magnesium-27 was chemically separated, and thick-target yields were measured by absolute gamma counting. A second aluminum foil behind the target was used to determine the amount of Mg^{27} produced by neutrons in the target. The ratio of front to back foil Mg^{27} yield was 1.54:1.00. Thick targets of ZnO were used to measure the yield of $O^{16}(N^{14},3p)Mg^{27}$. The cross section, at 27.6 Mev, was found to be 110 μb. The yield of Mg^{27} in the 10-A oxide layer of the special aluminum foil targets was estimated to be 1.5% of the total yield. The thick-target yield of 9.45-min Mg^{27} in aluminum, measured at 27.6 Mev incident energy, was found to be 13.6×10^{-12} atom per incident nitrogen ion after correction for neutron-induced Mg^{27}. The cross section is estimated to be 2.2 ± 1.0 μb.

The Mg^{27} cannot be produced by the evaporation of light particles as in $Al^{27}(N^{14},3\alpha 2p)Mg^{27}$. The reaction $Al^{27}(N^{14},Mg^{27})pN^{13}$ should be considered, either as a three-body disintegration or as the formation of Al^{28} in an excited state by neutron transfer and its subsequent de-excitation by proton evaporation.[15] In the latter case, the threshold for proton emission by Al^{28} is 9.5 Mev, and the exit barrier for the proton is 2.9 Mev, so that an excitation of about 13 Mev in the Al^{28} is needed for an appreciable yield of Mg^{27}. The "universal curve" for the neutron-transfer cross section[16] may be used to estimate the Mg^{27} cross section. From such an estimation the cross section is less than 0.5 μb. Certainly not more than 10% of these states in Al^{28} de-excite by proton emission, since the threshold for neutron emission is at 7.7 Mev. Thus, probably less than 0.05 μb can be attributed to this mechanism. Nothing is known about three-body disintegration in this type of reaction; however, since the cross section of transfer reactions is strongly Q dependent, it is likely that the exchange transfer is favored over the three-body disintegration. The cross section for the exchange-transfer (neutron in, neutron out) reaction near the barrier, according to the quasi-classical calculations of Goldansky,[17] is estimated to be 1–10 μb.

---

[15] A. Zucker, Phys. Rev. Letters 4(1), 21–22 (1960).

[16] M. L. Halbert et al., Phys. Rev. 106, 251 (1957).

[17] V. I. Goldansky, Nuclear Phys. 9, 551 (1958/1959).

Since proton and neutron single transfer have about the same cross section at low atomic number, one would expect the (p,n) exchange transfer cross-section calculation to predict the same value. In spite of the very approximate nature of the calculation, it is interesting to note that it agrees with the results of this experiment.

Optical Model Calculations

The optical model, which has been useful in the analyses of nucleon-nucleus scattering, has recently been used successfully in the interpretation of entrance channel phenomena initiated by particles heavier than nucleons. Good fits to the data were found for alpha-particle scattering, deuteron scattering, and the scattering of nitrogen ions from nitrogen.

With the advent of the nitrogen-beryllium and nitrogen-carbon scattering experiments, optical-model analysis of these experiments was simultaneously undertaken at ORNL and at UCLA. The purpose was to see if such a simple model could explain reactions between complex nuclei. These tests of the model, implied by the above experiments, are more severe than that proposed by the nitrogen-nitrogen scattering, because of the lack of identity of particles.

The calculations were made for two states. In phase 1 it was assumed that the elastic scattering is mainly caused by the interaction of the two nuclear tails, the absorption was represented by a Gaussian potential shape factor

$$W(r) = W_0 \exp\left[-(r - R_G)^2/b^2\right] ,$$

and the real potential was represented by the Woods-Saxon shape factor

$$V(r) = V_0[1 + \exp\,(r - r_0)/a]^{-1} \quad .$$

Phase 2 used Saxon forms for both real and imaginary wells. The range of parameters searched in our preliminary investigations is shown in Tables 1.1 and 1.2.

The best fit to the nitrogen-beryllium data found in phase 1 is plotted in Fig. 1.10. In general it was not possible (within this range of parameters) to fit the first few measured points without destroying

Table 1.1. Parameters Searched for 27.3-Mev Nitrogen-Beryllium Scattering

	Phase 1			Phase 2		
V, Mev	0	V_0	60	0	V_0	60
W, Mev	1	W_0	20	1	W_0	70
r_0, fermis	1.2	r_0	1.3	1.2	r_0	1.3
a, fermis	0.5	a	0.7	0.5	a	0.75
b, fermis	0.95	b	1.3			
R_G, fermis	5.0	R_G	6.0			

Table 1.2. Parameters Searched for 27.3-, 23.5-, and 21.5-Mev Nitrogen-Carbon Scattering

	Phase 1			Phase 2		
V, Mev	0	V_0	80	0	V_0	80
W, Mev	1	W_0	20	1	W_0	15
r_0, fermis	1.2	r_0	1.3	1.2	r_0	1.3
a, fermis	0.45	a	0.7	0.45	a	0.7
b, fermis	0.95	b	1.4			
R_G, fermis	5.5	R_G	6.5			

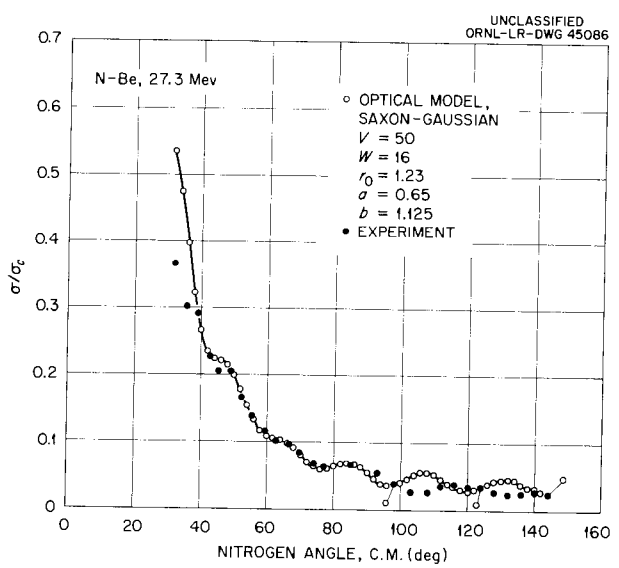

Fig. 1.10. Nitrogen Scattering from Beryllium, Comparison Between Experiment and Theory.

the fit at larger angles, a problem encountered in all experiments analyzed to date. Another common feature found in all cases was the departure of the theoretical prediction from the measured cross section at angles greater than 90–100°. This is most strongly illustrated in Fig. 1.11, where the phase-1 fit to the 27.3-Mev nitrogen-carbon data is

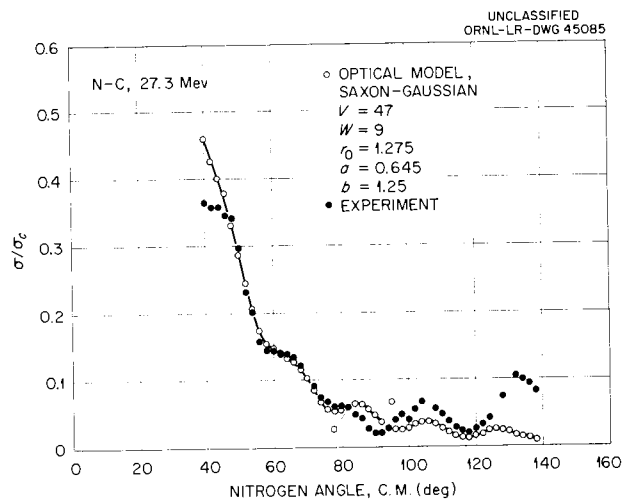

Fig. 1.11. Nitrogen Scattering from Carbon, Comparison Between Experiment and Theory. The real well is represented by the Saxon shape, the imaginary well by a Gaussian.

shown. The reasons for this failure are, perhaps, as follows: (1) The optical model is perforce a two-body description of the many-body scattering problem. For heavy ions this condition appears to be probable for large impact parameters and apparently extends to a large overlap of the nuclear tails. When the two nuclei have appreciably interpenetrated (large scattering angle), this simple description may break down. (2) The interaction used in these calculations is assumed to be spherical; it is doubtful that it would hold in the case of heavy-ion scattering. (3) In the carbon case, there is the possibility of a competing deuteron transfer reaction which may predominate at large angles.

Figure 1.12 is the phase-2 27.3-Mev nitrogen-carbon solution which can be seen to be as good a representation of the data as that found in the phase-1 calculations. It should be emphasized that the potentials found in the phase-1 and -2 results have very little similarity in the important surface region; however, both calculations predict the same reaction cross section and the same partial-wave amplitudes.

As yet we have not found good fits to the 23.5- and 21.5-Mev nitrogen-carbon experiments, nor have we been able to find parameters to fit the nitrogen-beryllium data by using Woods-Saxon wells for both real and imaginary potentials.

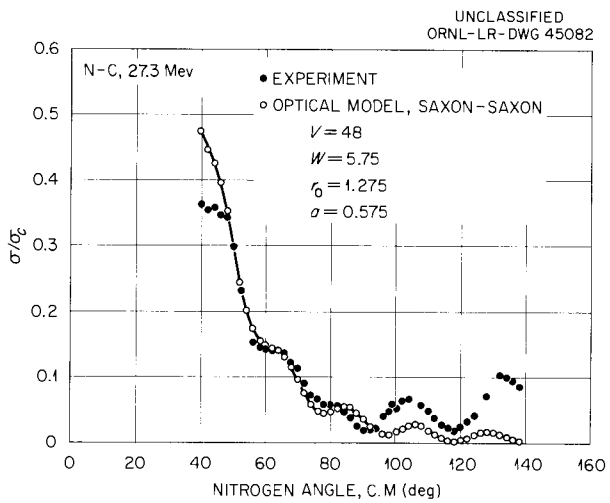

Fig. 1.12. Nitrogen Scattering from Carbon, Comparison Between Experiment and Theory. Saxon potential shapes used for both real and imaginary wells.

2. PHYSICS RESEARCH WITH 22-Mev PROTONS

The emphasis of the work with the ORNL 86-Inch Cyclotron for this period was on the acquisition of precise nuclear data collected in a systematic manner which aids in the interpretation of the data in terms of models of nuclear reaction mechanisms and of nuclear structure. To acquire the data with reasonably efficient use of cyclotron time, major improvements were made in instrumentation. At the same time, the electronic counting equipment was moved from its old location (with a neutron level above tolerance) to a low-radiation area.

The particle-selective counting system, Fig. 2.1, was improved to achieve long-term stability and to permit simultaneous recording of proton, deuteron, triton, and alpha-particle spectra. For this purpose a 400-channel pulse-height analyzer was purchased, and associated circuitry was designed and constructed by the cyclotron group. This includes a new pulse multiplier to replace the Los Alamos circuit,[1] which was found to

[1]W. L. Briscoe, Rev. Sci. Instr. 29, 401 (1958).

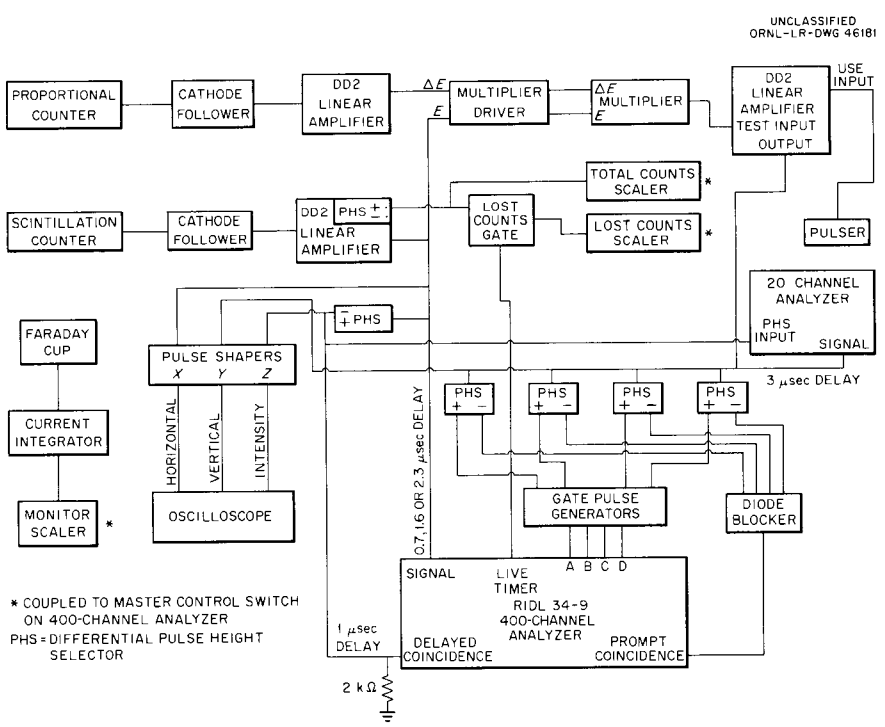

Fig. 2.1. Block Diagram of Particle-Selective Counting System.

be unstable. A data readout system, Fig. 2.2, was also designed and constructed by the group; it punches the data onto IBM cards for use with CONDAC, a data analysis code which has been in use for several years by the cyclotron groups. The punch system is programmed in a manner which avoids the possibility of synchronization errors, which are often a problem in data readout systems.

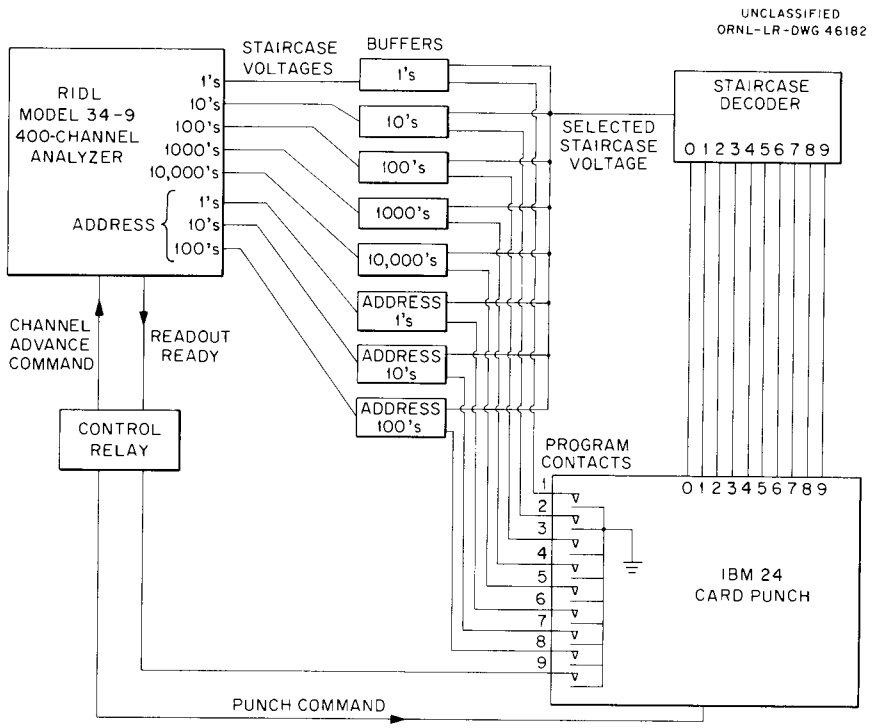

Fig. 2.2. Block Diagram of Card Punch Readout.

A newly constructed time-of-flight system makes use of the natural bunching of the proton beam in the cyclotron. Seven out of each eight pulses are eliminated in a beam sweeping arrangement to allow a longer period of timing. The over-all system gives a time resolution of 2 to 3 mμsec, which is believed to be mostly due to the width of the proton bunches.

(p,d) and (p,t) Reactions

Detailed studies of the energy spectra of deuterons from (p,d) reactions were begun. These spectra show gross structure indicating that

only a few of the known levels in the residual nuclei are strongly excited. Examination of the spectra suggested that the selection rules for these levels involve nuclear shell structure; this suggestion was borne out in more detail by a study of the deuteron spectra from targets of separated zirconium isotopes. A major neutron shell, N = 50, closes at Zr^{90}, and the difference in binding energy between the 50th and 51st neutron is about 5 Mev. This large energy difference makes possible a clear interpretation of the spectra, even with poor energy resolution.

Figure 2.3 shows the deuteron spectra from targets with neutron numbers near 50. An interpretation of the spectra is that (1) the (p,d) reaction proceeds as a pickup of a neutron, (2) the neutrons in the target should be regarded as being in shell-model bound states, and (3) the probability is small that any nucleon other than the picked-up neutron changes its shell-model state. The several peaks in the spectra are thus to be assigned to the picking up of neutrons from the various shell-model states.

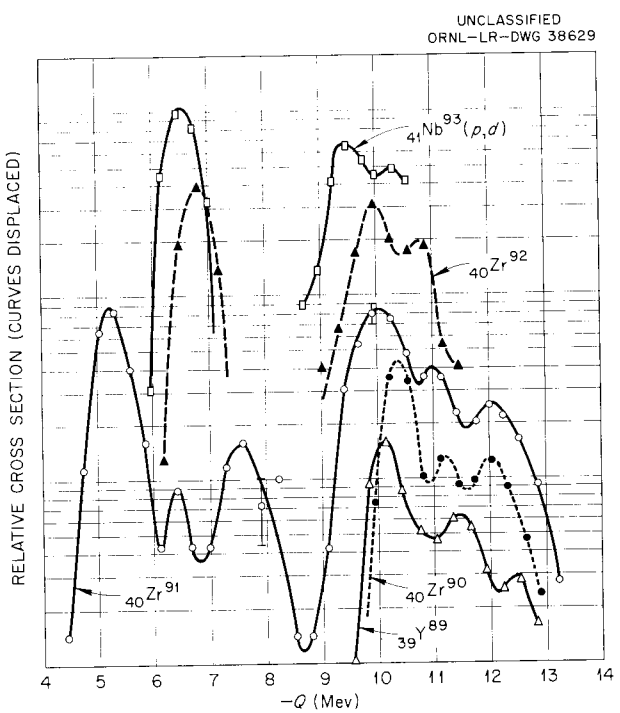

Fig. 2.3. Spectra of Deuterons from Proton Bombardment of Separated Zirconium Isotopes, Yttrium, and Niobium. A peak appears near Q = −8 Mev for all these targets, but has been omitted in this drawing except for the Zr^{91} target. The peak is apparently due to nitrogen on the target.

Angular distributions of the peaks from Zr^{91} and Zr^{92} leading to the ground states of Zr^{90} and Zr^{91}, respectively (Fig. 2.4), agree with the expected shell assignments of $2d_{5/2}$ for the 51st and 52nd neutrons. The difference in Q values for these two cases also gives reasonable pairing energy, about 1.5 Mev, for the $2d_{5/2}$ shell.

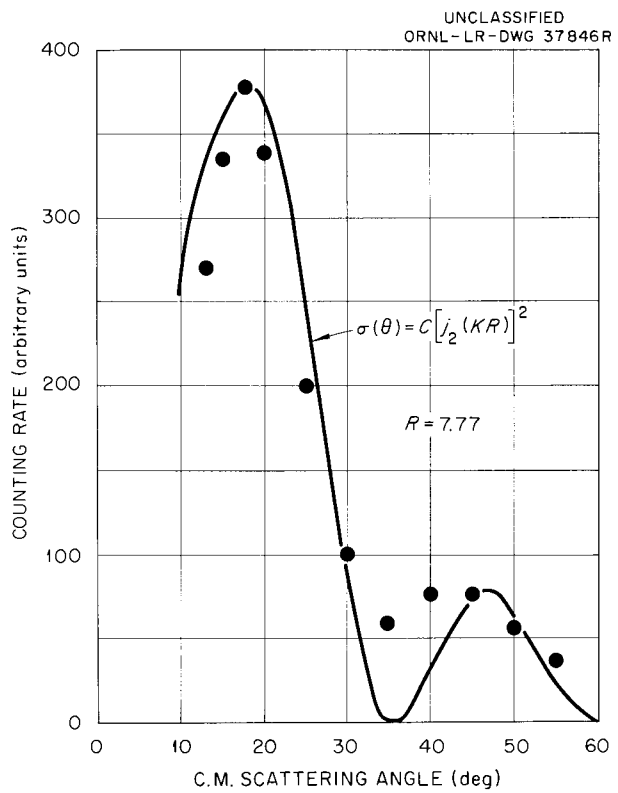

Fig. 2.4. Angular Distribution of the Deuteron Group from $Zr^{91}(p,d)Zr^{90}$ to the Ground State of Zr^{90}.

Triton spectra from the targets near N = 50 suggest that the (p,t) reaction proceeds as a double neutron pickup, and the same type of selection rules apply to (p,t) as to (p,d). When two neutrons in the same shell are picked up, as in the case of $Zr^{92}(p,t)Zr^{90}$ to the ground state, the peak in the spectrum is strong. When the two neutrons come from different shells, as in $Zr^{91}(p,t)Zr^{89}$ to the ground state, the peak is an order of magnitude weaker than the peak apparently due to $Zr^{91}(p,t)Zr^{89}$ to an excited state leaving two holes in the $1g_{9/2}$ shell.

Since (p,t) and (p,d) data are easiest to interpret if they are available for sequences of neighboring isotopes, it was decided to study iron

isotopes, for which targets could be obtained. The $Fe^{56}(p,d)Fe^{55}$ spectrum in Fig. 2.5 has a group with an $\ell = 1$ angular distribution at Q = −8.9 Mev and an $\ell = 3$ group at Q = −10.3 Mev (Fig. 2.6). In $Fe^{57}(p,d)Fe^{56}$ these

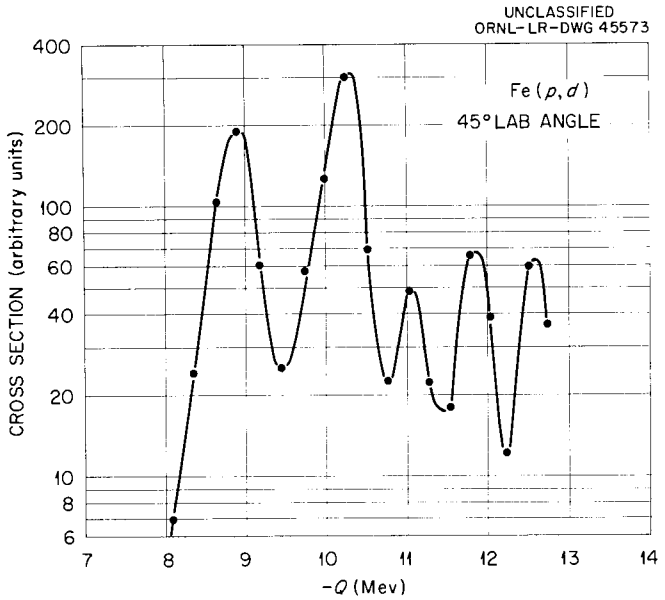

Fig. 2.5. The (p,d) Spectrum from Natural Iron (91.6% Fe^{56}).

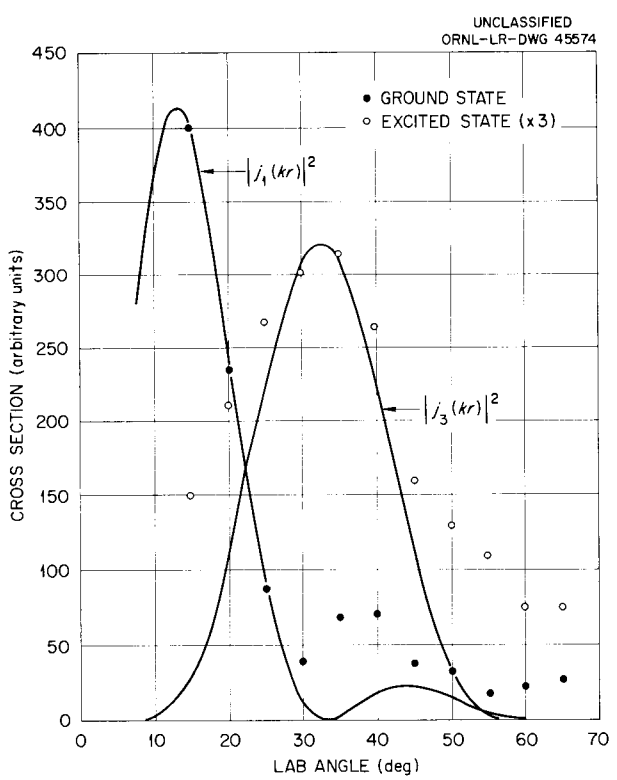

Fig. 2.6. Angular Distribution for Q = −10.3-Mev Groups from $Fe^{56}(p,d)Fe^{55}$.

groups (Fig. 2.7) occur also with an apparent doubling, probably due to coupling of the hole with the odd particle. In addition, new $\ell = 1$ groups appear at Q = −5.4 and −6.2, suggesting a new shell at N = 31. This should not occur for the simple shell model based on a spherically symmetric potential, but may occur in a nonspherical potential. It appears that the unified model may fit the data. An Fe^{58} target has been obtained, and the study is being continued.

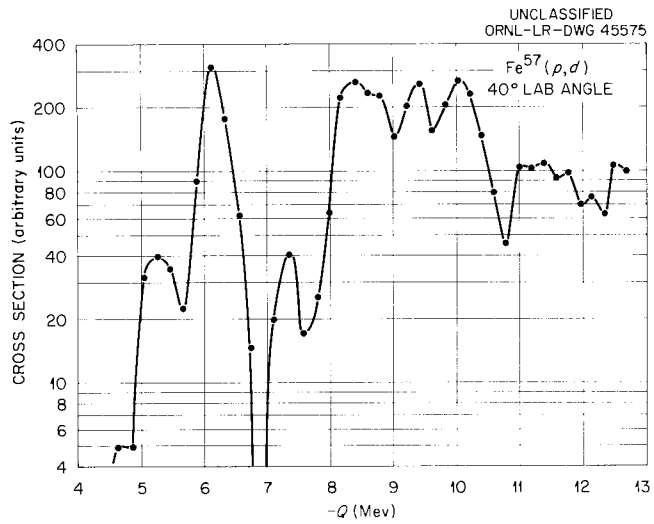

Fig. 2.7. The (p,d) Spectrum from an Enriched Fe^{57} Target.

Anomalous Scattering

It has been reported[2] that the selection rules for inelastic proton scattering favored excitation of certain collective states, with the suggestion that an octupole vibrational state would account for "anomalous inelastic scattering." Inasmuch as the (p,d) and (p,t) spectra seem to be well described by single-particle selection rules, it seemed attractive to re-examine "anomalous scattering" in comparison with the single-particle selection rules. Certain cases seem to fit the shell picture.[3] Similarities in (p,d) and (p,p′) spectra such as are shown for Fe^{56} in Fig. 2.8 occur also for Fe^{57} and Co^{59}.

---

[2]B. L. Cohen and A. G. Rubin, Phys. Rev. 111, 1568 (1958).
[3]C. D. Goodman, Phys. Rev. Letters 3, 230 (1959).

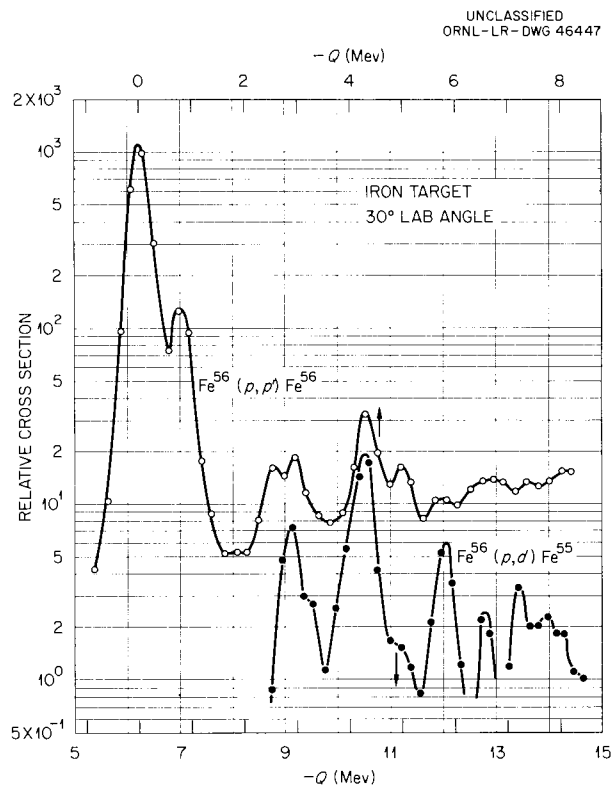

Fig. 2.8. Comparison of (p,p′) and (p,d) Spectra from a Natural Iron Target (91.6% Fe^{56}). The energy scales are placed so that a (p,d) peak due to removal of a neutron from a particular bound state will coincide with the (p,p′) peak due to promotion of a neutron from the same bound state to a state with 8.4-Mev binding energy.

(p,α) Reactions

The (p,α) spectra from rhodium and nickel were measured at several proton bombarding energies between 11 and 23 Mev. The maxima in the spectra do not shift in energy as would be predicted by the barrier penetrabilities and the compound nucleus theory given by Blatt and Weisskopf.[4] Earlier work[5] showed that the Coulomb barrier for (p,α) reactions at 23 Mev was lower than that given by Blatt and Weisskopf. The new data are consistent with the assumption that the barrier effectively becomes lower for excited nuclei, perhaps due to an increased diffuseness of the nuclear potential.

---

[4]J. M. Blatt and V. F. Weisskopf, Theoretical Nuclear Physics, Wiley, New York, 1952.

[5]C. B. Fulmer and B. L. Cohen, Phys. Rev. 112, 1672 (1958).

Elastic Scattering from Isobars

Elastic-scattering angular distributions from Ni^{64} and Zn^{64} and from Cd^{116} and Sn^{116}, and various other targets, were measured in a search for a possible dependence of the nuclear potential on the nuclear symmetry parameter (N-Z)/A. The data taken with 22-Mev protons show no appreciable differences with respect to the symmetry parameter. The data taken with 9.5-Mev protons, however, show changes in the positions of the maxima and minima consistent with a dependence of the real nuclear potential well depth on (N-Z)/A.

Nuclear Levels in Yb^{169}

Excited nuclear levels in Yb^{169} were studied with electron-capturing Lu^{169} ($T_{1/2}$ = 1.5 days) produced in the 22-Mev proton cyclotron. By use of high-intensity, "mass-free" activities electroplated onto fine wires, it has been possible to observe over 60 transitions up to 1.6 Mev energy in the internal-conversion spectrum.[6] A partial decay scheme, Fig. 2.9, is proposed on the basis of this data.

The criteria employed in the construction of the scheme were (1) energy fits of precisely measured transitions; (2) multipole assignments[7] based on K/L ratios and L- and M-subshell ratios in the range 20 to 350 kev; (3) transition intensities, measured or deduced; and (4) internal consistency of moments of inertia (i) and log (ft) estimates. Mottelson and Nilsson[8] have made an analysis of intrinsic states for odd-A nuclei in the region of Yb^{169}. They have described the intrinsic levels in terms of the asymptotic quantum numbers: K, the symmetry-axis component of nuclear angular momentum; π, the parity; N, the principal oscillator quantum number; n_z, the symmetry-axis oscillator quantum number; and Λ, the symmetry-axis component of orbital angular momentum. The notation used here is $K\pi[Nn_z\Lambda]$.

---

[6]B. Harmatz, T. H. Handley, and J. W. Mihelich, Phys. Rev. 114, 1082 (1959).

[7]M. E. Rose, Internal Conversion Coefficients, North-Holland, Amsterdam, 1958.

[8]B. R. Mottelson and S. G. Nilsson, Kgl. Danske Videnskab. Selskab, Mat-fys. Skrifter 1(8), 1 (1959).

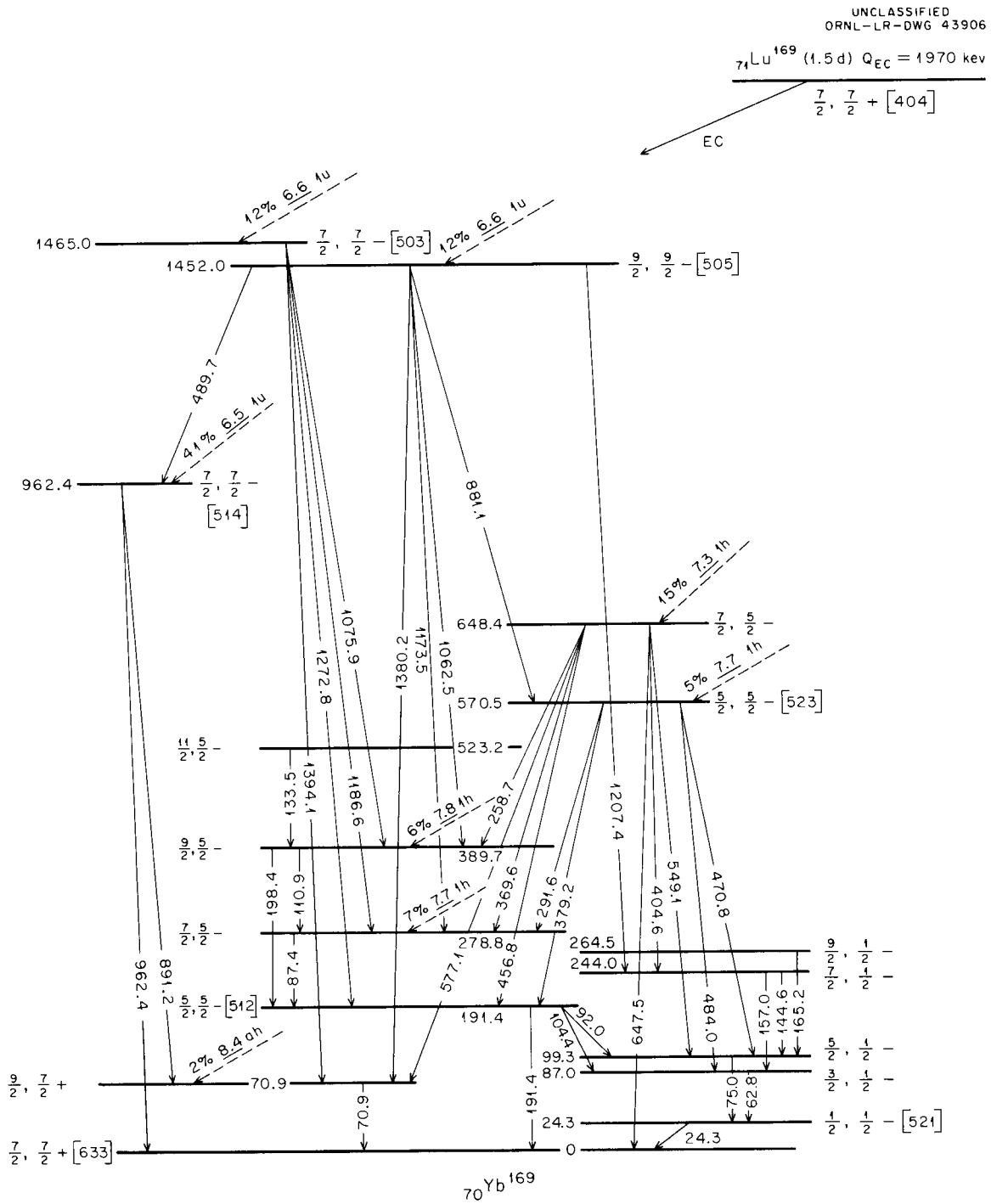

Fig. 2.9. Levels in Yb^{169} Populated by Electron-Capture Decay of Lu^{169}. The convention employed in the designation of intrinsic states is I, $K\pi[Nn_z\Lambda]$. Those levels following a rotational sequence are aligned vertically. All energy values are given in kev.

Transitions de-exciting the proposed states in Yb^{169} are listed in Table 2.1. An isomeric state is predicted for Yb^{169}; isomeric states arise from similar configurations of 99 neutrons in Dy^{165} and Er^{167}. The conversion spectrum shows a 24.2-kev transition of probable E3 multipolarity which may depopulate the (1/2- [521]) state to ground (7/2+ [633]). A 20- to 30-kev radiation of 50-sec half-life has been previously observed[9] in ytterbium, mass unknown.

The decay scheme of Yb^{169} shows an anomalous (K = 1/2) rotational band based at 24 kev, a well-developed band based on a (5/2- [512]) state at 191 kev, and an intrinsic (5/2- [523]) state at 570 kev with a rotational excitation (I = 7/2) at 648 kev. The rotational parameters, $3\hbar^2/i$, for these bands are 70, 75, and 67 kev respectively. For the relevant rotational parameters, one obtains a predicted value[6] of 265.4 kev for the proposed state at 264.5 kev (I = 9/2) and a predicted value of 523.1 kev for the proposed 523.2-kev (I = 11/2) state. The postulation of a 70.9-kev rotational state (I = 9/2) is consistent with the high moment of inertia expected[10] for the ground-state orbital (7/2+ [633]).

An intense transition of 962.5 kev energy is shown to de-excite a proposed 962-kev (7/2- [514]) state to ground. This radiation is interpreted as of E1 character, based on a rough comparison of photon and conversion-electron intensities. Two close-lying levels at 1465 and 1452 kev are tentatively designated as the expected[8] (7/2- [503]) and (9/2- [505]) states respectively.

Electron-capture branches to various levels are designated in Fig. 2.9 by dashed arrows, with relative intensities given in per cent and log (ft) estimates[11] underlined. The classification of these branches according to selection rules[12] follows the notation: allowed (a), first forbidden (1), hindered (h), and unhindered (u). For a disintegration energy (Q_{EC}) of 2 Mev, as calculated from a semiempirical mass formula,[13] the most likely classification of the ground state of Lu^{169} is (7/2+ [404]).

---

[9] E. der Mateosian and M. Goldhaber, Phys. Rev. 76, 187A (1949).

[10] O. Prior, Arkiv Fysik 14(28), 451 (1958).

[11] S. A. Mozkowski, Phys. Rev. 82, 35 (1951).

[12] G. Alaga, Phys. Rev. 100, 432 (1955); Nuclear Phys. 4, 625 (1957).

[13] A. G. W. Cameron, A Revised Semi-Empirical Atomic Mass Formula, AECL-433 (1957).

Table 2.1. Intensity and Multipolarity Assigned to Transitions Depopulating Levels Shown in Decay Scheme of Yb^{169}

See also Fig. 2.9

Proposed Excited States		De-Exciting Transitions (kev)	Multipole[a] Assignment	Deduced Relative Intensities[b]	
(I,Kπ)	(kev)			$N_\gamma + N_{ce}$	N_γ
(7/2, 7/2+)	0				
(9/2, 7/2+)	70.85	70.85	M1 + E2	6480[c]	680
(1/2, 1/2−)	24.3	24.3	E3	> 1700	0
(3/2, 1/2−)	87.0	62.75	M1 + E2	3630[c]	240
(5/2, 1/2−)	99.3	75.0	E2	1080	110
(7/2, 1/2−)	244.0	144.6	M1 + E2	310	140
		157.0	E2	610	360
(9/2, 1/2−)	264.5	165.2	E2	800	480
(5/2, 5/2−)	191.4	92.0	(M1)	510	90
		104.4	(M1)	470	112
		191.4	E1	5820	5470
(7/2, 5/2−)	278.8	87.4	M1 + E2	5200[c]	850
(9/2, 5/2−)	389.7	110.9	M1 + E2	2060	600
		198.4	E2	230	182
(11/2, 5/2−)	523.2	133.5	M1	155	62
(5/2, 5/2−)	570.5	291.6	(M1)	195	165
		379.2	(M1)	835	770
		470.8	(M1)	205	195
		484.0	(M1)	105	100
(7/2, 5/2−)	648.4	258.7	(M1)	165	135
		369.6	(M1)	350	320
		404.6	(M1)	70	67
		456.8	(M1)	265	253
		549.1	(M1)	130	127
		577.1	(E1)	1745	1737
		647.5	(E1)	435	433

Table 2.1 (continued)

Proposed Excited States		De-Exciting Transitions (kev)	Multipole[a] Assignment	Deduced Relative Intensities[b]	
(I,Kπ)	(kev)			$N_\gamma + N_{ce}$	N_γ
(7/2, 7/2−)	962.4	891.2	(E1)	1743	1740
		962.4	(E1)	7010	7000
(9/2, 9/2−)	1452.0	489.7	(M1)	48	45
		881.1	(E2)	241	240
		1062.5	(M1)	530	527
		1173.5	(M1)	293	292
		1207.4	(M1)	132	132
		1380.2	(E1)	1250	1249
(7/2, 7/2−)	1465.0	1075.9	(M1)	257	255
		1186.6	(M1)	759	750
		1272.8	(M1)	180	179
		1394.1	(E1)	1270	1269

[a]Multipolarities are assigned either from conversion electron data, as a member of a rotational band, or from consistency with angular momentum selection rules; latter assignments are in parentheses and are shown unmixed since we have no way of estimating mixing ratios.

[b]Estimates of photon intensity are based on electron data and theoretical conversion coefficients. Total transition intensity is listed in column $N_\gamma + N_{ce}$.

[c]Photon and K-electron intensities are deduced from L-electron data.

Applied Physics

The quantities of radioisotopes produced in service irradiations for commercial concerns who handle the processing and distribution have continued to rise. There were, however, no new additions to the list. In this period some 22 runs were made for As^{74}, with a total production of 2786 mc. Another isotope, Bi^{206}, also exceeded the curie mark with 1242 mc produced in eight runs. Full yield data for these commercially produced isotopes are summarized in Table 2.2.

Table 2.2. Summary of Yield Data of Isotopes Produced by Cyclotron Bombardment for Commercial Distribution

Isotope	Reaction	Number of Runs	Amount Produced (mc)	Production Rate (mc/hr)	Production Rate (mc/ma-hr)	Target	Max Average Current (ma)	Max Run Length (hr)
Be^{7}	$Li^{7}(p,n)$	2	314	39	182	Li cast on Cu	225	4
V^{48}	$Ti^{48}(p,n)$	1	42	21	105	TiO_2 in Al capsule	200	2
Mn^{52}	$Cr^{52}(p,n)$	2	84	42	210	Cr powder in Al capsule	200	1
Mn^{54}	$Cr^{54}(p,n)$	1	387	19	11	Enriched Cr^{54}-plated Cu	1730	20
Fe^{55}	$Mn^{55}(p,n)$	1	71	11	12	Mn plated on Al	950	6
Co^{57}	$Ni^{58}(p,2n)$ + (p,pn) + $(p,2p)$	3	812	33	25	High-purity Ni plated on Cu	1570	14
Ge^{68}	$Ga^{69}(p,2n)$	6	20	1	4	Ga cast on Cu	680	4
As^{74}	$Ge^{74}(p,n)$	22	2786	15	758	Ge powder in Al capsule	190	12
Sr^{85}	$Rb^{85}(p,n)$	4	162	4	22	RbCl in vented Ni capsule	190	10
Y^{88}	$Sr^{88}(p,n)$	3	39	4	18	SrO in Al capsule	190	4
Cd^{109}	$Ag^{109}(p,n)$	1	52	9	3	Solid Ag	2550	6
Bi^{206}	$Pb^{206}(p,n)$ + $Pb^{207}(p,2n)$	8	1242	33	167	Pb plug in Al capsule	200	10
Zn^{65}	$Cu^{65}(p,n)$	1	86	22	9	Solid Cu	2410	4

Other radioisotopes, produced for research programs at other laboratories, for which full yield data are not available were F^{18}, Co^{56}, As^{73}, Y^{87}, I^{124}, Ce^{137}, Ce^{139}, Pm^{148}, Eu^{149}, Dy^{159}, and Hg^{197}. The isotopes Y^{88}, Tc^{95m}, and Pm^{146} were made for other divisions of the Laboratory.

Altogether, 142 internal bombardments were attempted and 122 of these were successfully completed. In addition, there were 55 external beam irradiations for the experimental program of the Applied Physics Group. Six of the unsuccessful runs were deliberate failures, ones in which the current was increased until the target failed. Most of the others were on development runs.

Several runs were made in a study of the effect of the first-harmonic beam-centering coils on the energy and maximum current possible. For most cases the targets are power-limited. It was found that the yields (per hour) for (p,n) isotopes increase if the energy is lowered and the current increased so as to keep the target power constant. On the other hand, for the maximum production of isotopes by the (p,2n) reaction the machine must be run at the maximum energy available, consistent with steady operation of the cyclotron. From the results of the study, the optimum operating conditions were determined for these two cases.

During this period another target of chromium enriched in Cr^{54} was bombarded for the production of Mn^{54}. The target contained 1/3 g of enriched chromium and was run for 20 hr at an average current of 1730 μa. Other high-current runs were as follows: a 4-hr run at 2410 μa average on a copper target for Zn^{65} production and a 6-hr run at 2550 μa on a solid silver target for the production of Cd^{109}.

Further bombardments of CaF_2 targets were made. The fluoride does evaporate under bombardment, but 60% recovery is possible even at 400 μa on the target. The yield obtained for natural calcium is 0.3 mc/ma-hr on a target from which 50 mg of calcium was recovered. A flat copper target with grooves milled over a 4-in. area and with calcium oxide placed in these grooves as an alcohol paste was operated at 200 μa for 3 hr. The evaporation problems with this target have not been studied.

A target of titanium metal powder was bombarded with neutrons produced in a thick beryllium target in the external proton beam. The neutron spectrum from such a target is unknown, but it is thought to peak

at about 8 Mev and to extend up to 20 Mev. The target, 0.25 lb of titanium metal powder, was placed directly behind the beryllium. The neutron flux is estimated to have been 3×10^{10} neutrons cm^{-2} sec^{-1}; the bombardment lasted 12 hr. The yields obtained are 0.65 μc of Ca^{47} and 2.0 μc of Ca^{45}. This indicates that the effective cross section on Ti^{48} is six times that of Ti^{50}.

For the proton bombardment of gallium the metal is cast directly into a 0.030-in. depression in the copper target plate. Since the plate is level during bombardment, the melted gallium does not pour out of the depression. These targets can be run successfully at 400 μa with no great loss of target material or deterioration of cyclotron operation. The yield of Ge^{68} is 1.4 mc/hr. This 280-day isotope is of interest because it has a 67-min daughter that can easily be separated from it. This gives a convenient portable source ("cow") of short-lived activity for a number of tracer applications.

Interest in Co^{57} stems from its use in the determination of the gravitational red shift of gamma rays. One target of high-purity nickel was bombarded for 14 hr at an average current of 1730 μa and produced 610 mc. There is also interest in this isotope as a replacement for Co^{60} in the labeling of vitamin B_{12}.

Further work was done on soft-soldered targets. Two targets were made by soft-soldering a sheet of copper 1/16 in. thick into a depression 0.050 in. deep on a copper target plate. These targets were run to failure. The failure currents were 2070 and 2100 μa for the two targets. Soft-soldered targets of platinum were since run at 785 μa and of iron at 1000 μa.

A vanadium target, a 2 × 1-5/8 × 0.030 in. sheet, nickel-plated on one side and then soft-soldered to a copper target plate, was operated at 500 μa for 2 hr. The Cr^{51} yield was 226 μc/μa-hr. A thick target of vanadium was also run in the external beam; a yield of 595 μc/μa-hr was obtained. The difference can easily be explained on the basis of the small size of the internal target; it was smaller than the beam.

The isotope Ce^{137} free of Ce^{139} was made by bombarding a 0.003-in. layer of lanthanum vacuum-evaporated on the outside of an aluminum tube. The evaporation was performed at Berkeley. The tube was run in the capsule

header. This technique exposes the target material to only the highest-energy protons.

Two test targets of rhodium sheet 3-1/2 × 1-5/8 × 0.003 in. thick were bombarded for the production of Pd^{103}. One was soft-soldered to a copper target plate and the other was silver-soldered. The soft-soldered target melted at 900 μa and became inoperable. With the silver-soldered target, satisfactory operation was achieved at 1500 μa; the yield was 97 mc/ma-hr. As a check, a thick rhodium target was irradiated in the external beam; the yield was 219 mc/ma-hr.

A preliminary study of the decay of In^{117m} was made with $In^{117,117m}$ grown in from Cd^{117} produced by reactor neutron irradiation of enriched Cd^{116}. The half-life of In^{117} was found to be 40 ± 3 min; this is at variance with reported values of 66 and 72 min.

The following excitation functions were measured: $Sn^{120}(p,n)Sb^{120,120m}$; $Sb^{121}(p,pn)Sb^{120,120m}$; $Rh^{103}(p,n)Pd^{103}$; $Ge^{70}(p,n)As^{70}$; $Ge^{72}(p,2n)As^{71}$; $Ge^{74}(p,n)As^{74}$; $Sn^{120}(p,\alpha)In^{117,117m}$; $[Ge^{70}(p,pn) + Ge^{70}(p,2n)]Ge^{69}$; $[Ge^{74}(p,pn) + Ge^{73}(p,n)]As^{73}$; and $[Ge^{72}(p,n) + Ge^{73}(p,2n)]As^{72}$. The results will be published in the open literature.

3. CYCLOTRON OPERATION

Both the 86-in. 22-Mev proton cyclotron and the 63-in. 27-Mev nitrogen cyclotron have operated routinely; no major shutdowns were required. The in-service time of the heavy-particle machine was markedly improved by increased protection of the dee-stem insulators.

Detailed measurements of variations of the beam current in the 86-Inch Cyclotron demonstrate that the beam intensity is very sensitive to minor fluctuations in the power supply to the oscillator. A regulator is being developed to maintain the plate voltage constant to within 0.1%. These beam improvement efforts on the 86-Inch Cyclotron also contribute toward the development of components for the Isochronous Cyclotron, now under construction.

Time Dependence of the Beam in the 86-Inch Cyclotron

In the preliminary stages of setting up a time-of-flight system for measuring neutron spectra from proton reactions, a study was made of the time dependence of the beam in the 86-Inch Cyclotron. The expected short bursts of protons were found on each cycle of the 13.4-Mc/sec accelerating voltage. In addition to this rf structure, however, there is a 360-cps modulation of the beam pulses and a complicated pattern built upon that.

The accompanying photographs, Fig. 3.1, show the beam pattern obtained by displaying the output of a fast plastic scintillation counter on an oscilloscope. The counter was exposed to the beam scattered from an aluminum foil. The 60-cps line voltage and the envelope of the 13.4-Mc/sec accelerating voltage are shown on the same time scale for reference. Apparently the beam intensity is critically dependent on the accelerating voltage but is not a monotonic function of that voltage.

The evidence shown in Fig. 3.1 does not in itself prove that there is a relationship between accelerating voltage and beam current; for example, the 360-cycle modulation of the beam could possibly be introduced through the ion source. It would be synchronized with the modulation of the accelerating voltage, because both power supplies operate from the same power line. To show that the beam current is truly a function of accelerating voltage, an oscilloscope was set up to display beam current vs accelerating voltage (see Fig. 3.2). The ripple in voltage provides

UNCLASSIFIED
PHOTO 47421

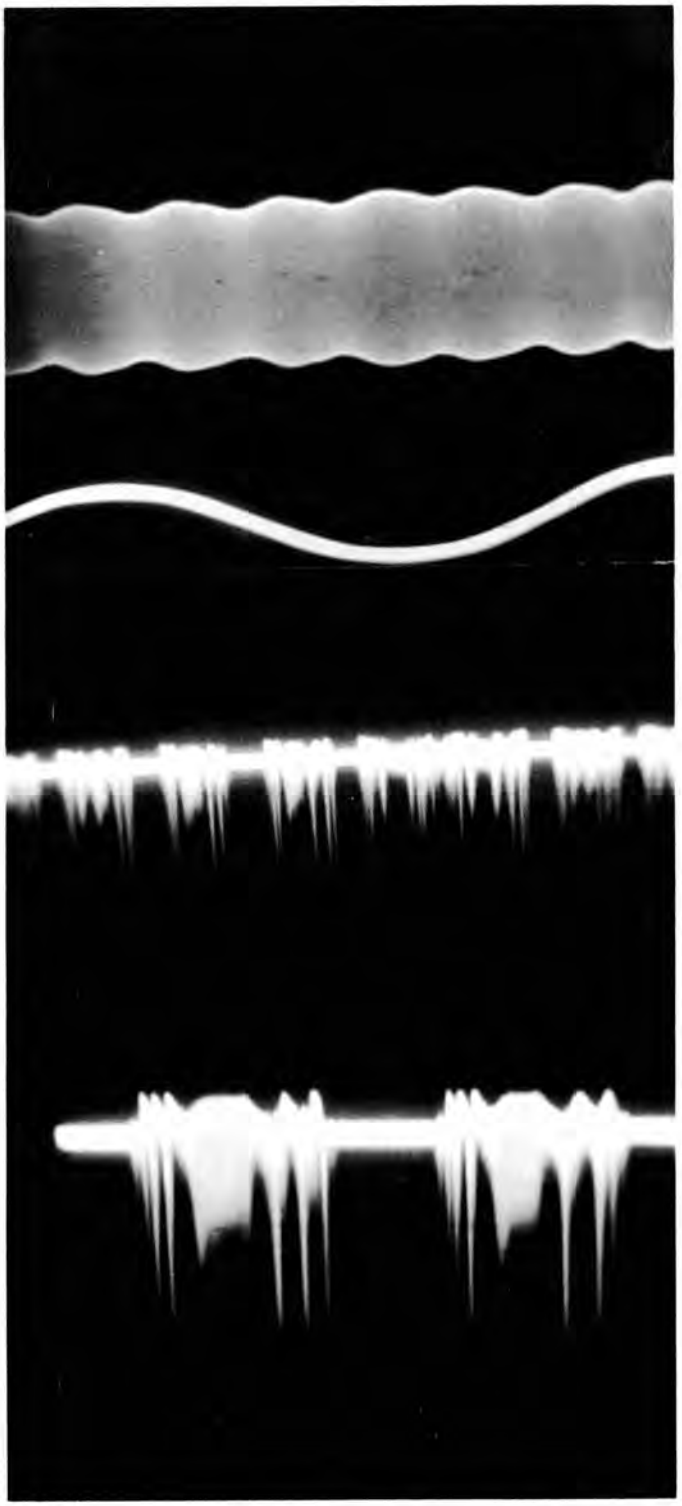

Fig. 3.1. Oscilloscope Patterns of 86-Inch Cyclotron Beam. Top pattern: envelope of the rf accelerating voltage. Second pattern: 60-cps line voltage to show time scale. Third pattern: cyclotron beam intensity. Fourth pattern: cyclotron beam intensity displayed on faster oscilloscope sweep.

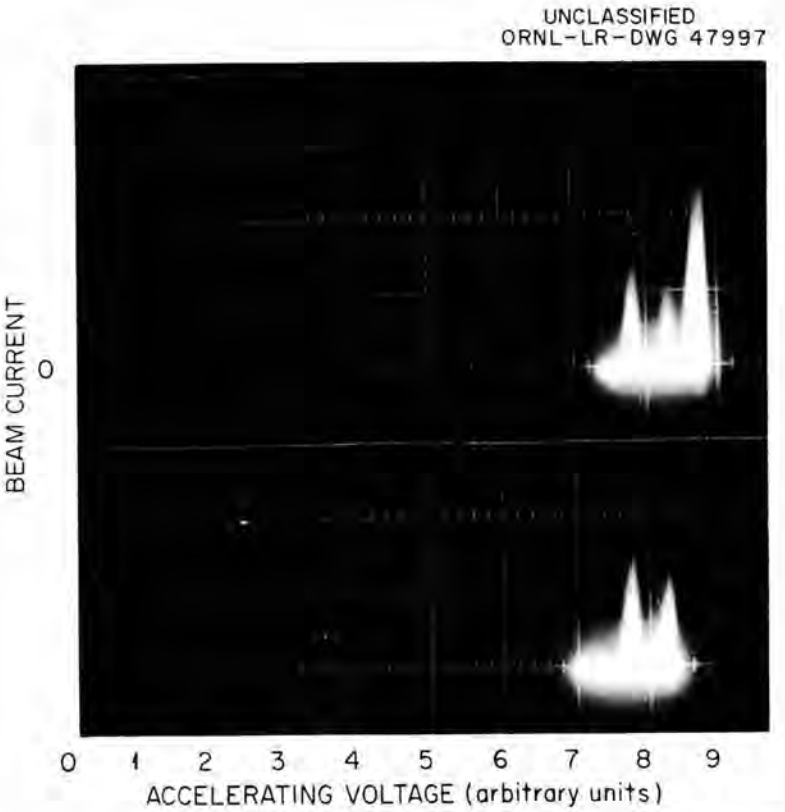

Fig. 3.2. Beam Current vs Accelerating Voltage in 86-Inch Cyclotron. The upper trace is at normal rf power, while the lower trace is at reduced power. The ripple in accelerating voltage provides the horizontal sweep. The beam peaks remain at the same voltage values and do not follow the phase of the ripple.

the horizontal sweep. The amplitude of the accelerating voltage as a function of time was then changed by decreasing the power to the oscillator. The beam peaks remain at the same voltage values and do not follow the phase of the ripple as they might be expected to do if they were generated by the effect of the ripple on the ion source.

A plausible explanation of the data is that as the accelerating voltage is increased and the energy gain per turn increases, the turns structure moves radially outward. The beam is maximum when a turn reaches the septum in optimum position for extraction. As the turns structure moves out, or in, from this position, much of the beam strikes the septum and is not extracted. Since the turns structure moves in time, it is not possible to keep the septum and deflection channel parameters continuously optimized.

The pictures suggest that if the rf voltage could be held constant, the extracted beam could be increased perhaps tenfold. The ratio of average to peak beam would be greatly improved; this would also be quite beneficial to counting experiments. The beam intercepted by the septum would be reduced so that the septum life would be increased. Also, the increased brightness of the beam would permit better energy resolution in external beam experiments and probably a cleaner pulse separation in the time-of-flight system.

The oscilloscope pictures also indicate that a 1% change in the accelerating voltage makes a significant change in the extracted beam. The 360-cps ripple is about 15% of the peak accelerating voltage.

The 86-Inch Cyclotron Dee Voltage Regulation

As described above, it has been determined that variations in the cyclotron dee voltage have a very detrimental effect on the extracted beam of the cyclotron. If the dee voltage could be maintained relatively constant, the external beam would be increased perhaps tenfold. Regulation of the dee voltage should also result in increased septum life, since the amount of beam striking the septum would be greatly reduced.

The design of a regulator for the oscillator plate voltage supply is essentially complete. This regulator should maintain the plate voltage constant to within ±0.1%. A second loop may be added later which will feed back a signal proportional to the variation of the rf dee voltage into the plate voltage regulator. This second loop would tend to remove any variations in dee voltage produced by vibration and thermal effects. A block diagram of the regulator is shown in Fig. 3.3. Federal type 6921 triodes (three in parallel) will be employed in the system. The grid voltage of the 6921 triodes will be supplied by a two-stage dc amplifier having a gain of about 8000. The dc voltage drop across the series regulator tubes will be maintained at approx 3.5 kv by a slow regulator loop controlling the ac input to the high-voltage rectifiers.

A fast protective system will also be installed on the cyclotron along with the regulator and will consist of crowbars and a vacuum-switch circuit breaker. This system will protect the regulator and the oscillator tubes from damage due to sparking in the cyclotron.

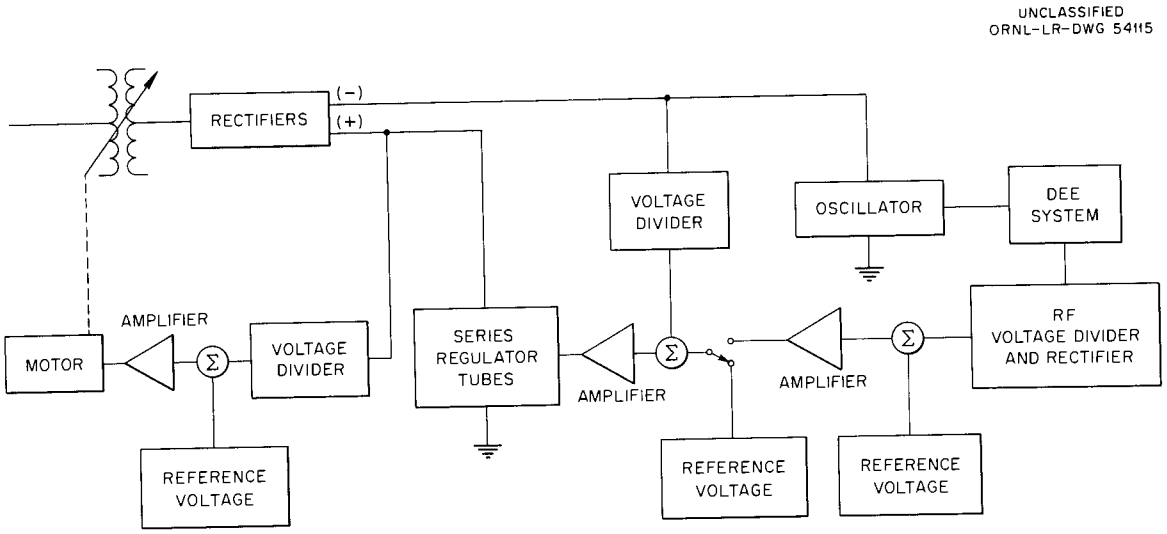

Fig. 3.3. Block Diagram of the Dee Voltage Regulator for 86-Inch Cyclotron.

Operation of the 86-Inch Cyclotron

Operation for the year was quite varied in the number and types of bombardments made, as is indicated below:

Type of Bombardment	Runs
Physics, deflected beam	138
Physics, internal beam	51
Experimental, deflected beam	50
Experimental, internal beam	36
Isotope production, deflected beam	5
Isotope production, internal beam	67
Total	347

The operation schedule varied somewhat; the average was 76.3 hr per week. A breakdown of the scheduled operation time is as follows:

	Per Cent
Normal Operational Conditions	
Bakeout	8.1
Beam improvement	0.7
Beam on target	61.6
Source changes and source adjustments	1.6
Target installation	3.9
Operation Interruptions	
Vacuum troubles	7.3
Electrical troubles	2.3
Target and dolly troubles	1.2
Radiation hazard	0.6
Major shutdown (pulling dees and/or liner for repairs)	0.4
Source and vacuum-lock troubles	0.2
Utilities troubles	0.1
Miscellaneous	12.0
	100.0

Most of the major shutdowns (removing the dees and/or liner) were due to water leaks in the septum or the dee and to breakage of the dee-support insulator. These mechanical failures of components were attributable primarily to radiation damage.

Some typical operating conditions for the 86-Inch Cyclotron are as follows:

Operation frequency	13.241 Mc/sec
Magnetic field	9000 gauss
Dee-to-dee potential	400–500 kv
Energy	20–23 Mev
Gas (hydrogen) flow rate	2–3 cc/min
Plate voltage, internal beam	17.2 kv
Plate voltage, external beam	18.7 kv

Plate current, internal beam	12.0 amp
Plate current, external beam	14.0 amp
Vacuum	6×10^{-6} mm Hg
Arc conditions	
Filament current	350–450 amp
Arc voltage	165–250 v
Arc current	0.07–0.66 amp

The beam level is, of course, dictated by the type of target being bombarded and the sponsor's experiment. The proton beam currents available vary from 0.1 to 20 μa for the external targets and from 30 to a maximum of 2500 μa on internal targets.

Operation of the 63-Inch Cyclotron

During the past year the 63-Inch Cyclotron was available for experimental work about 75% of the scheduled operating time; there were no major breakdowns. A marked improvement in operation resulted from the installation of a centrifugal-type fan to direct cooling air flow over the external surfaces of the dee-stem insulators. Previously, failure of these insulators due to thermal stresses resulting from high-voltage sparking had caused a shutdown about every two months. It has not been necessary to replace any insulators since the installation of the additional cooling. The chief cause of outage has been water leaks in the liner.

The length of the N^{+++} bombardments varied from a few minutes to days, or even weeks. The chemistry runs, which are of short duration, were more numerous. The type and number of bombardments made for the Heavy Particle Physics and Chemistry Groups are listed below:

Type of Bombardment	Runs
Elastic and inelastic scattering	33
Light-particle spectra	9
Chemistry	126
Transfer reactions	28
Miscellaneous	9
Total	205

The following analysis of the operation of the machine is based on an average operating schedule of 49.2 hr per week:

	Per Cent
Normal Operational Conditions	
Bakeout – tuning up machine	6.7
Beam improvement – getting beam up to acceptable bombardment intensities	1.2
Target setup time – installing and adjusting targets	17.5
Beam on target – actual bombardment time	56.7
Source changes	4.4
Operation Interruptions	
Electrical troubles	3.3
Vacuum troubles	3.2
Miscellaneous, including routing maintenance	7.0
	100.0

Stable operation and satisfactory beam conditions are obtained at a vacuum of about 4×10^{-6} mm Hg; serious difficulties are encountered when the pressure rises to approx 1×10^{-5} mm Hg. Other conditions and values of the 63-Inch Cyclotron during normal operation are as follows:

Operating frequency	~4.855 Mc/sec
Magnetic field	15,000 gauss
Dee-to-dee potential	40–42 kv
Energy	27.3 ± 0.3 Mev
Gas (nitrogen) flow rate	1.4–1.5 cc/min
Arc conditions	
Filament current	360–520 amp
Arc voltage	150–250 v
Arc current	1.5–2.1 amp

Various combinations of the arc conditions noted can prevail; generally, the higher the arc values, the higher the beam output. The life of the tantalum filament was increased from 8 hr to about 14 hr by increasing the thickness from 125 mils to 160 mils; space limitations permit no further increase.

4. ACCELERATOR DEVELOPMENT

Interest continues in design and feasibility studies for a proposed azimuthally-varying-field fixed-frequency cyclotron for the acceleration of protons to approx 850 Mev. While the major effort has been directed toward the design of the intermediate-energy machine, the Oak Ridge Isochronous Cyclotron now under construction, substantial progress has also been made on the design and fabrication problems of the electron model of the larger machine.

Cyclotron Analogue II

Cyclotron Analogue II is a fixed-frequency electron cyclotron with a spiraled eight-sector azimuthally varying magnetic field. It is being built to accelerate electrons to, and possibly through, the $\nu_r = 8/4$ resonance, which will occur in this machine when the kinetic energy of the electrons is nearly equal to the rest mass. The Analogue models the beam dynamics of the 850-Mev proton cyclotron proposed for construction at ORNL; it is being built to permit a detailed experimental study of the conditions required for the efficient extraction of a high-quality (optically bright) beam from that machine by means of the 8/4 resonance. The feasibility of accelerating particles through the $\nu_r = 8/4$ resonance can also be examined.

A brief tabulation of the basic properties of the Analogue follows:

Central magnetic field (B_0)	41.926 gauss
Electron rotation frequency	117.399 Mc/sec
Cyclotron unit (c/ω)	16.000 in.
Axial focusing frequency (ν_z)	~0.2
Electron energy for $\nu_r = 8/4$	~470 kev
Maximum energy	~510 kev

Magnetic Field Design

The desired magnetic field in the median plane has the form

$$B(r,\theta) = \overline{B}(r)\ \{1 + \sum f_n(r) \cos 8n\ [\theta - \xi(r)]\} \quad .$$

The spiral law $\xi = r^2$ was chosen because it yields a substantial reduction in maximum flutter required without introducing difficulties which

result from changing the spiral angle too rapidly. The required flutter for a $\theta = r^2$ angular variation is shown in Fig. 4.1; the careful control required to achieve $\nu_z = 0.2$ is indicated.

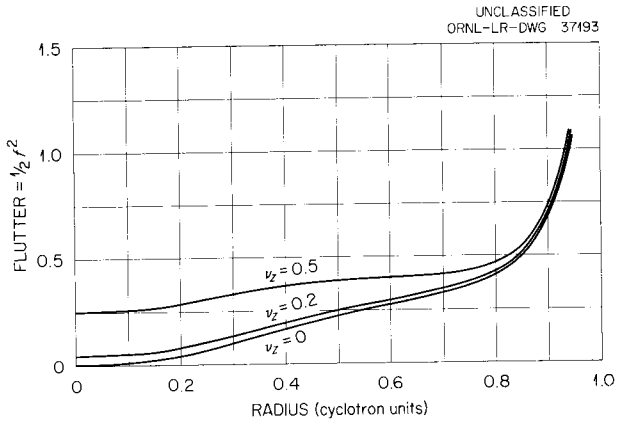

Fig. 4.1. Flutter Required for $\nu_z = 0.0$, 0.2, and 0.5.

The method[1] of shaping the sector coils to produce the desired radial variation of flutter and spiral angle by flaring the coil symmetrically about the normal to the $\theta = r^2$ curve was found to be unsatisfactory; it produced serious deviations of the spiral angle from the desired value. The system finally used to achieve the proper spiral angle of the field is to flare the coil symmetrically in angle about the desired $\theta = r^2$ curve. This system is imperfect in that small but rapid deviations from the desired spiral law occur. These small (±0.5°) variations caused ±10% variations in the focusing strength through the $(d\theta/dr)^2$ term in the first-order equation for the axial focusing:

$$\nu_z^2 = -\frac{R}{\bar{B}}\frac{d\bar{B}}{dr} + \frac{1}{2}f^2\left[1 + 2r^2\left(\frac{d\theta}{dr}\right)^2\right] .$$

To achieve smooth focusing properties the coil was adjusted point by point angularly to minimize the deviations of the 8th harmonic from the desired $\theta = r^2$ dependence.

The focusing perturbations caused by deviations of higher-order harmonics are compensated by adjusting the flutter appropriately. This is illustrated in Figs. 4.2 and 4.3, which show the amplitude and angular

[1]Electronuclear Ann. Prog. Rep. Oct. 1, 1958, ORNL-2740, p 26.

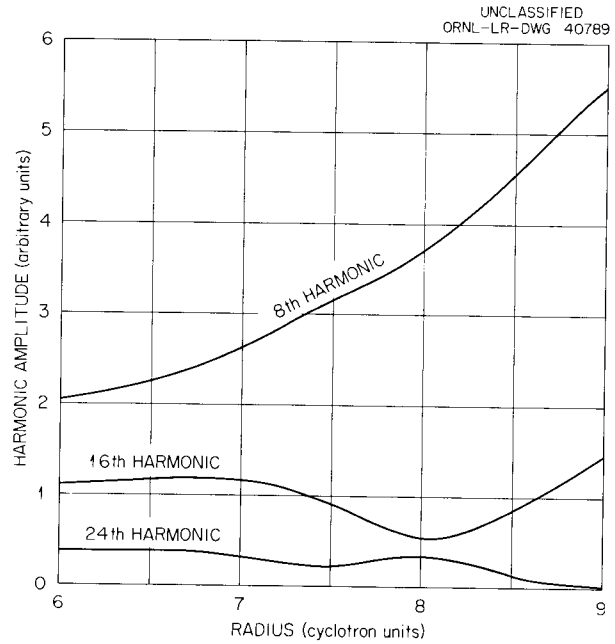

Fig. 4.2. Magnetic Field Harmonics, Cyclotron Analogue II.

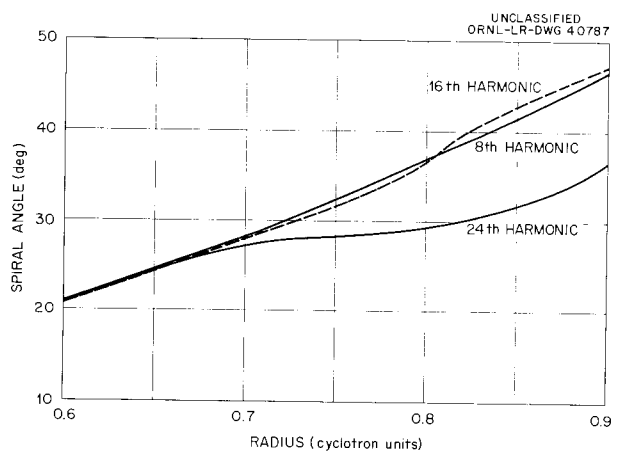

Fig. 4.3. Spiral of Various Harmonics, Cyclotron Analogue II.

variation of the 8th, 16th, and 24th harmonics, and by the flutter for the same magnetic field, Fig. 4.4. The small irregularity in the flutter in the region r equals 0.7 to 0.85 is required to compensate for the deviations of the 16th and 24th harmonic angles. The equilibrium orbit properties obtained by numerical integration of the equations of motion in this magnetic field are shown in Fig. 4.5. The shape derived for a sector coil carrying 530 amp is shown in Fig. 4.6.

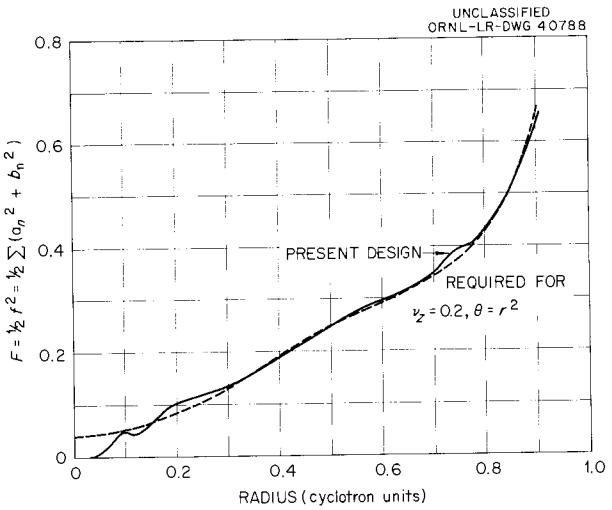

Fig. 4.4. Azimuthal Variation, Cyclotron Analogue II.

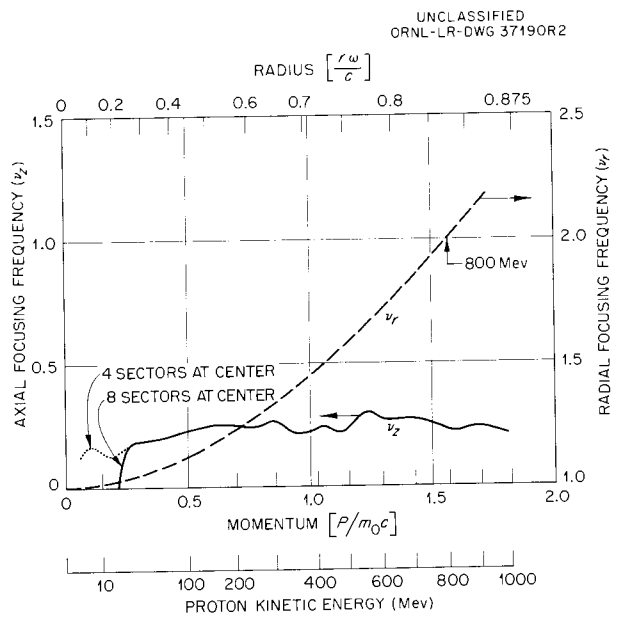

Fig. 4.5. Equilibrium Orbit Properties for Analogue II Magnetic Field.

At the center of the magnetic field for the Analogue the azimuthal variation is zero; it increases radially at a rate depending on the gap and the pole number. The tips of the sector coils are arranged so that near the center the configuration is predominantly four-sector; an abrupt transition to eight-sector geometry is made as soon as adequate axial focusing is obtained. Figures 4.7 and 4.8 show the coil geometry near the center and the resultant harmonic content of the magnetic field.

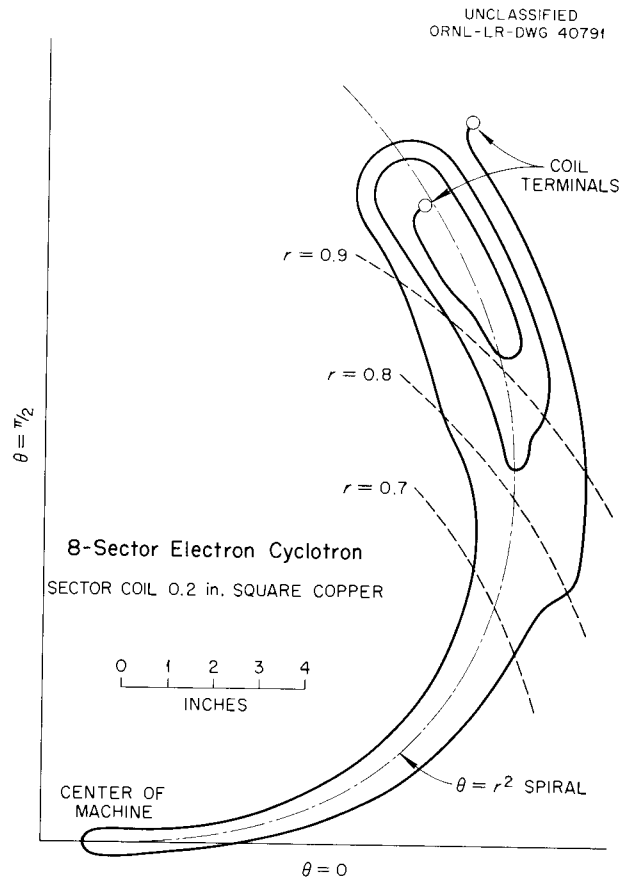

Fig. 4.6. Configuration of Analogue II Sector Coils.

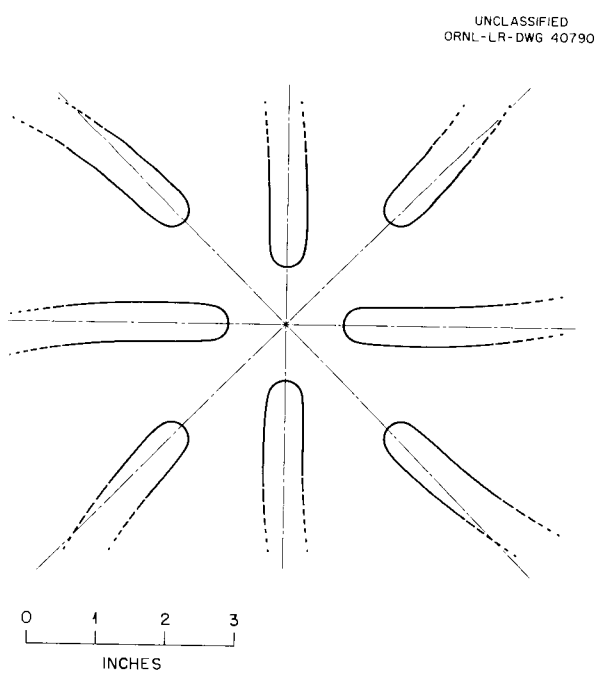

Fig. 4.7. Central Geometry, Cyclotron Analogue II.

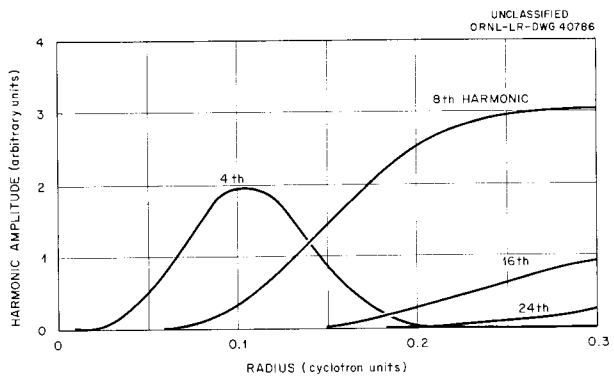

Fig. 4.8. Magnetic Field Harmonics at Center, Cyclotron Analogue II.

The sector coils provide only a portion of the isochronous magnetic field; the remainder is supplied by a set of circular coils. By a judicious choice of coil location and current the average field is fitted to within 1%, except near the center, by four windings located 6.5 cm from the median plane. Final trimming to reduce the error to about 1 part in 10,000 is accomplished by adjusting the current in 36 uniformly spaced windings located 2 cm from the median plane. The location of the various coils within the machine is shown in Fig. 4.9.

Sector Coil Fabrication

In the design of the magnetic field the goal has been to achieve the desired field accuracy of 1 part in 10,000 by construction accuracy wherever possible. This is to minimize, or perhaps eliminate, the field trimming required after construction of the machine. No suitable means has been devised to wind satisfactory sector coils with many turns of relatively small-gage wire to achieve the required number of ampere turns. The system finally devised makes maximum use of the most modern automatic machining techniques and also of newly developed resin adhesives. The choice of fabrication methods has generally been dictated by the desire to achieve a structural accuracy of ±0.001 in. wherever feasible.

The sector-coil assembly drawing, Fig. 4.10, illustrates the fabrication method. Water passages exactly the shape of the conductor are machined in an aluminum plate approx 5/8 in. thick. The plate is then resin-bonded to a plate of identical shape but without grooves; this provides water passages of the required shape. After the assembly is

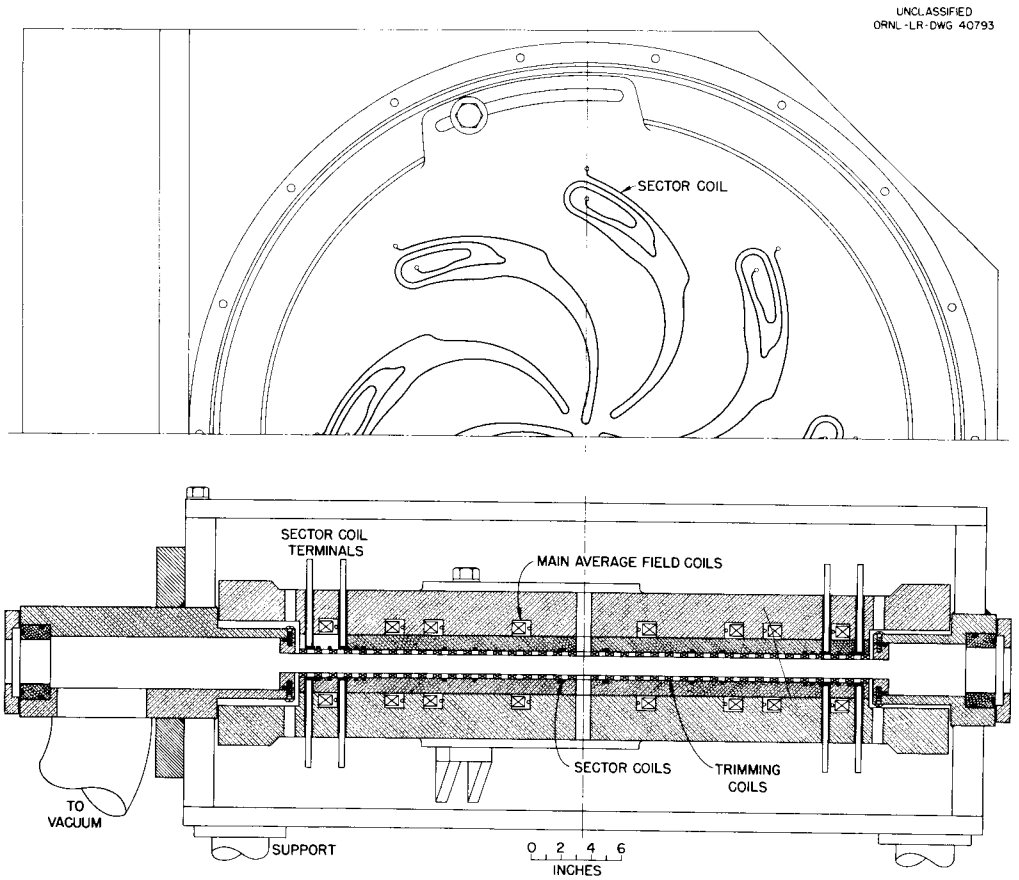

Fig. 4.9. Analogue II Vacuum Tank and Coils in Section.

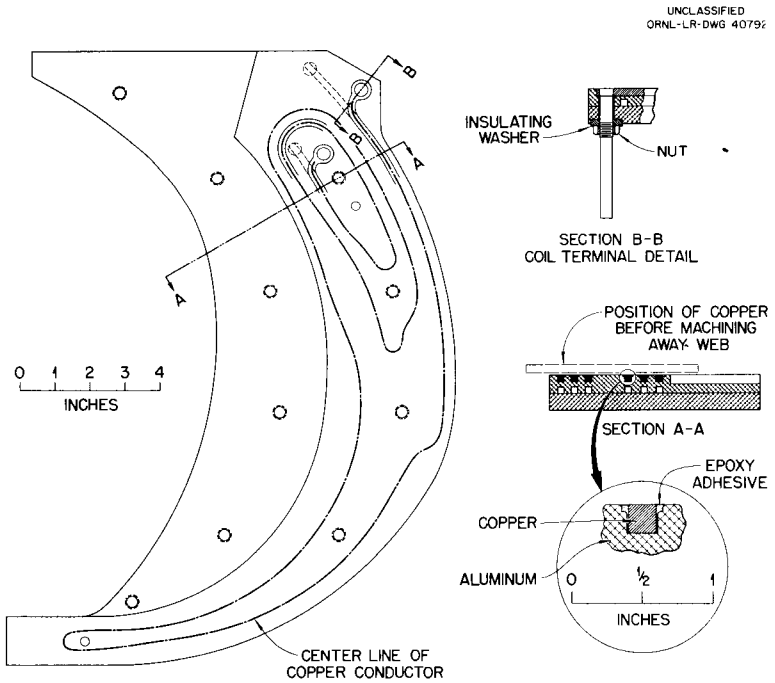

Fig. 4.10. Analogue II Sector-Coil Assembly.

machined to the required flatness, a groove to match exactly the required conductor shape is machined in the reverse side of the first plate, see Fig. 4.11. The grooved aluminum plate is then anodized to a thickness of 0.0002 in. to provide electrical insulation. A copper plate, machined to produce ridges the exact shape of the conductor, Fig. 4.12, is bonded

Fig. 4.11. Anodized Aluminum Sector-Coil Plate.

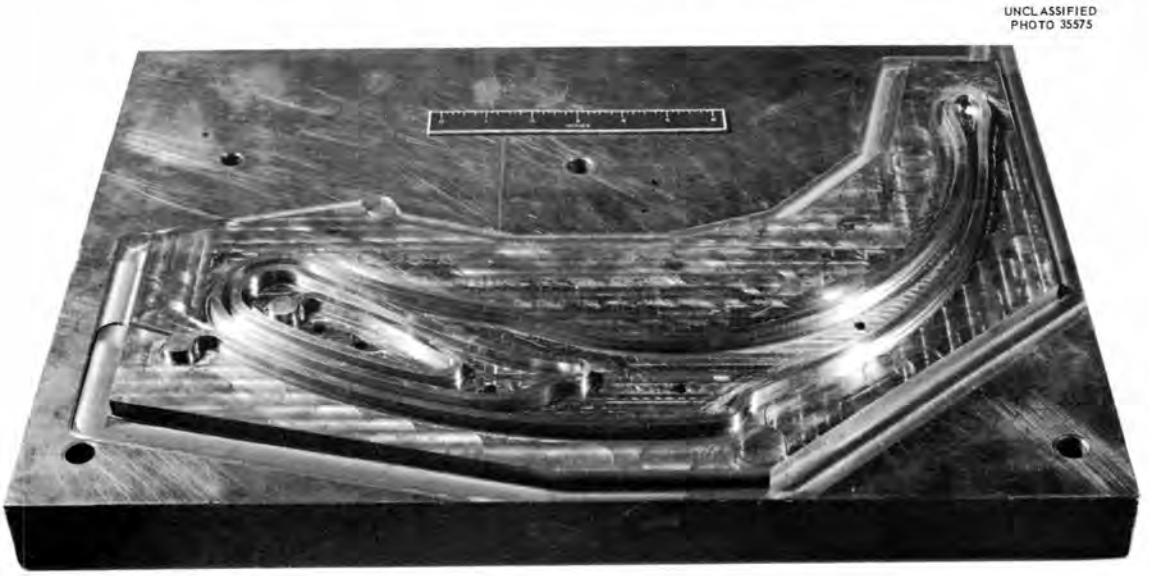

Fig. 4.12. Sector-Coil Conductor, Prior to Bonding in Aluminum Plate.

into the matching grooves in the aluminum. After the resin is cured, the back of the copper is machined away; this leaves the required depth of conductor accurately located and bonded in the aluminum plate, see Fig. 4.13.

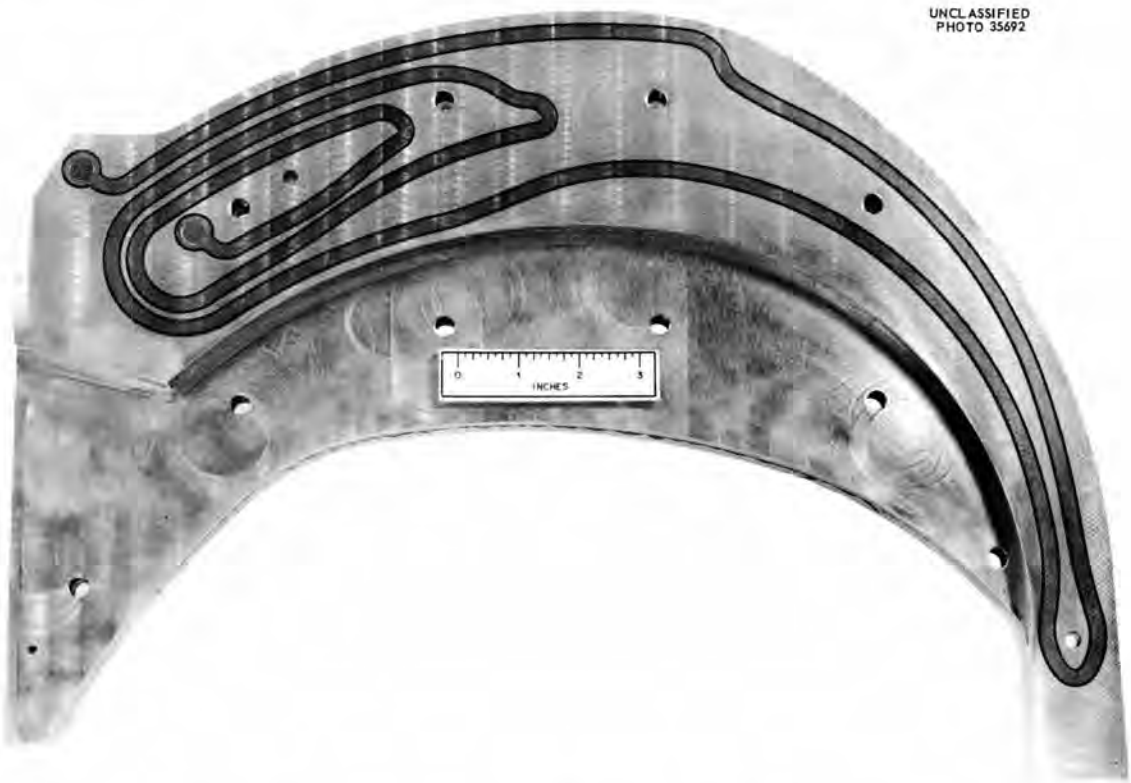

Fig. 4.13. Completed Sector-Coil Assembly.

Tests of this system have shown that, with ordinary water pressures of approx 60 psi, a temperature rise of only 5°C will be experienced with a 550-amp current.

Mechanical Arrangement and Vacuum System

The main coil support system consists of two large aluminum disks to locate accurately the various coils in precise parallel planes, Fig. 4.9. The main average-field coils are held in grooves in the disks. The trimming coils are supported against the surface of the sector coils.

The whole magnet system is mounted within the vacuum chamber to simplify the support of atmospheric pressure loads. A double vacuum

system is used to avoid difficulty from outgassing of the various bonding agents. The beam space is to be maintained at a pressure of 10^{-6} mm Hg, the regions containing the coils at about 10^{-2} mm Hg. The two regions are separated by thin aluminum plates located against the average-field trimming coils. A 4-in. mercury diffusion pump is used for the high-vacuum system.

Radio-Frequency System

The accelerating system is designed to ensure the efficient extraction of a high-quality beam. A single-dee resonant system, similar to that used in the four-sector electron cyclotron, is driven by a regulated master-oscillator power-amplifier system which includes the dee as a part of the regulating loop. The voltage on the dee will be regulated to within about 0.05%. The addition of a third harmonic to approximate a square wave form is planned. The system was described in more detail in the previous progress report.[2]

---

[2]Electronuclear Ann. Prog. Rep. Oct. 1, 1958, ORNL-2740, p 32.

5. THE OAK RIDGE ISOCHRONOUS CYCLOTRON

Considerable progress has been made in the design and construction of the Oak Ridge Isochronous Cyclotron (ORIC) since authorization for its construction was received in October 1958. The specifications for this variable-energy, multiple-particle, azimuthally-varying-field cyclotron are given in Table 5.1 and in Fig. 5.1; they are essentially as outlined

Table 5.1. Design Specifications for ORIC

Performance goals	
Proton energy	Variable, up to 75 Mev
Heavy ion energies	Variable, up to 10 Mev/nucleon
Beam power, maximum	75 kw
Magnet, 3-sector, with slight spiral	
Pole diameter, base and tip	76 in.
Orbit radius, average maximum	31.5 in.
Magnet gap	
Hill	7.5 in.
Valley	28 in.
Central field, average maximum	17 kilogauss
Field rise with radius, maximum	8%
Winding, water-cooled aluminum	1.137 in. square
Power	
Valley coils	750 kw
Main coils	1000 kw
Weight	
Aluminum	9 tons
Steel	200 tons
Radio-frequency system, variable	
Oscillator frequency	7.5–22.5 Mc/sec
Orbit frequency, with harmonics 3 and 5	1.5–22.5 Mc/sec
Dee	
Aperture	1.89 in.
Diameter	71 in.
Dee-to-ground potential	100 kv
Power	
Maximum input	500 kw
Output	350 kw

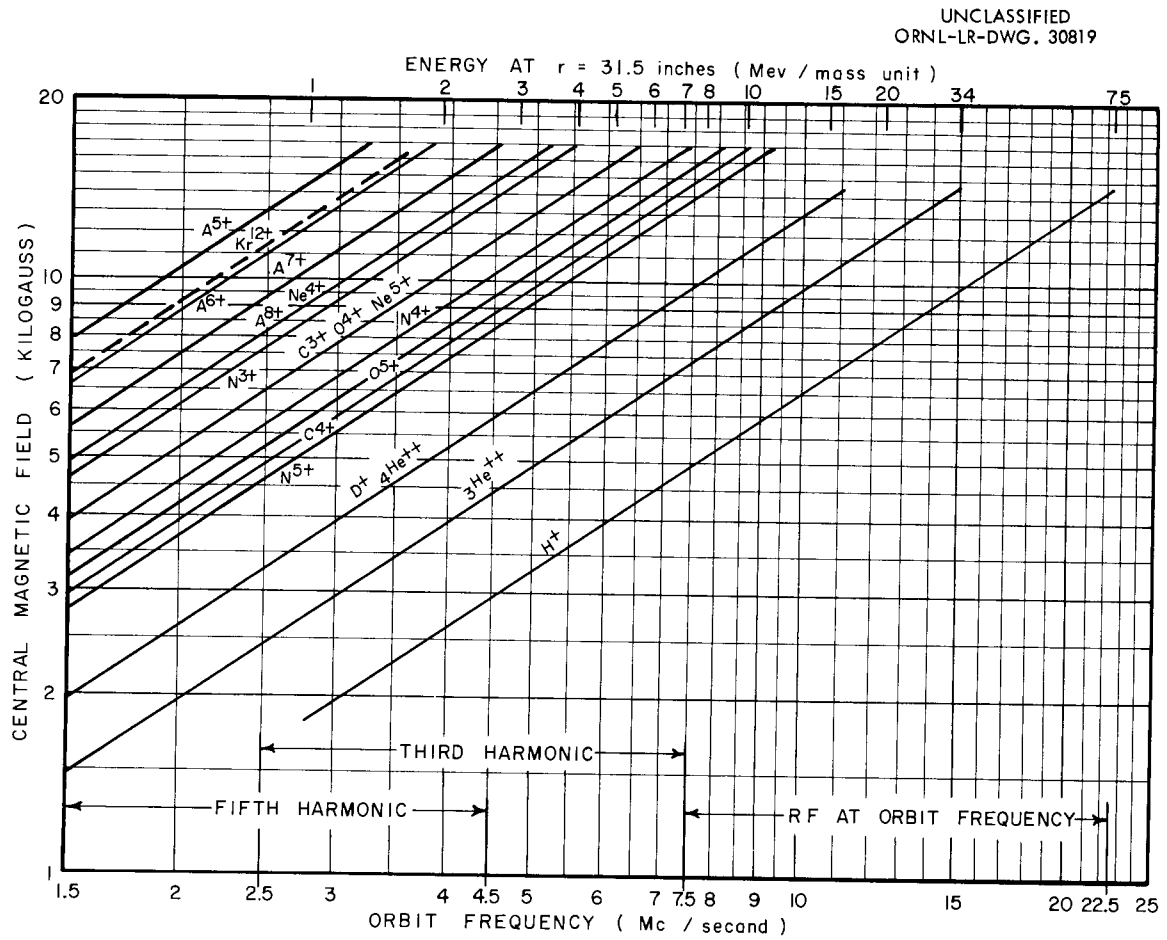

Fig. 5.1. Resonance Conditions for Acceleration of Various Ions in ORIC.

in the preceding report.[1] Protons will be accelerated to energies up to 75 Mev; heavier particles, with mass-to-charge ratios as high as 8:1, can be accelerated up to 10 Mev/nucleon. Since a detailed description of the cyclotron has recently been published,[2] only the major areas of progress will be reviewed here.

Design Studies

The previous successful operation of Cyclotron Analogue I clearly demonstrated that an azimuthally varying field could be used to maintain isochronism efficiently at relativistic energies.[3] Model magnet studies

[1] Electronuclear Research Ann. Prog. Rep. Oct. 1, 1958, ORNL-2740.

[2] R. S. Livingston and F. T. Howard (eds.), Nuclear Instr. & Methods 6, 1–25 (1959); 6, 105–25, 221–37 (1960).

[3] H. G. Blosser et al., Rev. Sci. Instr. 29, 819–34 (1958).

served to establish the over-all specifications for the ORIC. Much design work remains to be done, however, especially for establishing the final specifications for the complex arrangement of pole-tip sectors and magnet windings (see Figs. 5.2 and 5.3), to produce and control the AVF configuration, and to provide a radio-frequency system continuously variable over a 3:1 frequency range.

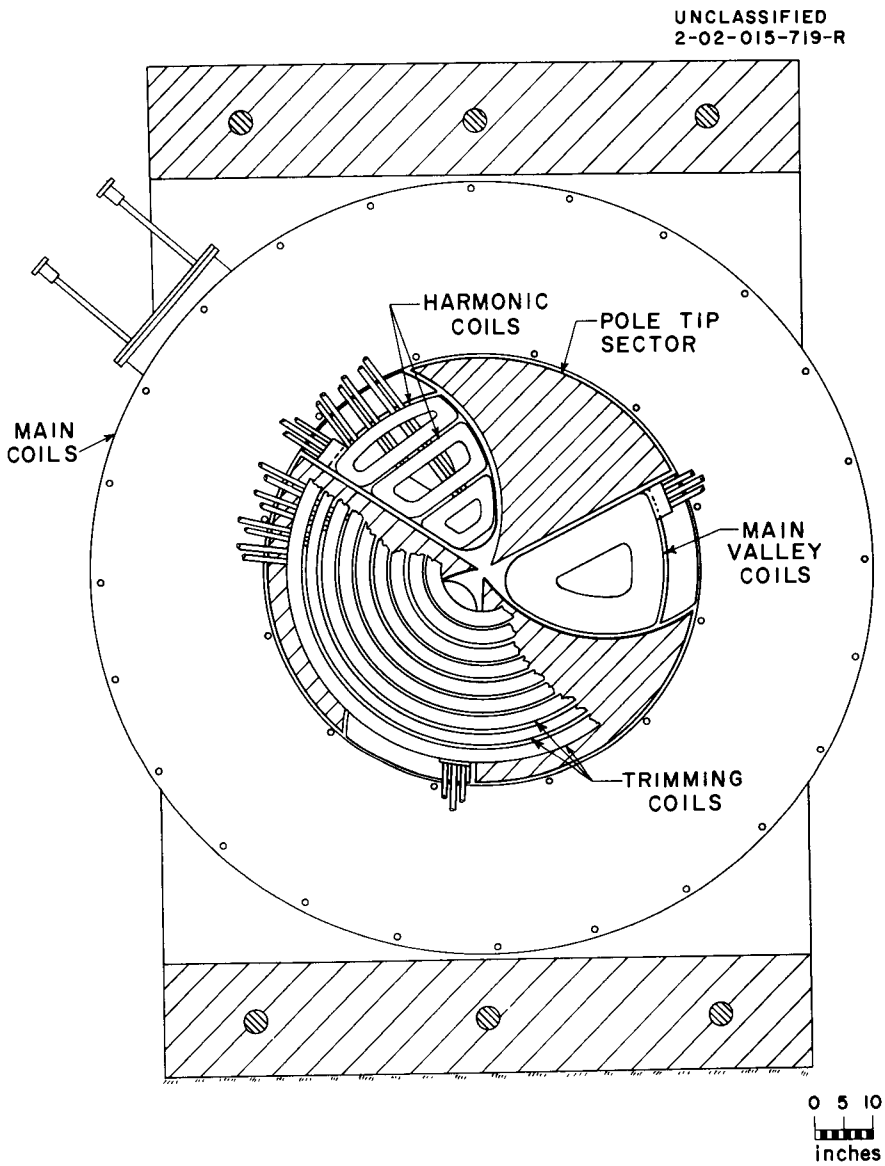

Fig. 5.2. Section Through ORIC Magnet Showing Orientation of Pole Face Windings.

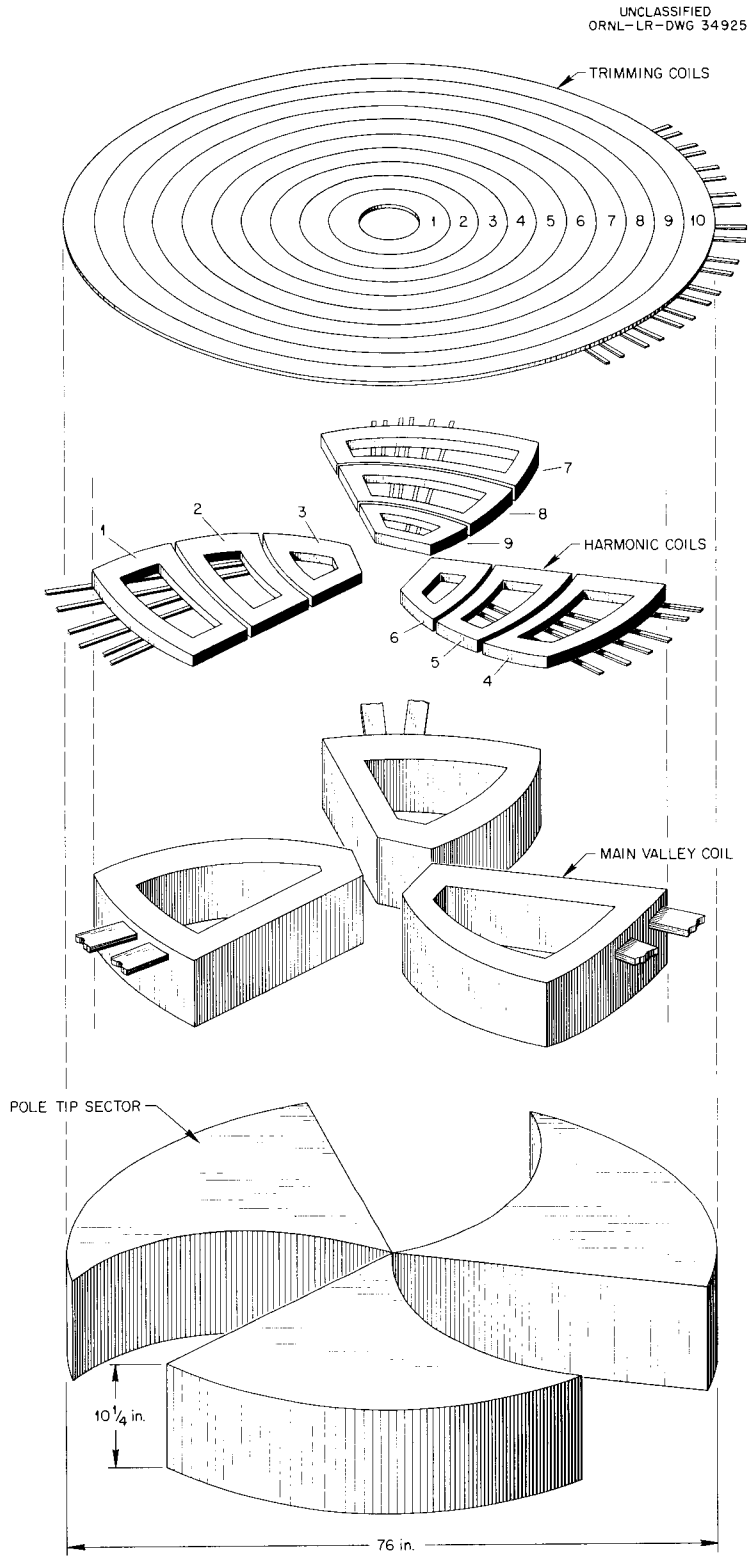

Fig. 5.3. Expanded Schematic View of Coils to Provide Control of the AVF Configurations.

Magnet Design and Testing

Initially, magnetic field measurements were obtained in a one-ninth-scale model magnet; the field was measured at points over a rectangular grid with a Rawson rotating coil fluxmeter as the sensing element. The probe was positioned with a milling machine table which automatically stopped at each data point long enough for the field signal to reach equilibrium and be registered on a Brown strip chart recorder (see Fig. 5.4). The system was accurate to within about 0.6%.

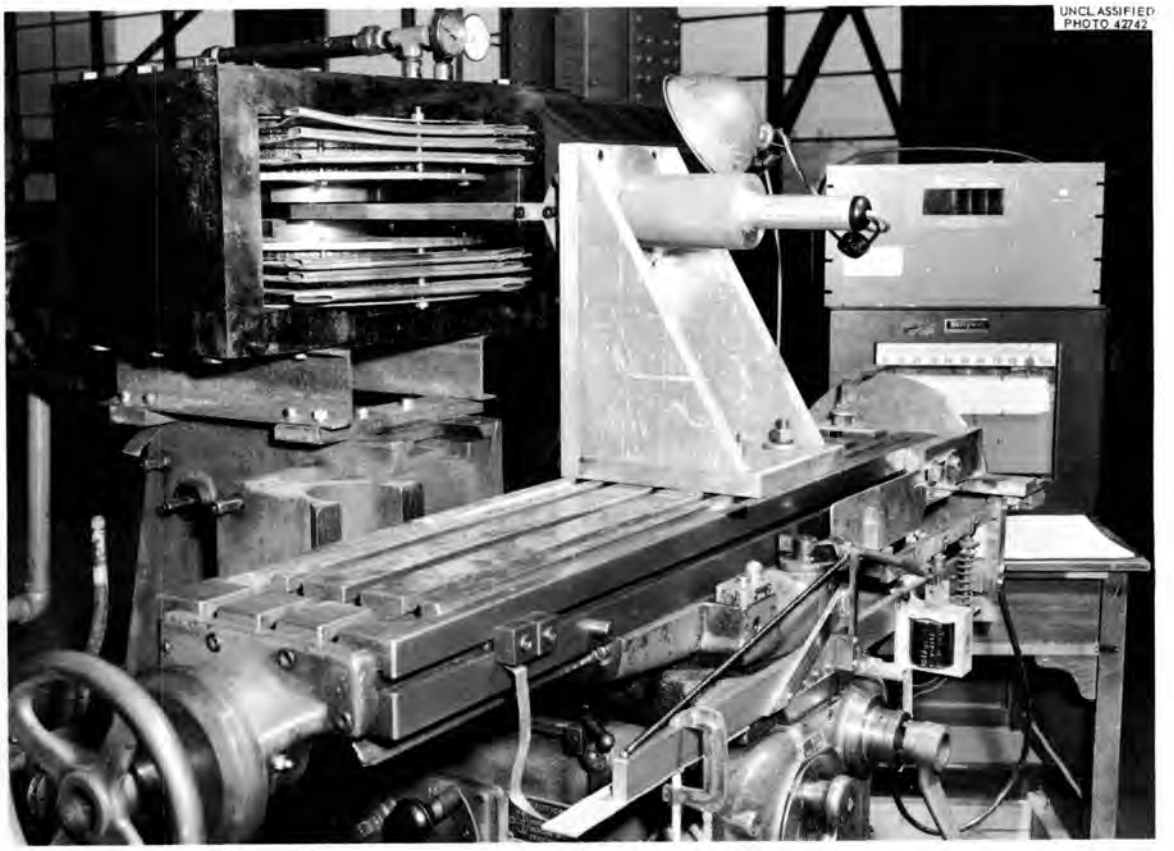

Fig. 5.4. Arrangement for Field Measurements in Ninth-Scale Magnet.

Measurements obtained with the one-ninth-scale magnet were inadequate for detailed orbit and deflection studies. Some of the factors limiting the accuracy of the system were the size of the model, the instruments used to record the data, inaccuracy in positioning the probe, and errors introduced by manually transcribing the data.

To improve the accuracy of field measurements a completely new system was assembled. A new quarter-scale model magnet, shown in Fig. 5.5, was constructed with a tolerance of ±0.001 in. on the pole tips. The probe

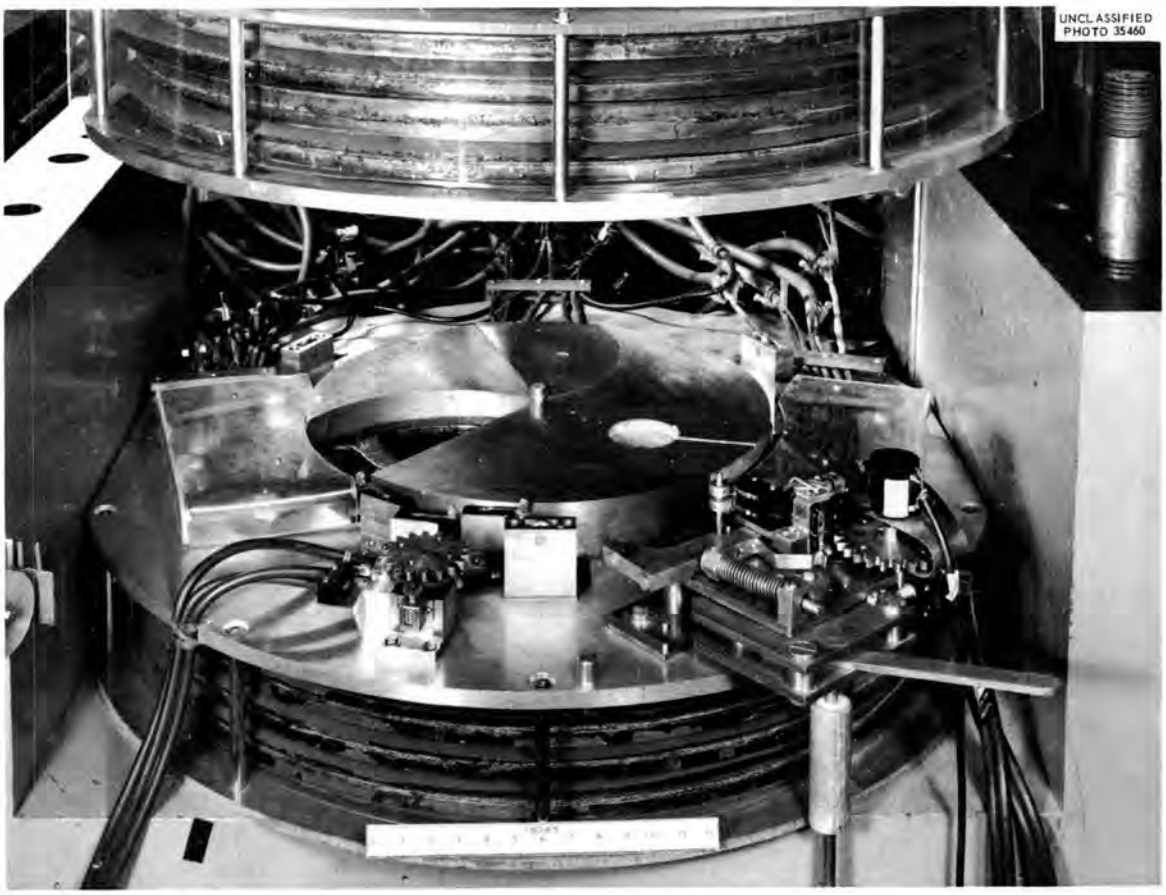

Fig. 5.5. Quarter-Scale Model Magnet for ORIC.

positioning gear (see Fig. 5.6) is capable of locating the probe in polar coordinates to ±13 sec (about 0.0005 in. at the maximum beam radius) and ±0.003 in. radially. An automatic digital data recording system records the data on punched paper tape for direct input to a digital computer.

A Hall generator was chosen as the sensing element because it is easily adapted to an automatic data recording system. The Hall generator output varies with temperature, and, moreover, the temperature coefficient varies with magnetic field, as shown in Fig. 5.7. A simple compensation network is used to hold the output voltage constant to ±0.01% over a 10°C range (see Fig. 5.8). If the temperature rises, the output voltage of the Hall generator decreases, but the resistance of the thermistor also

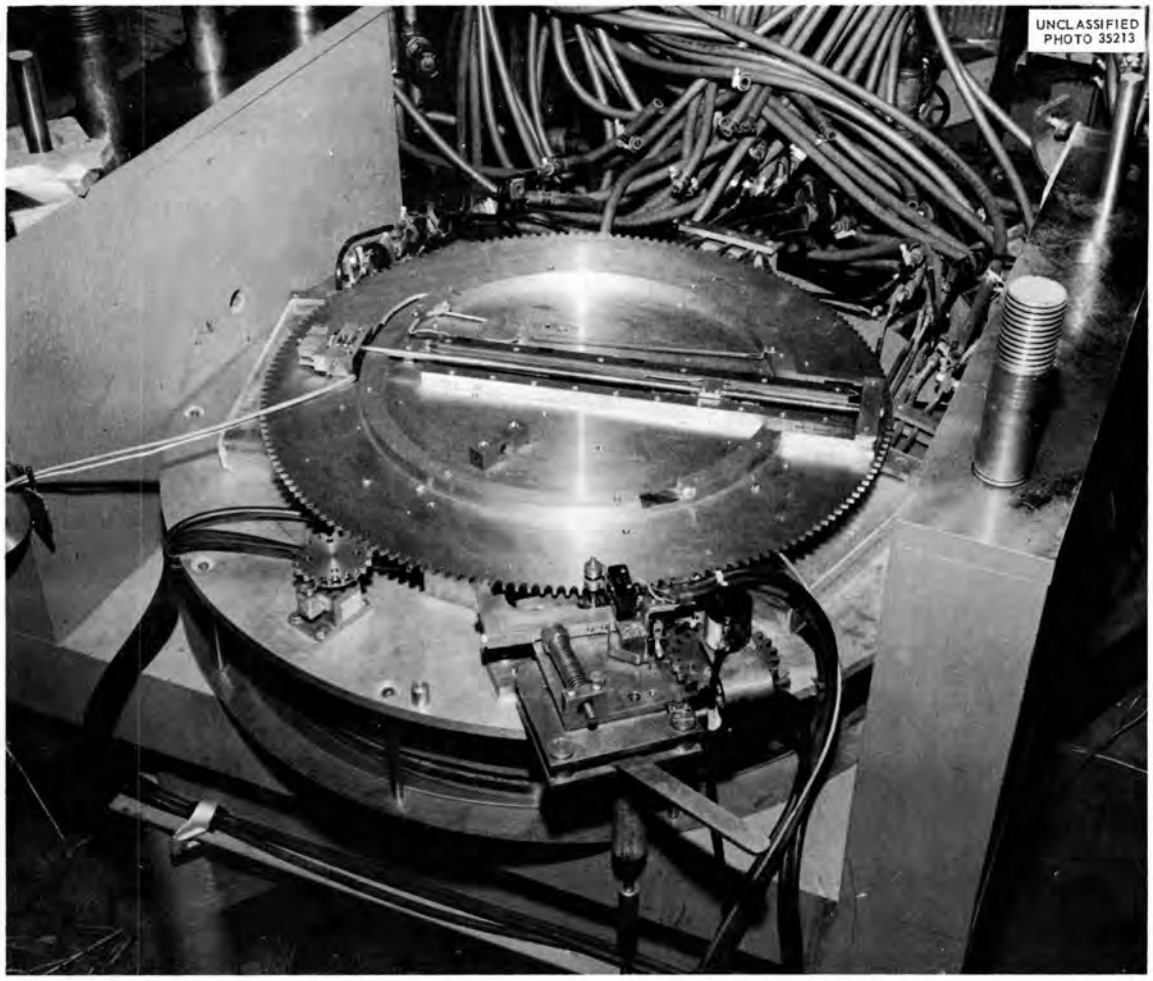

Fig. 5.6. Quarter-Scale Magnet with Positioning Gear.

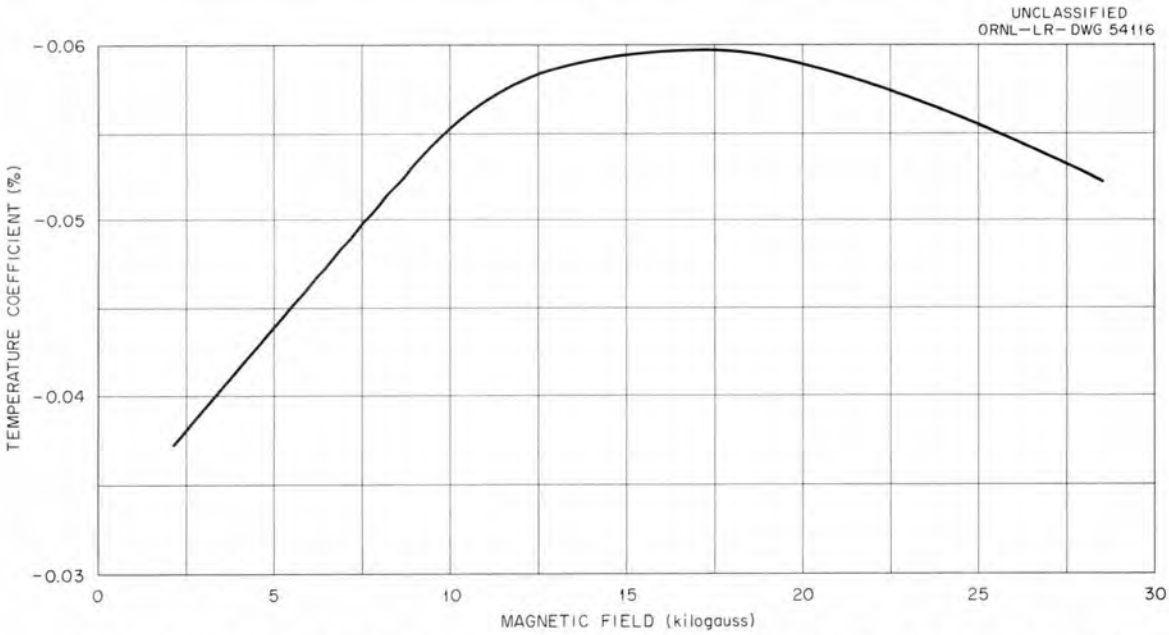

Fig. 5.7. Variation of Temperature Coefficient of Hall Probe with Temperature.

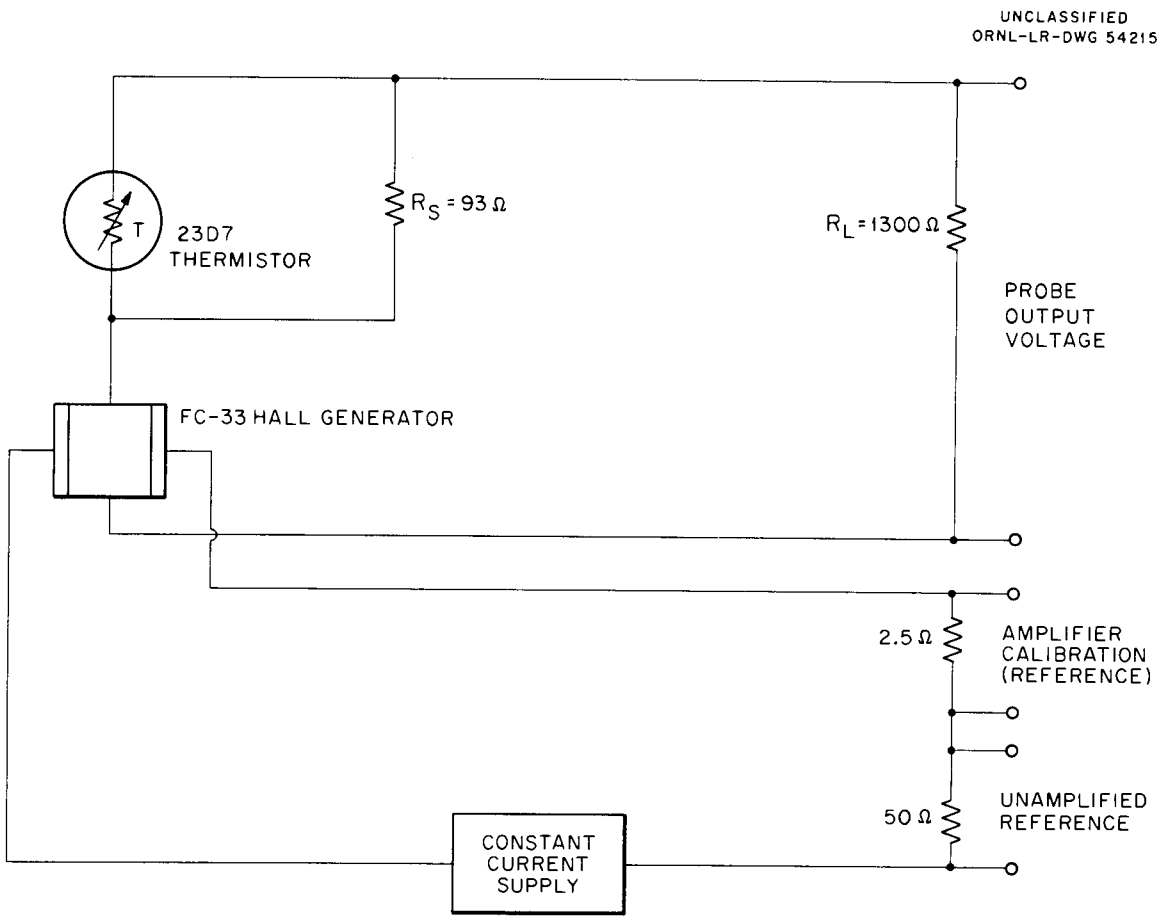

Fig. 5.8. Circuit of Hall Generator with Temperature Compensation.

decreases, so the total resistance in the load circuit is less and the current in the load resistor remains constant. If the load resistance and shunt resistance across the thermistor are adjusted to give the best compensation at 20,000 gauss, the compensation is adequate for any magnetic field from 5000 to 25,000 gauss.

The system, including probe positioning and current regulation, is accurate to about ±0.03%. Most of this error is in the positioning of the probe; the error in the measuring device is only about ±0.01%.

Approximately 4 hr is required to scan a 120° sector of the quarter-scale model, recording 2400 field values at 2° azimuthal increments and at radial increments equivalent to 1 in. in the full-scale magnet.

Orbit Studies

An extensive programming effort to permit the designing of the magnetic field, the ion source, and the rf field for optimum performance of the cyclotron is progressing satisfactorily. New codes, such as the approximate formula program which shows how to modify the magnetic field for better performance, have been debugged and found extremely useful. Two new codes for use in a quantitative study of beam luminosity, which is a critical quantity for nuclear physics experiments, are in process and should be available by this summer. The data from the quarter-scale model magnet measurements indicate that there should be no problem in attaining both isochronism and sufficient focusing.

The emphasis now is on small modifications of the field in the deflection region. Here, the problem is complicated by conflicting requirements which make it necessary to compromise. For resonance deflection, the size of the stable region must be controlled. Once the amplitude of oscillation about the equilibrium orbit exceeds this region, the amplitude and gain in radius per revolution are determined by a calculable quantity called the driving term, D. If the frequency of oscillation does not depend strongly on amplitude, that is, if the frequency shifting term is small, the increase in radius for one revolution is proportional to D times the square of the amplitude. Thus, it is desirable to maximize D and minimize the frequency shifting effect. In addition, the departure from isochronism must be kept small and the average magnetic field must be designed to reduce the stable region. A control of the flutter gradient affects D strongly, as well as ν_r and the possibility of coupling to an axial mode of oscillation. Measurements are now being made for the purpose of determining how much the magnetic field in this region can be changed by judicious use of coils and iron inserts. Once the conditions for deflection are settled, emphasis will be placed on the task of obtaining a high-intensity beam of small angular divergence and on the task of adjusting the turns in the various exciting coils so that the operator can readily shift from one ion and energy to another.

Radio-Frequency System

A major requirement for the resonator is continuous tuning over a 3:1 frequency range, from 7.5 to 22.5 Mc/sec. Several different systems were considered, and models of some were tested. On the basis of more reliable estimates, the specification for an energy gain of 400 kev/turn was reduced to 200 kev/turn. The system finally selected uses a single 180° dee coupled to an RCA 6949 tube.

To achieve reliability and ease of tuning the resonator, one of the early goals in design was to avoid sliding contacts which must carry large rf currents. This consideration led to the so-called "barn-door" method of tuning. In this scheme the resonant frequency is varied by moving the liner surrounding the dee stems toward or away from the stems to change their characteristic impedance. Within the limitations imposed by available space in the magnet, it was not possible to get the 3:1 frequency range without the addition of a movable shorting plane.

Another method of tuning which uses no movable contacts and which might be applicable to the ORIC case is the three-quarter wave system used on some synchrocyclotrons.[4] A resonator of this type is shown in Fig. 5.9. This circuit configuration may be considered as two coupled circuits. The mutual inductance which couples the circuits is the central stem which also physically supports the dees and the dee stems. The tuning is accomplished by adjusting the large outer circuit and leaving the inner (dee) circuit fixed. The natural resonant frequencies of two coupled lumped circuits are given in Fig. 5.10. The circuit shown has a fixed value of mutual inductance; the system can be tuned only along two of the lines of constant k. It is impossible, therefore, to tune to the region around the self-resonant frequency, $f = f_{01}$. In the ORIC this self-resonant frequency of the dee circuit necessarily falls in the 7.5 to 22.5 Mc/sec range; a fixed mutual inductance would require that a portion of the frequency spectrum be left out. Although the resonator does not have lumped inductive and capacitive elements, the behavior of the system is, of course, quite similar to that shown in Fig. 5.10.

---

[4]K. R. MacKenzie, Preliminary Report on the "Three-Quarter-Wave" R-F System for Frequency Modulated Cyclotrons, AECD-1860 (Sept. 12, 1947).

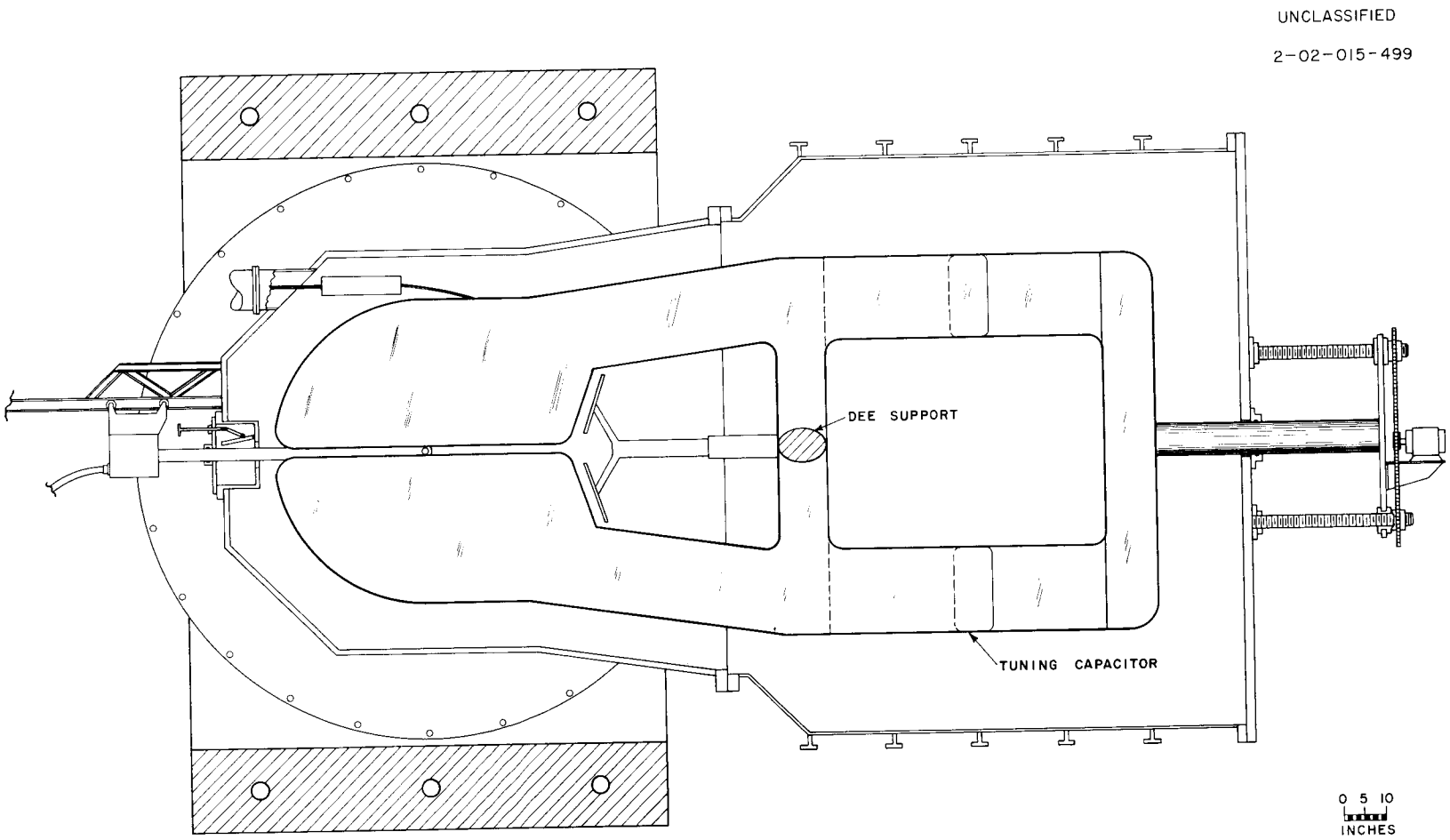

Fig. 5.9. Resonant System with Fixed Mutual Inductance.

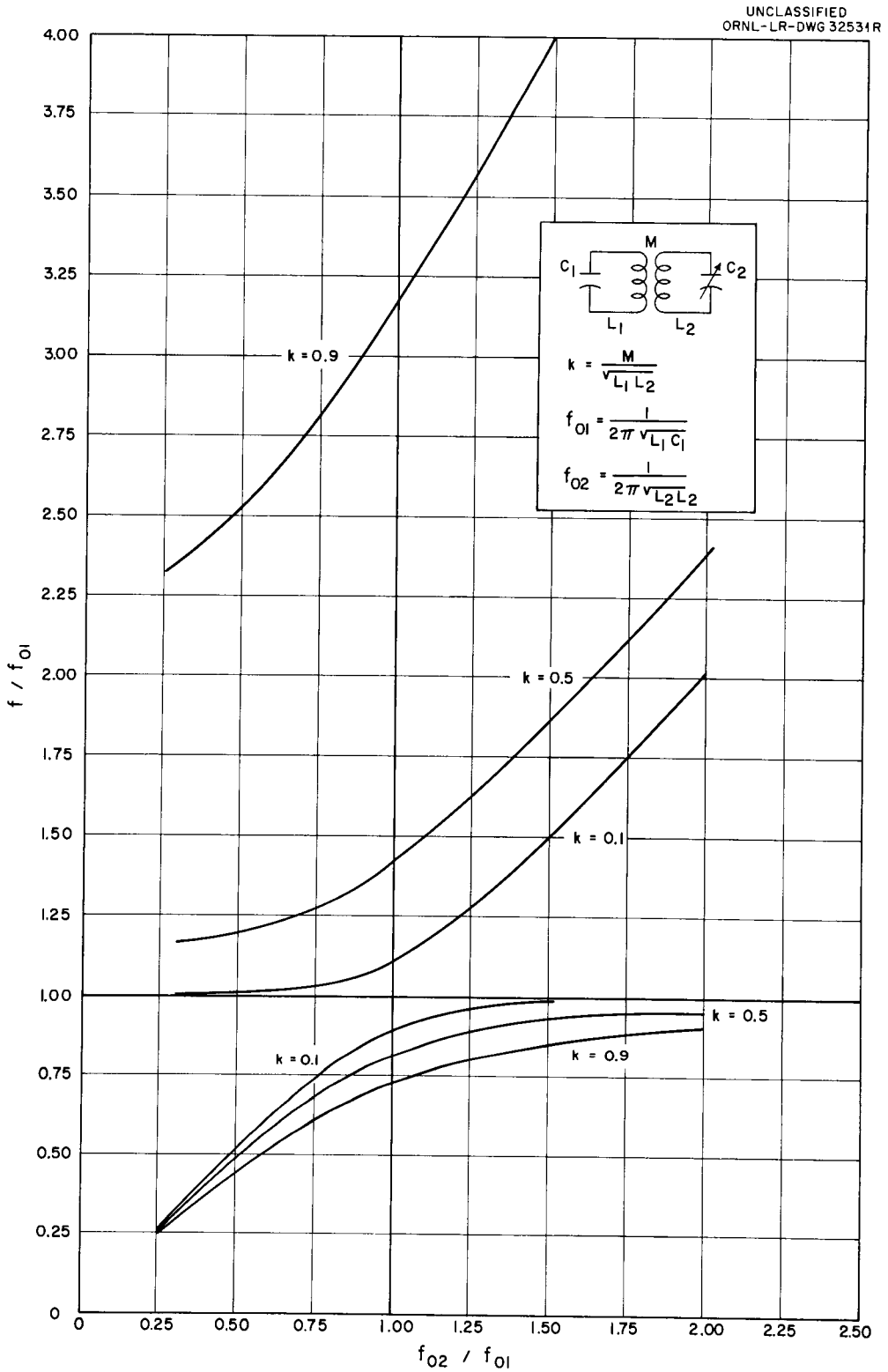

Fig. 5.10. Natural Resonant Frequencies of Two Coupled Lumped Circuits.

A quarter-scale rf model was built along the lines shown in Fig. 5.11. A second model with tighter coupling between the two circuits was built to a one-eighth scale as shown in Fig. 5.12. With variable mutual inductance the system could be tuned to all frequencies over a range greater than 3:1. To get a peak dee voltage of 100 kv and keep the rf excitation power less than about 400 to 500 kw, a coefficient of coupling of nearly unity must be achieved in the coupled transmission line region.

Further investigation of the required threshold rf voltage allowed a reduction from the originally planned 400 kev/turn to 200 kev/turn. This can be provided with a single 180° dee. Unfortunately, it is essential to use movable contacts on the shorting plane to achieve the wide frequency range. The characteristics of a quarter-scale model were promising, and a more precise full-scale model of the rf system was constructed, as shown in Fig. 5.13. The general characteristics of the full-scale model are listed in Table 5.2.

At 22.5 Mc/sec with full beam, the total rf power to drive the resonator will be approx 300 kw. This power is to be supplied by an RCA 6949 tube coupled to the resonator through a capacitor and an approx 100-ohm drive line. The tube will in turn be driven by a 2-kw exciter. The master frequency will be determined by an oscillator located in the console.

To achieve a stable external beam of high quality the dee voltage must be regulated to about 1 part in 1000. The power amplifier plate voltage will be controlled by a series regulator tube in the plate power supply to obtain this regulation. A block diagram of the drive system is shown in Fig. 5.14.

Cyclotron Components

The various components of the cyclotron are being designed by the Electronuclear Research Division staff with the assistance of personnel from the Instrumentation and Controls Division and from the architect-engineer, Catalytic Construction Company. Some unusual components, such as the magnet coils, are being fabricated locally, but contracts for the fabrication of most components are being placed through usual channels by the Laboratory's Purchasing Department.

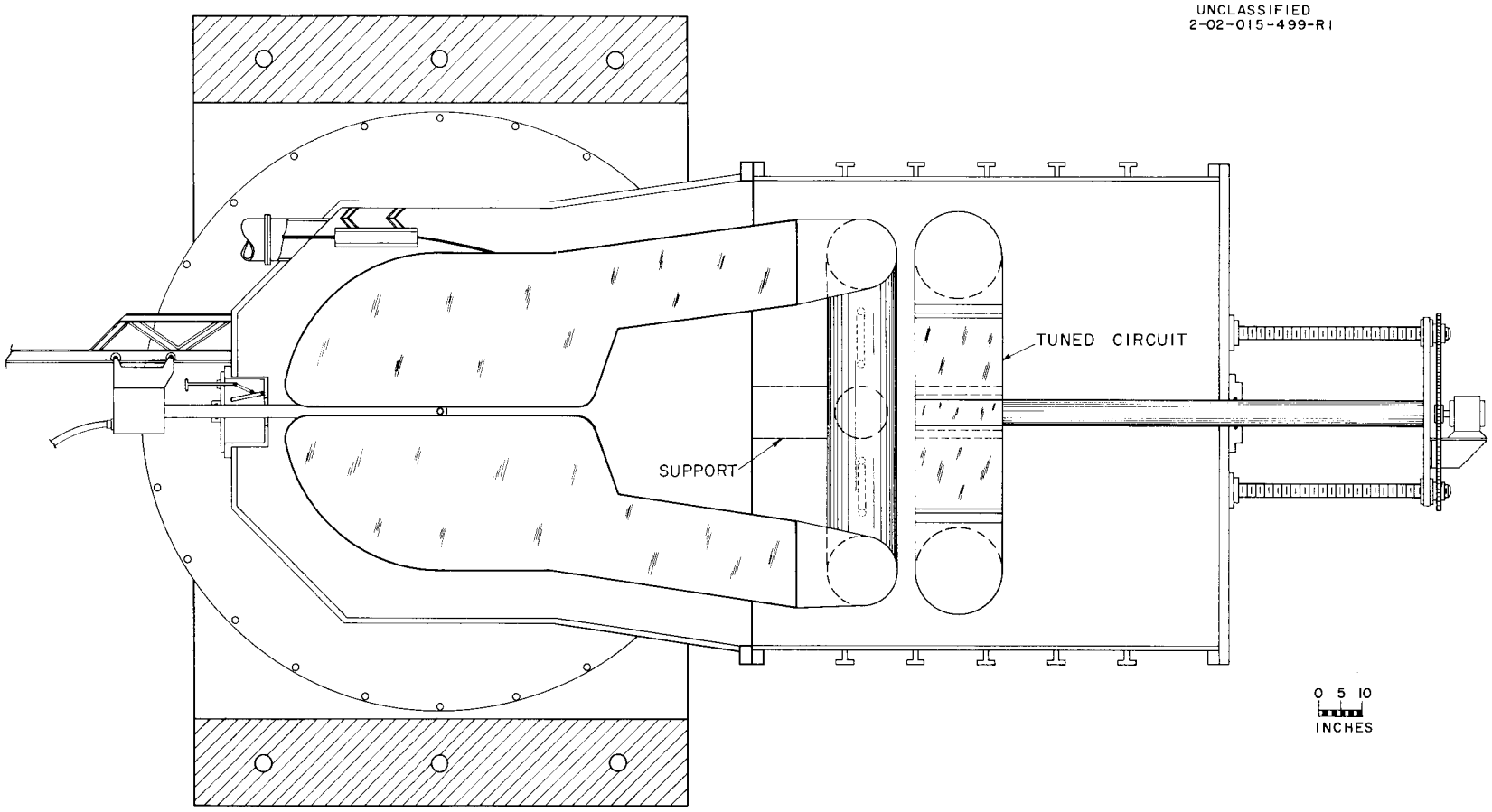

Fig. 5.11. Resonant System with Variable Mutual Inductance.

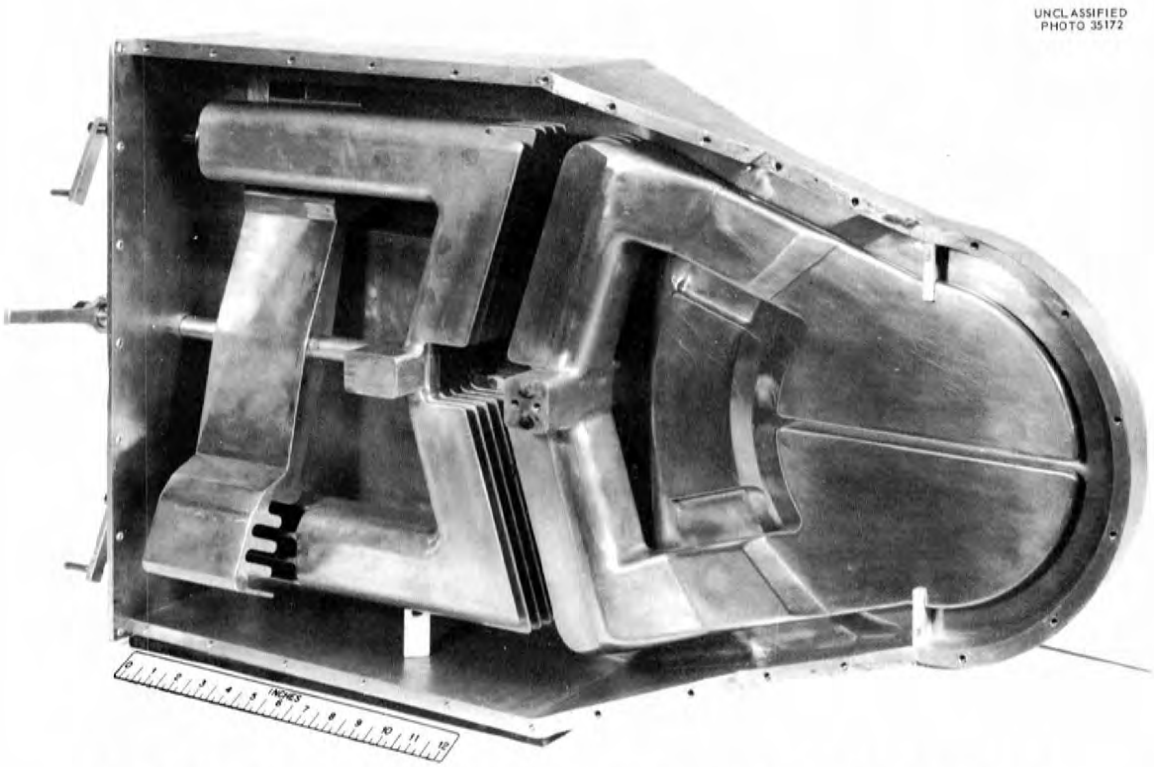

Fig. 5.12. Eighth-Scale Model of System Shown in Fig. 5.11.

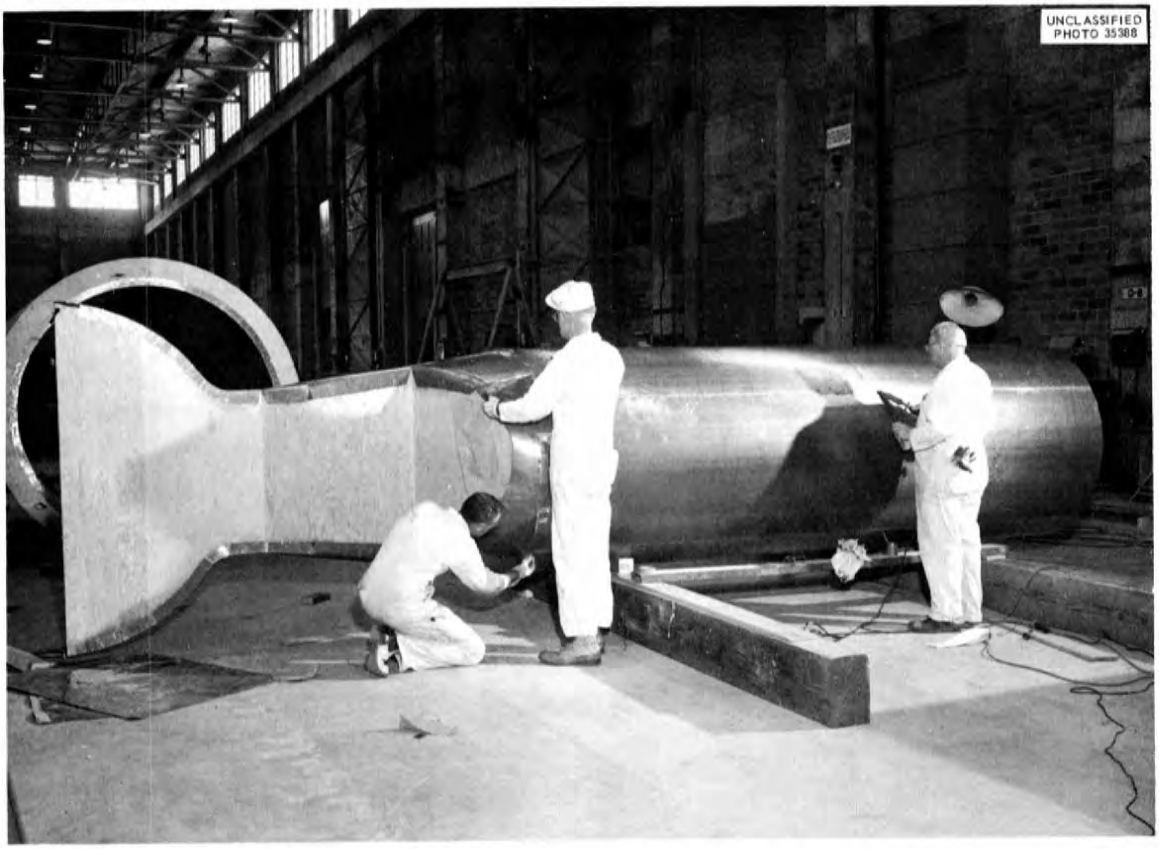

Fig. 5.13. Full-Scale Mockup of ORIC Resonator.

Table 5.2. Characteristics of RF System with Single 180° Dee

Frequency	7.5–22.5 Mc/sec
Dee voltage, maximum	100 kv
Voltage variation at dee lip, center to edge	+2%
Dee diameter	70 in.
Dee-stem diameter	50 in.
Shorting-plane travel	130 in.
Shorting-plane current density, peak	83 amp/in.
Rf drive	~300 kw
Dee-stem characteristic impedance near dee	~11.9 ohms
Dee-stem characteristic impedance near forward shorting position	~5.0 ohms

The specifications for the main magnet structure were determined from field measurements obtained with the one-ninth-scale model magnet. The low-carbon steel castings for the magnet, four for the yoke and two for the 76-in. pole bases, were fabricated by United States Steel. The two main coils required about 9.2 tons of aluminum conductor; they were wound at Oak Ridge (see Fig. 5.15). The magnet is about 113 × 113 × 180 in. and weighs about 210 tons. It has been installed in a temporary structure (see Fig. 5.16) to permit preliminary magnetic field measurements while the building is under construction.

The design of the pole-tip coils is not complete; however, they can be described with reasonable accuracy at this time since probably only the size will vary. The valley coils will be wound with square 5/8-in. copper conductor with a round coolant passage through the center. The coils will be "canned" in a vacuum-tight close-fitting metal container with the leads being brought out through the accelerating tank wall inside specially shaped pipes. All electrical and coolant connections can then be made outside the accelerating tank.

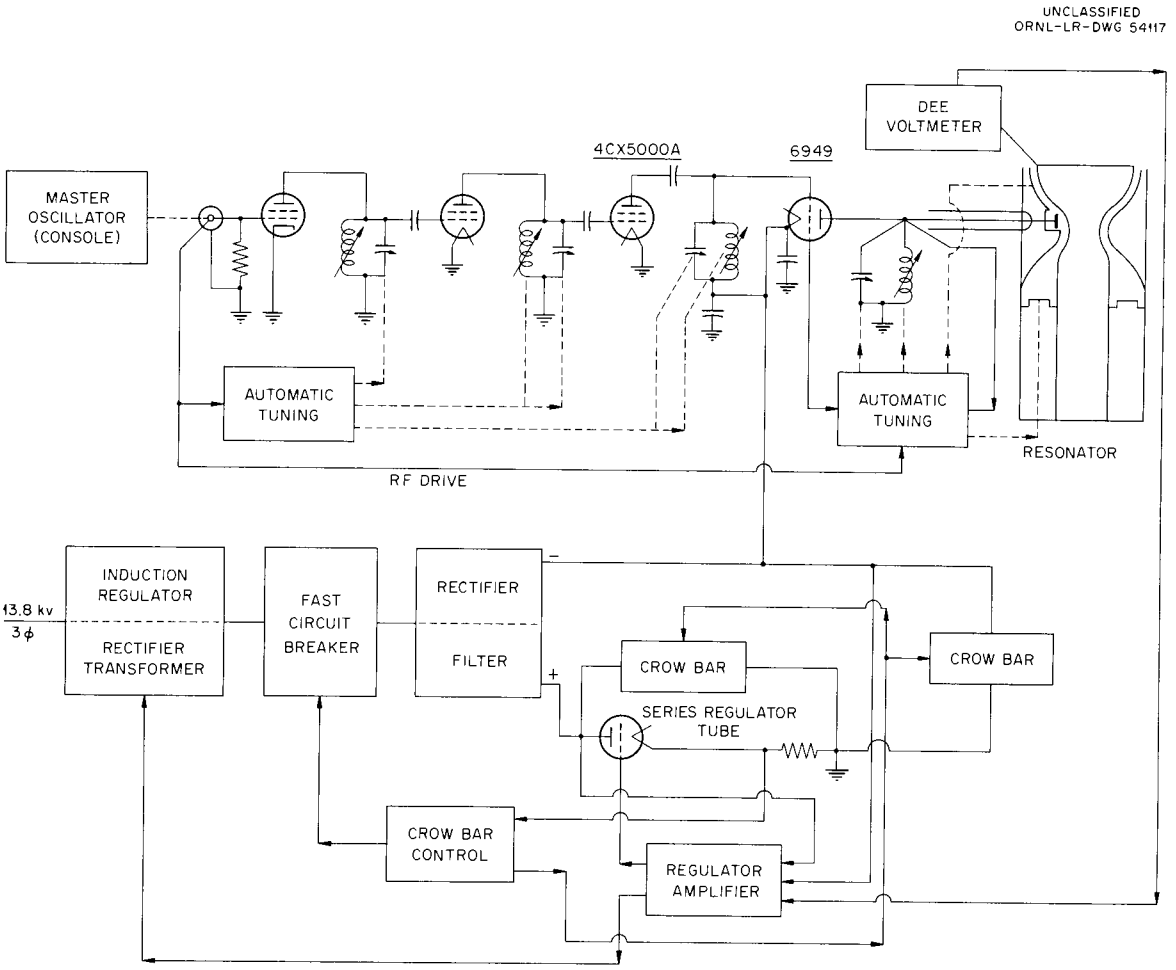

Fig. 5.14. Block Diagram of RF System Selected for ORIC.

The final design chosen for the resonant system, shown schematically in Fig. 5.17, consists of a horizontally mounted quarter-wave circular-section coaxial line with a remotely controlled variable shorting plane. The 50-in. center element of the coaxial line serves as a cantilever support for a single 180° dee. The 75-in. outer shell of the line undergoes a transition in shape near the magnet, where it joins the accelerating tank to form a vacuum enclosure for the entire accelerating system. More details of the structure are shown in Fig. 5.18.

The dee stem has been designed and is being fabricated. It is made of 3/8-in. copper-clad carbon steel; the 20% thick cladding covers the outer surface. The stem is stiffened by five internal rings of carbon steel. The inside surface is traced with copper lines for water-cooling the structure.

Fig. 5.15. The Main Coils of the ORIC Magnet Were Wound with 1170-ft Strands of Hollow Aluminum Conductor, 1.137 in. square and 0.7 in. ID.

Fig. 5.16. The ORIC Magnet Is Installed in a Temporary Location to Permit Measurements to Proceed While the Building is Under Construction.

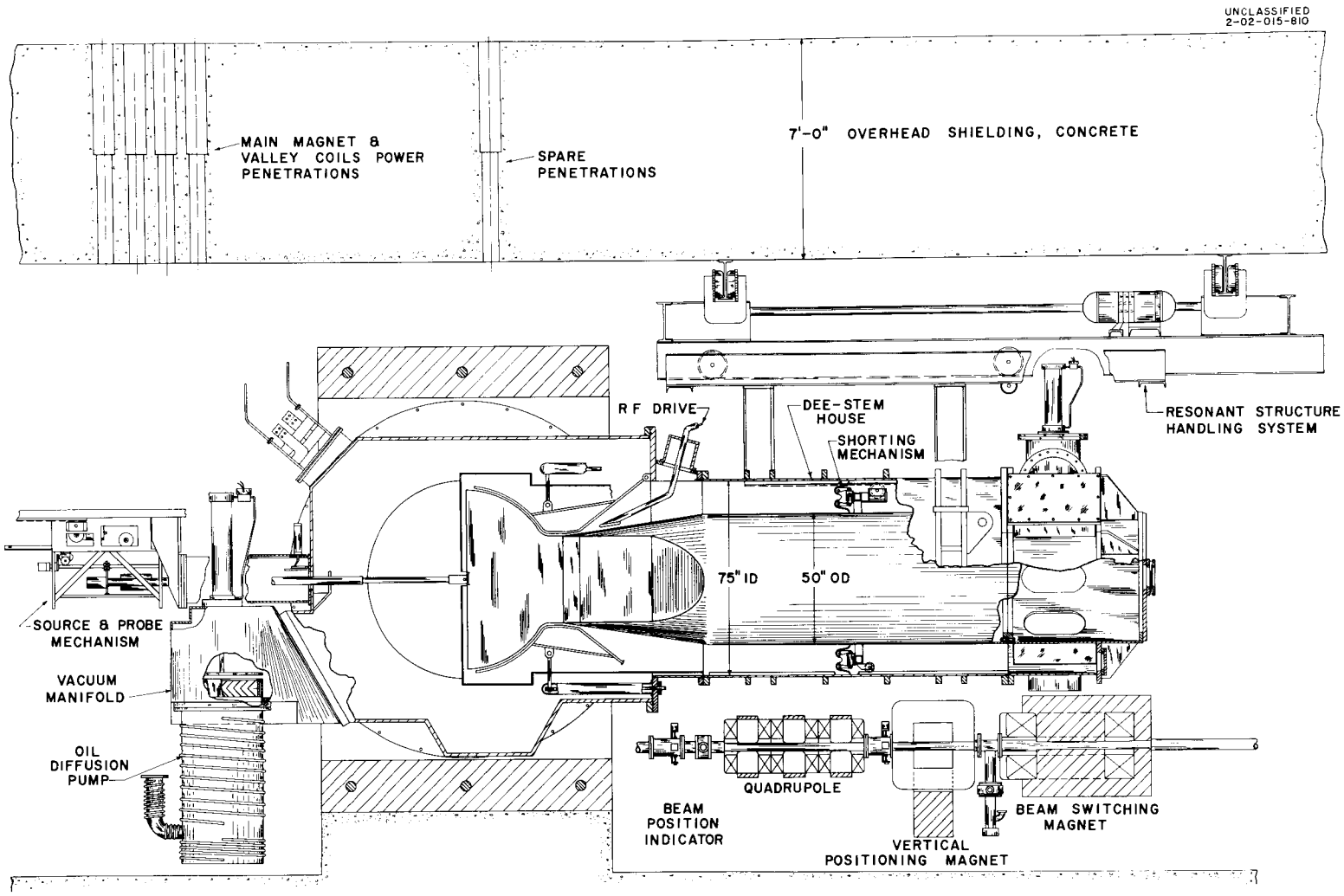

Fig. 5.17. Section of ORIC Showing Main Features of Resonant and Vacuum System.

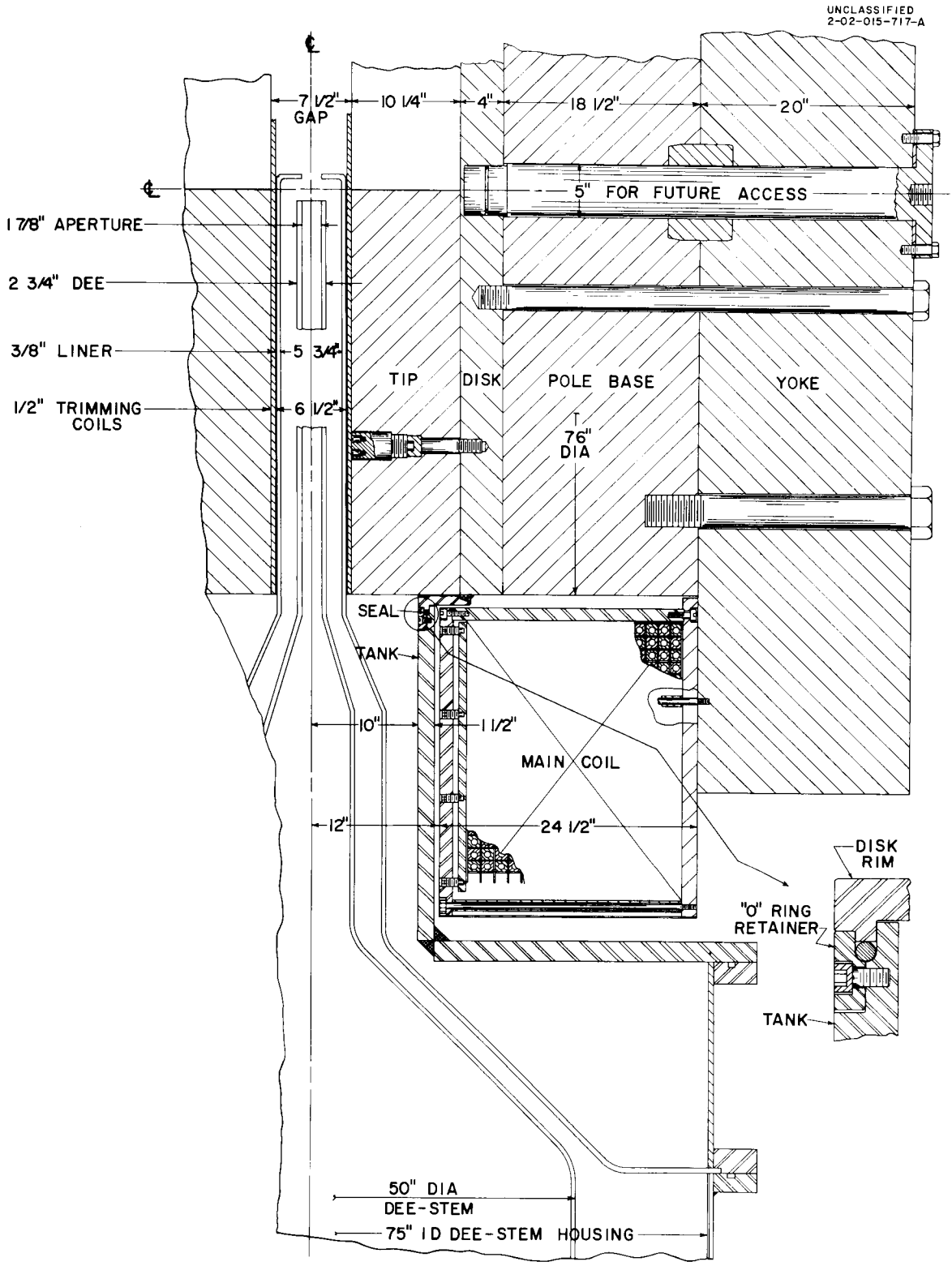

Fig. 5.18. Horizontal Section of ORIC Showing Structural Details.

The rf shorting plane is composed of 48 identical units; each contains two pivoted contact arms actuated by a bellows. The general design characteristics are shown in Fig. 5.19. Note that revolving the arms (shoes) about two fixed centers allows a connecting foil to be used with a minimum of distortion during operation. Each shoe is divided into several fingers by radial saw cuts to allow conformity to surface irregularities of dee stem and dee-stem house wall. This design is complete and a working model is being tested.

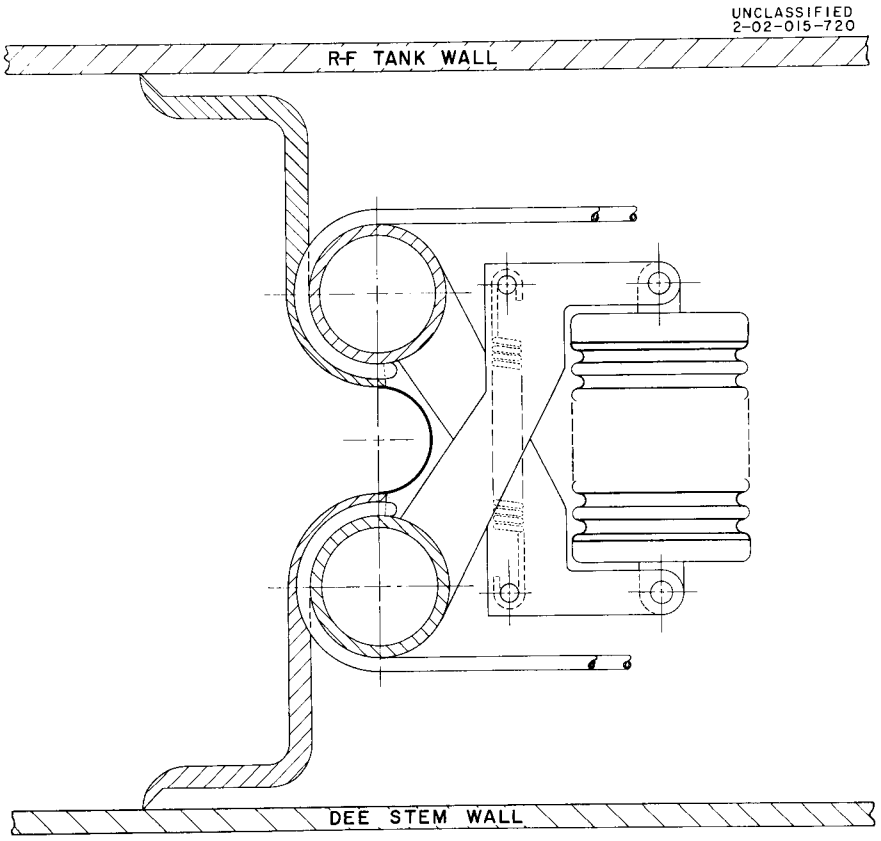

Fig. 5.19. A Component of the Movable rf Shorting Mechanism.

A vacuum manifold supporting the two main 32-in. oil diffusion pumps is attached to the accelerating tank opposite the dee-stem housing. An auxiliary 20-in. oil diffusion pump will be mounted on the dee-stem support flange at the grounded end of the coaxial stub; this pump evacuates the volume inside the dee stem and also pumps on the annulus between dee stem and dee-stem house behind the shorting plane.

The source and probe system rides on rails supported from the ceiling and enters the machine through a vacuum lock mounted on the horizontal center line above the vacuum manifold.

Instrumentation and Controls

Design of the console and control board for the ORIC is nearing completion; although many engineering details remain to be worked out, most of the general concepts are complete. A plywood model was used during preliminary studies of instrument placement (see Fig. 5.20).

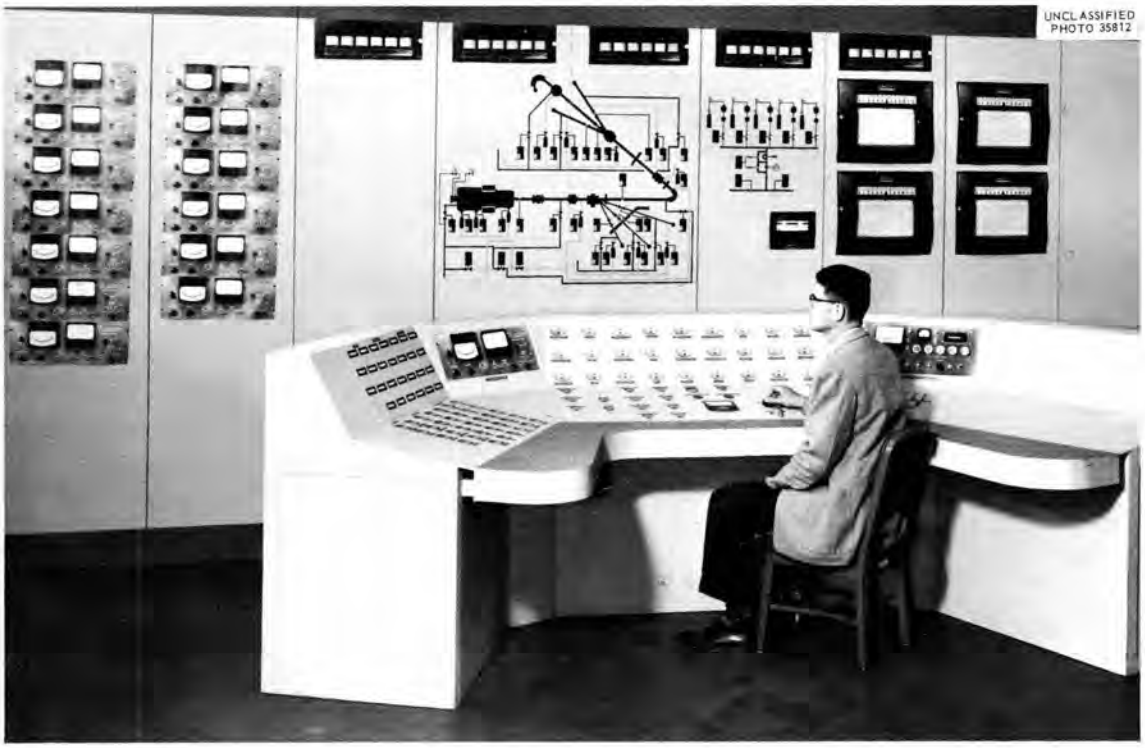

Fig. 5.20. Full-Scale Mockup of Console and Control Board for ORIC.

Locations assigned to the various cyclotron controls and indicators depend upon the frequency of use and importance to the operation. The controls for the magnet trimming currents, the radio-frequency oscillator and power amplifier, the probe and source motions and position indicators, and the major controls for the external beam system are located on the center section of the console; important radio-frequency tuning and television camera controls are located on the right; and controls for the main,

valley, and AVF coils and for the beam focusing, positioning, and analyzing magnets are on the left.

The instruments and controls on the control board behind the console are generally related to ancillary cyclotron services. A large graphic display of the external beam system is placed centrally; push-button switches and indicator lights relate to and control the corresponding vacuum pump, beam-pipe valve, and other auxiliary equipment.

Considerable attention has been given to the development of an inexpensive and reliable method of protecting the magnet coils from loss of coolant during operation; full protection involves over 100 separate water-cooling circuits. Several methods have been considered. A spring-loaded switch held in position with a low-melting-point alloy in thermal contact with the water-cooled conductor was considered. The alloys tested began to creep at temperatures considerably below the desired trip point and thus gave unpredictable results. Other methods considered but untested include the use of flow switches, thermocouples, and bridge-unbalance detectors. It is likely that a combination of such methods will be used to give as much protection as possible at reasonable cost.

AVF Coil Power Supplies

Specifications for the 19 current-regulated power supplies for the trimming and harmonic coils were completed and details of the design are being worked out. Specifications for these supplies are as follows:

Type	Number	Voltage (v)	Current (amp)	Output (kw)
A	1	28	1200	33.6
B	4	36	800	28.8
C	5	48	500	24.0
D	9	25	250	6.25

Each unit is to have output voltage adjustable from 0 to 100%, to maintain current regulation to within 0.01% of rated output current, and to have less than 0.01% voltage ripple in the output regardless of load. Polarity is to be reversed by switching at or near zero current.

A typical power supply is outlined in Fig. 5.21. Power is converted from 460-v, three-phase ac to magnetic-amplifier-controlled dc with suitable transformers, rectifiers, and control elements. Output from the magnetic amplifier, which is expected to be variable from 5 to 100% voltage and with about 2% ripple, is stabilized by a series-transistor current regulator. The transistor regulator will at all times respond directly to the preset field coil current; the magnetic amplifier will hold the collector voltage across the transistors essentially constant. This system offers the advantages of fast response, excellent ripple reduction, and controlled short-circuit behavior. Cost is expected to be comparable with other methods of obtaining similar regulation characteristics.

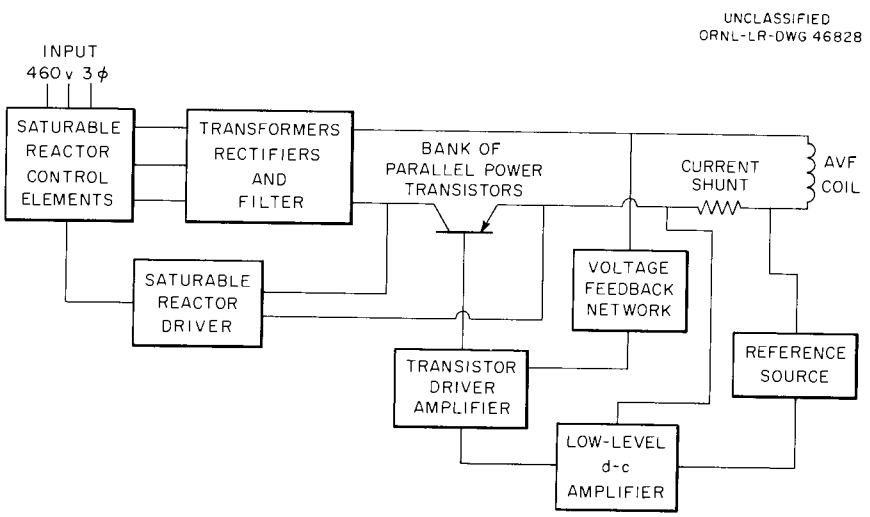

Fig. 5.21. Block Diagram Typical of Regulated Power Supplies for AVF Coils.

Field Regulator for 1750-kva Generator

A field supply and current regulator for the 350-v, 5000-amp, 1750-kva motor-generator was fabricated and is being used in the quarter-scale magnet studies. In preliminary tests this regulator maintained a current stability of 0.01% over several hours. Nominal output ratings for this unit are 250 v dc at 15 amp.

A block diagram of the regulator is shown in Fig. 5.22. The 460-v, three-phase input power is transformed to 24 v rms and then transformed

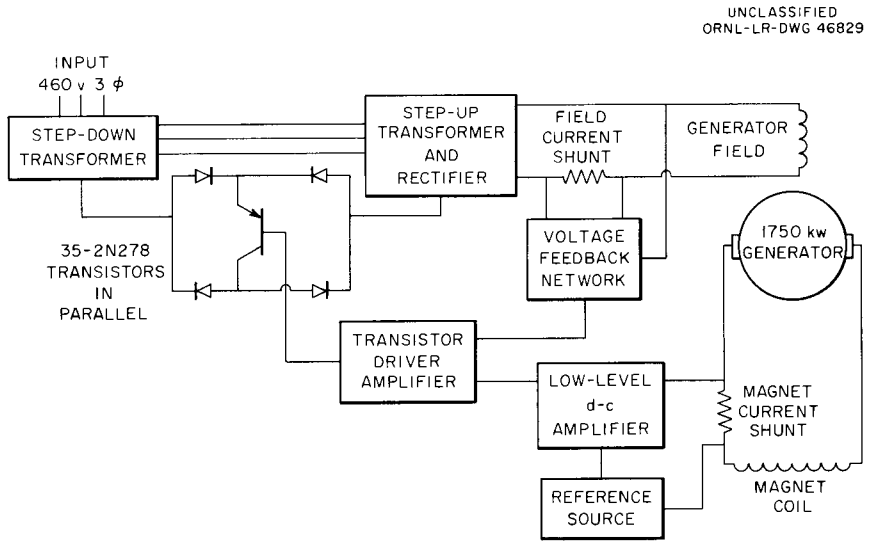

Fig. 5.22. Block Diagram of Magnet Regulator.

upward and rectified into direct current for the field supply. A dynamic series impedance consisting of 35 parallel transistors is inserted in the 24-v leg of the system, and the magnitude of the impedance is changed through a feedback path so as to result in the proper value of armature current.

The ORIC Building

Catalytic Construction Company of Philadelphia was selected as the architect-engineer for the building and to assist the Laboratory with the design of cyclotron components. To expedite construction of the cyclotron building, the site was prepared while the title-II drawings and specifications were being prepared. The building site was excavated to bedrock and backfilled by local contractors.

The ORIC building is a 100 × 200 ft rectangular masonry structure (see Fig. 5.23). The first floor (see Fig. 5.24) contains the cyclotron and target rooms with heavy (7-ft concrete) shielding walls, control and counting rooms, laboratories, and work space for service personnel. The shielded areas extend into the second floor, which also contains laboratories and offices. A smaller third floor contains such heavy equipment as magnet power supplies, vacuum pumps, and heat exchangers, all supported by the heavy shielding structure.

Fig. 5.23. Artist's Sketch of ORIC Building.

The title-II drawings and specifications were completed in October 1959. Fifteen bids for construction of the cyclotron buildings and facilities were examined in early December. On December 14 the contract was awarded to Foster and Creighton Construction Company of Nashville at the bid price of $1,484,000. The contract includes erection of the building and cooling tower and the installation of some equipment associated with the cyclotron. (Components of the cyclotron, now being fabricated, will be installed later.) The special piping, electrical, and reinforced concrete work constitute about 50% of the total. The contract specifies completion of the building in 330 days (by Nov. 8, 1960). The contractor began work promptly; most of the footings and first-floor walls are in place, and concrete for the shield (7 ft thick) is now being poured (see Fig. 5.25).

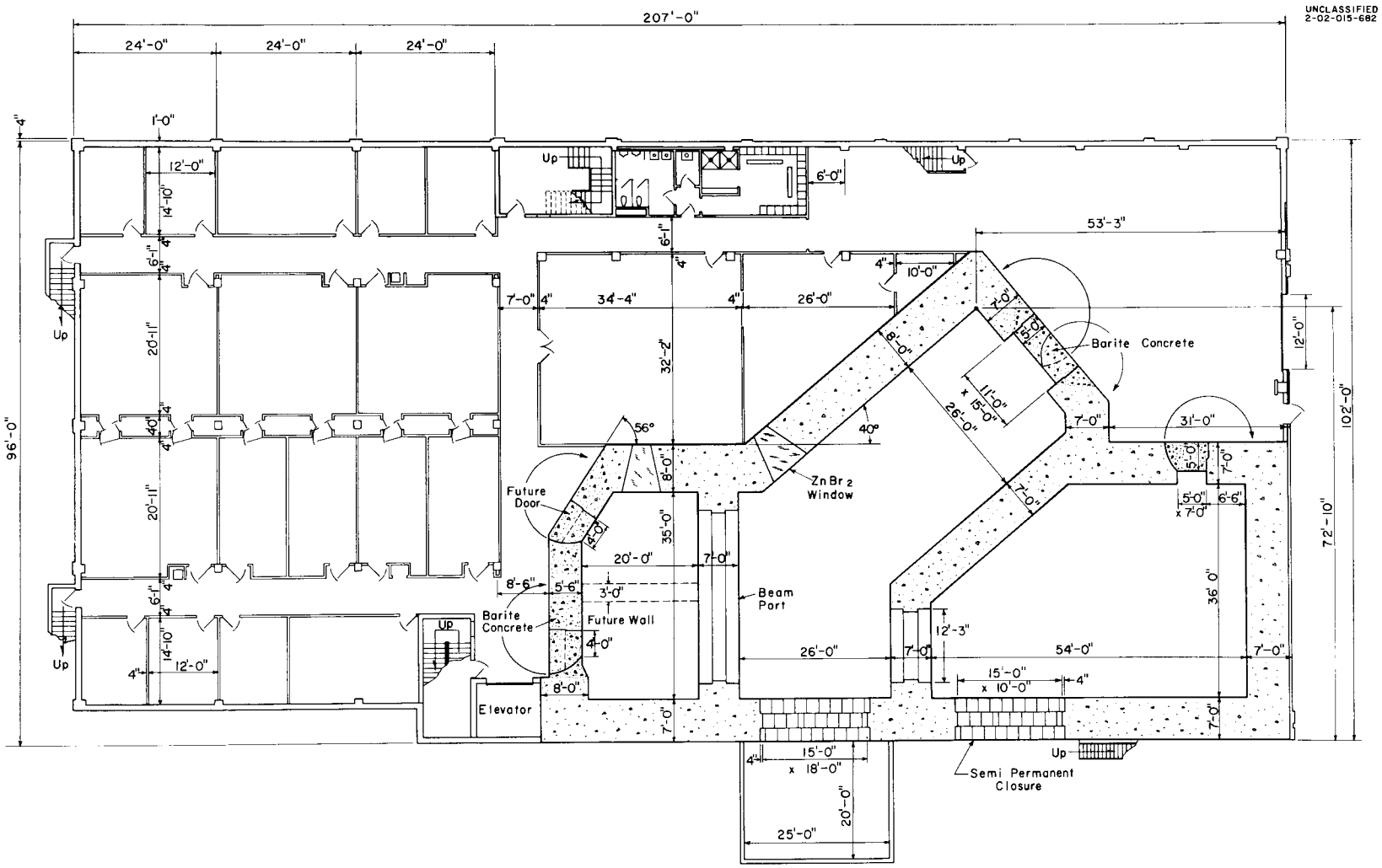

Fig. 5.24. ORIC Building 6000, First Floor Plan.

Fig. 5.25. ORIC Building 6000 Under Construction (Mar. 1, 1960).

PUBLICATIONS

Bassel, R. H., and R. S. Bender, "The Oak Ridge Relativistic Isochronous Cyclotron. Addendum. Some Recent Results of Orbit Studies," Nuclear Instr. & Methods 6, 234–37 (1960).

Bichard, J. W., J. W. Mihelich, and B. Harmatz, "Electron Capture Decay of Lu^{173} to Levels in Yb^{173}," Phys. Rev. 116, 720–24 (1959).

Blosser, H. G., R. E. Worsham, C. D. Goodman, R. S. Livingston, J. E. Mann, H. M. Moseley, G. T. Trammel, and T. A. Welton, "Four-Sector Azimuthally Varying Field Cyclotron," Rev. Sci. Instr. 29, 819–34 (1958).

Cohen, B. L., "Cyclotrons and Synchrocyclotrons," in Handbuch der Physik, vol 44, Springer, Berlin (1959).

Cohen, B. L., H. G. Blosser, E. D. Hudson, R. S. Lord, and R. S. Bender, "The Oak Ridge Relativistic Isochronous Cyclotron. Part II. Magnetic Field Design for the Isochronous Cyclotron," Nuclear Instr. & Methods 6, 105–25 (1960).

Cohen, B. L., and A. G. Rubin, "Determination of Nuclear Reaction Mechanisms from Energy Spectra of Emitted Particles," Phys. Rev. 114, 1143–45 (1959).

Cohen, B. L., and A. G. Rubin, "Further Studies of Anomalous Inelastic Proton Scattering," Phys. Rev. 111, 1568–77 (1958).

Cohen, B. L., and A. G. Rubin, "Inelastic Proton Scattering in Medium-Weight Elements," Phys. Rev. 113, 579–84 (1959).

Fisher, D. E., A. Zucker, and A. Gropp, "Nuclear Reactions Induced by the Nitrogen Bombardment of Sulfur," Phys. Rev. 113, 542–47 (1959).

Fulmer, C. B., "Total Reaction and Elastic Scattering Cross Sections for 22.8-Mev Protons on Uranium Isotopes," Phys. Rev. 116, 418–23 (1959).

Fulmer, C. B., and B. L. Cohen, "Magnetic Analysis of the Long-Range Particles from Fission of U^{235}," Phys. Rev. 108, 370–72 (1957).

Fulmer, C. B., and B. L. Cohen, "(p,α) Reactions Induced by 23-Mev Protons," Phys. Rev. 112, 1672–78 (1958).

Goodman, C. D., "An Interpretation of Anomalous Inelastic Proton Scattering," Phys. Rev. Letters 3, 230 (1959).

Gordon, M. M., and T. A. Welton, "The Oak Ridge Relativistic Isochronous Cyclotron. Part III. Analysis of Ion Orbits in the Isochronous Cyclotron," Nuclear Instr. & Methods 6, 221–33 (1960).

Halbert, M. L., and A. Zucker, "Elastic Scattering of N^{14} by Be^{9}," Phys. Rev. 115, 1635 (1959).

Halbert, M. L., and A. Zucker, "Light-Particle Spectra from the Nitrogen Bombardment of Oxygen," Phys. Rev. 114, 132–36 (1959).

Harmatz, B., T. H. Handley, and J. W. Mihelich, "Nuclear Spectroscopy of Odd-Mass (161–173) Nuclides Produced by Proton Irradiation of Er and Yb," Phys. Rev. 114, 1082–94 (1959).

Howard, F. T., Cyclotrons and High Energy Accelerators, ORNL-2644 (November 1958).

Howard, F. T., ed., Sector Focused Cyclotrons, Proceedings of the Conference on Sector-Focused Cyclotrons, Sea Island, Georgia, Feb. 2–4, 1959, Natl. Acad. Sci.–Natl. Research Council, Publ. No. 656 (Nuclear Sci. Ser., Rept. No. 26).

Jacob, K. P., J. W. Mihelich, B. Harmatz, and T. H. Handley, "Electron Capture Decay of Tm^{168} and Tm^{166}," Phys. Rev. 117, 1102–11 (1960).

Livingston, R. S., and F. T. Howard, eds., "The Oak Ridge Relativistic Isochronous Cyclotron, Part I," Nuclear Instr. & Methods 6, 1–25 (1959).

Pinajian, J. J., and M. L. Halbert, "Nitrogen-Induced Nuclear Reactions in Potassium," Phys. Rev. 113, 589–94 (1959).

Ziegler, N. F., The Admittance and Transfer Function of Solid Core Electromagnets, ORNL-2860 (December 1958).

Zucker, A., "Mechanism of Transfer Reactions with Heavy Ions," Phys. Rev. Letters 4, 21 (1960).

PAPERS PRESENTED AT SCIENTIFIC AND TECHNICAL MEETINGS

American Physical Society, Chicago, November 28–29, 1958

J. W. Bichard, J. W. Mihelich, and B. Harmatz, "The Electron Capture Decay of Lu^{173} to Levels in Yb^{173}."

K. P. Jacob, J. W. Mihelich, B. Harmatz, and T. H. Handley, "Electron Capture Decay of Tm^{168} and Tm^{166}."

J. W. Mihelich, B. Harmatz, and T. H. Handley, "Nuclear Spectroscopy of Odd Mass (161–173) Rare Earth Nuclides."

American Physical Society, New York City, January 28–31, 1959

C. B. Fulmer and C. D. Goodman, "(p,α) Reactions Induced by Protons in the Energy Range of 11–23 Mev."

C. D. Goodman and J. B. Ball, "(p,d) Reactions at 23 and 19 Mev."

M. L. Halbert and A. Zucker, "Elastic Scattering of N^{14} by Be^{9}."

A. Zucker, M. L. Halbert, and C. E. Hunting, "Measurement of a Plasma Density with 27-Mev Nitrogen Ions."

Conference on Sector-Focused Cyclotrons, Sea Island, Georgia, February 2–4, 1959

R. H. Bassel, "Beam Extraction Studies for the ORIC."
R. S. Bender, "Beam Facilities Planned for the ORIC."
H. G. Blosser, "Adjustment of Trimming-Coil Currents."
H. G. Blosser, "Beam Quality Measurements and Focusing Grid Studies."
B. L. Cohen, "Selection of Magnet Configuration for the ORIC."
E. D. Hudson, "Oak Ridge Model Magnet Studies."
R. J. Jones, "Ion Source and Beam Quality Studies."
R. E. Worsham, "Preliminary Design of the RF System for ORIC."

Southeastern Section of American Physical Society, New Orleans, April 9–11, 1959

C. B. Fulmer, "22-Mev Proton Elastic Scattering from Ni^{64}, Zn^{64}, and Cu."

F. T. Howard, "A Survey of Cyclotrons and Other High-Energy Accelerators."

M. L. Halbert, C. E. Hunting, and A. Zucker, "Energy Dependence of N^{14}-C^{12} Elastic Scattering."

J. A. Martin, "Eight-Sector AVF Electron Cyclotron."

American Physical Society, Washington, D.C., April 30–May 2, 1959

J. B. Ball and C. D. Goodman, "Mechanism of (p,t) Reactions at 22 Mev."

C. E. Hunting, M. L. Halbert, and A. Zucker, "Elastic Scattering of N^{14} by Carbon."

J. J. Pinajian, "The Exchange Transfer Reaction $Al^{27}(N^{14},Mg^{27})O^{14}$."

American Physical Society, Milwaukee, June 18–20, 1959

M. L. Halbert, "Elastic Scattering of Nitrogen Ions by Light Nuclei."

Gordon Research Conference on Nuclear Chemistry, Meriden, N.H., June 29–July 3, 1959

A. Zucker, "Nuclear Reactions and Scattering with 27-Mev Nitrogen Ions."

International Conference on High Energy Accelerators and Instrumentation at CERN, Geneva, September 14–19, 1959

J. A. Martin, "A 450-kev Eight-Sector Fixed-Frequency Electron Cyclotron."

American Physical Society, New York, January 27–30, 1960

R. H. Bassel, R. M. Drisko, and M. A. Melkanoff, "Optical Model Analysis of Heavy Ion Scattering."

C. B. Fulmer, "Elastic Scattering of Protons by Single Isotopes."

C. D. Goodman, "Evidence for Pickup Mechanism in $Nb^{93}(p,\alpha)Zr^{90}$."

M. L. Halbert, J. L. Blankenship, and M. V. Goldman, "Response of Surface-Barrier Semiconductor Counters to N^{14} Ions."

C. E. Hunting, "Alpha-Particle Spectra from the Bombardment of F^{19} by N^{14}."

A. Zucker and M. L. Halbert, "Elastic Scattering of 27.3-Mev Nitrogen by Aluminum."

ANNOUNCEMENTS

The following physicists have joined the staff of the Electronuclear Research Division:

J. B. Ball, University of Washington
R. H. Bassel, University of Pittsburgh
R. W. Boom, University of California, Los Angeles
D. M. Smith, University of Texas
K. S. Toth, University of California, Berkeley

Temporary assignments to the Division have included:

John Baker, student trainee, Lincoln Memorial University
R. M. Drisko, University of Pittsburgh
M. P. Fricke, Co-op student, Drexel Institute
P. C. Gugelot, Institut voor Kernphysisch Onderzoek, Amsterdam
M. V. Goldman, Princeton University
G. L. Kochanny, Michigan State University
B. Linder, Florida State University
M. S. Maxon, Indiana University
J. W. Mihelich, University of Notre Dame
D. C. Peaslee, Purdue University
A. Timnick, Michigan State University

J. L. Need left the Laboratory for a position with the National Aeronautics and Space Administration at Cleveland, Ohio. B. D. Williams is now with the Oak Ridge Gaseous Diffusion Plant (K-25).

ORNL-3047
Physics
TID-4500 (16th ed.)

INTERNAL DISTRIBUTION

1. C. E. Center
2. Biology Library
3. Health Physics Library
4-6. Central Research Library
7. Reactor Experimental Engineering Library
8-27. Laboratory Records Department
28. Laboratory Records, ORNL R.C.
29. A. M. Weinberg
30. L. B. Emlet (K-25)
31. J. P. Murray (Y-12)
32. J. A. Swartout
33. E. H. Taylor
34. E. D. Shipley
35. S. C. Lind
36. M. L. Nelson
37. W. H. Jordan
38. A. W. Riikola
39. C. P. Keim
40. R. S. Livingston
41. F. L. Culler
42. A. H. Snell
43. A. Hollaender
44. M. T. Kelley
45. G. E. Boyd
46. K. Z. Morgan
47. T. A. Lincoln
48. A. S. Householder
49. C. S. Harrill
50. C. E. Winters
51. H. E. Seagren
52. D. Phillips
53. P. M. Reyling
54. G. C. Williams
55. R. J. Jones
56. C. D. Goodman
57. F. T. Howard
58. R. E. Worsham
59. J. A. Martin
60. M. B. Marshall
61. A. Zucker
62. R. W. Johnson
63. J. A. Lane
64. M. J. Skinner
65. R. A. Charpie
66. R. S. Cockreham
67. R. S. Bender
68. E. D. Hudson
69. J. J. Pinajian
70. W. R. Smith
71. W. A. Fowler (consultant)
72. H. Feshback (consultant)
73. M. Goldhaber (consultant)
74. M. S. Livingston (consultant)
75. J. R. Richardson (consultant)
76. J. H. Van Vleck (consultant)
77. ORNL – Y-12 Technical Library, Document Reference Section

EXTERNAL DISTRIBUTION

78. Division of Research and Development, AEC, ORO
79-706. Given distribution as shown in TID-4500 (16th ed.) under Physics category (75 copies – OTS)

Progress reports have been issued by the Electronuclear Research Division for the periods ending on the dates listed below:

ORNL-1173	September 30, 1951, Part I
ORNL-1235	September 30, 1951, Part II
ORNL-1269	December 31, 1951, Part I
ORNL-1270	December 31, 1951, Part II
ORNL-1315	March 31, 1952, Part II
ORNL-1339	March 31, 1952, Part I
ORNL-1345	June 30, 1952, Part I
ORNL-1346	June 30, 1952, Part II
ORNL-1383	September 30, 1952
ORNL-1531	March 20, 1953
ORNL-1663	September 20, 1953
ORNL-1670	March 20, 1954
ORNL-1795	September 20, 1954
ORNL-1884	March 20, 1955
ORNL-2030	September 20, 1955
ORNL-2139	March 20, 1956
ORNL-2140	March 20, 1956
ORNL-2434	October 1, 1957
ORNL-2740	October 1, 1958